Unterschrift des Betreuers

TECHNISCHE UNIVERSITÄT WIEN
Vienna University of Technology

DIPLOMARBEIT

Development of a high temperature dilatometer for measuring magnetostriction

ausgeführt am

———————————————

Institut für Festkörperphysik
der Technischen Universität Wien

———————————————

unter der Anleitung von
Univ.-Prof. Dipl.-Ing. Dr.techn. Roland Grössinger

durch

Jürgen Möller
A-2153 Stronsdorf 307

———————————————   ———————————————
Datum   Unterschrift

Contents

Contents

1. Kurzfassung

Magnetoelastische Effekte eines Festkörpers sind Wechselwirkungen von äußeren Einflüssen, wie Temperatur T, Druck σ und der magnetischen Feldstärke H mit den inneren Parametern des Materials, wie Magnetisierung M, Dehnung ϵ und Entropie S. Die Magnetostriktion stellt dabei eine spezielle Art dieser Interaktionen zwischen magnetischer Feldstärke H und Dehnung ϵ dar. Deshalb ändert ein Material als Antwort auf ein Magnetfeld H seine Dimensionen, um seine Magnetisierung M dem angelegten Feld anzupassen. Atomar lässt sich dieses Verhalten durch zwei parallel ablaufende Mechanismen erklären: die Spin-Bahn-Wechselwirkung und das Kristallfeld des Festkörpers, welches die Energieniveaus der "magnetischen Elektronen" aufspaltet.

Um diese Formänderung der Kristalle festzustellen, gibt es einige Messmethoden, die sich jedoch aufgrund ihrer Auflösung, ihres Temperaturbereiches und der möglichen magnetischen Feldstärken unterscheiden. Besonders Dehnungsmessstreifen und kapazitive Dilatometer überzeugen durch ihr hohes Auflösungsvermögen und ihre breitgefächerte Funktionalität. Bisherige Studien mit kapazitiven Dilatometern wurden vor allem im Tieftemperaturbereich bis hin zu Raumtemperatur durchgeführt. In Verbindung mit Magnetostriktionsmessungen im Hochtemperaturbereich ergeben sich zusätzliche Problemstellungen, wie die Auswahl geeigneter Materialien.

Diese Diplomarbeit untersucht das Verhalten einer kapazitiven Messzelle oberhalb von Raumtemperatur und setzt sich mit der daraus ergebenden Problematik auseinander. Die Entwicklung dieses Messsystems, verbunden mit dem Aufbau der Kapazitätsmesszelle und einer dazu notwendigen Software zum Steuern des Messablaufes, findet vor allem im Raumtemperaturbereich statt. Erst nach einem adäquaten Abgleich mit gut dokumentierten Magnetostriktionsmessungen für Nickel bei Raumtemperatur wird der Messaufbau für Hochtemperatur adaptiert. Die grundlegenden Probleme werden dabei angesprochen und analysiert. Magnetostriktionsmessungen sind stark temperaturabhängig. Schwierigkeiten, die es zu lösen gibt, ergeben sich vor allem durch einen Temperaturgradienten auf der Zelle. Schließlich wird der optimale Einsatz der kapazitiven Messmethode erläutert und ein Ausblick auf die Realisierung verbesserter Messsysteme diskutiert.

2. Abstract

Magnetoelastic effects of a solid are interactions between external influences like temperature T, stress σ and magnetic field H and the internal parameters of the material, magnetization M, strain ϵ and entropy S. Magnetostriction represents thereby a specific interaction between the magnetic field H and the strain ϵ. As a consequence of the applied magnetic field H a material alters its dimensions in order to modulate its magnetization M with the external magnetic field H. Atomically this behaviour is explained with two parallel proceeding mechanisms: spin-orbit coupling and the crystal field of the solid body that splits the energy levels of the "magnetic electrons".

For detecting these deformation several different measuring methods are used, which alter however due to their sensitivity, their temperature range and their possible magnetic fields. Especially strain gauges and capacitive dilatometers satisfy with high resolution and a wide-ranging functionality. Up to now most studies with capacitive dilatometers were accomplished from cryogenic temperature up to room temperature. Magnetostriction measurements at high temperatures go hand in hand with additional difficulties, as the choice of qualified materials.

This diploma thesis examines the manners of a capacitive measuring cell at high temperatures and reflects its problems. The development of this gauging system, combined with the construction and assembly of the capacitance cell and a for that purpose necessary software for actuating the detection system, takes primarily place at room temperature. Not until after a adequate calibration with well documented magnetostriction measurements for nickel at room temperature, the gauging setup is adapted for the use at high temperatures. Basic problems are discussed and analyzed. Magnetostriction measurements are highly temperature-sensitive. Difficulties which have to be studied, arise from a temperature gradient on the cell. Finally the optimal operation of the capacitive measuring technique is elucidated and a perspective on the realisation of temperature improved measurement systems discussed.

3. Introduction

In this diploma thesis we investigate the effect a magnetic field H has on the physics of a solid body. The material gets magnetised and changes its magnetization due to the applied magnetic field H. As a further consequence the dimensions of the inter-atomic distance but also the crystal structure change. This effect is commonly called magnetostriction λ. For example the process of magnetostriction is best known and well audible as "100Hz hum" of transformators caused by the transformer sheets. Techno-logically it is used as well in voltage and force sensors as in microactuators. The atomic roots of magnetostriction are combined in two mechanisms: the spin-orbit coupling and the crystal field of the solid that splits the energy levels of the "magnetic electrons".

Microscopic measurement methods such as X-ray and neutron diffraction or macro-scopic methods like capacitance dilatometry, strain gauges , extensometers, twin mi-croscope, tunnel tip transducers and interferometry detects the length expansions or contractions. Most suitable are capacitive dilatometers and strain gauges because of their high sensitivity and their compatibility with high magnetic fields H.

The values of magnetostriction is up to now well known for many materials from cryo-genic temperature to room temperature. Even if electric motors and nearly all ordinary attachment have operating temperatures around 100°C, measurements above room tem-perature are rare and rather just theoretically forecasted than experimentally detected. As a central issue for the finite experimental knowledge about high temperature mea-surements is that temperatures over 600K make great demands on material and limit the choice of them. They have to be non magnetostrictive themselves and should resist high temperatures.

Notwithstanding it seems to be an interesting challenge to study a rather untouched region of physics and research new materials that dispute the high temperatures. For this reason first analyzes of such high temperature magnetostriction measurement setups are achieved. Unquestionable the application of strain gauges is limited in this temperature range because of the temperature limitations of the used materials. As a result of that capacitive dilatometers are preferred.

But the study of magnetostriction at high temperatures is not just industrially adap-tive. Materials science is also interested in values for magnetostriction λ at high tem-peratures. The reason for it is the correspondence between the magnetization M and the strain ϵ of a solid body. Both altitudes are compared with the aid of the so called inverse Brillouinfunction $\lambda \propto \mathcal{L} \left(\frac{\mu H}{k_B T} \right)^{-1}$, with the permeability μ, the magnetic field H, the Boltzmann constant k_B and the temperature T. As a matter of fact the Curie

temperature T_C is for most materials placed above 0°C and therefore the magnetization M of them does not disappear up to T_C. For statements based on the inverse Brillouin-function $\lambda \propto \mathcal{L}\left(\frac{\mu H}{k_B T}\right)^{-1}$ it is important to know the magnetostriction λ up to T_C in order to suggest the magnetization M and vice versa.

A solid depends besides the magnetic field H similarly on two other external parameters, temperature T and stress σ that affect pure magnetostriction measurements (figure 4.2). Thus pressures and temperature gradients should be avoided. That aggravates the demands on measurement systems for high temperatures.

The diploma thesis is organized as follows: In section 4 we introduce the basic principles of magnetostriction and testing methods to detect it. Chapter 5 provides a brief introduction of ideas and prinicples for a capacitive measurement method at room temperature. Its results are presented in chapter 6 where we also respond to arising problems with some improvements. On the basis of these succeeded results a high temperature system is adapted in section 7. Finally the results of high temperature experiments are presented and analyzed in chapter 8. The thesis concludes with a outlook and advices for further improvements.

4. Theory of magnetostriction

4.1. The phenomenon of magnetostriction

Magnetostriction is the changing of a material's physical dimensions due to applying a magnetic field. If the material is magnetically ordered the magnetostriction is proportional to the magnetization. In other words, a magnetostrictive body will alter its shape when it is subjected to a magnetic field (figure 4.1). The effect was first identified in 1842 by James Joule when observing a sample of nickel.
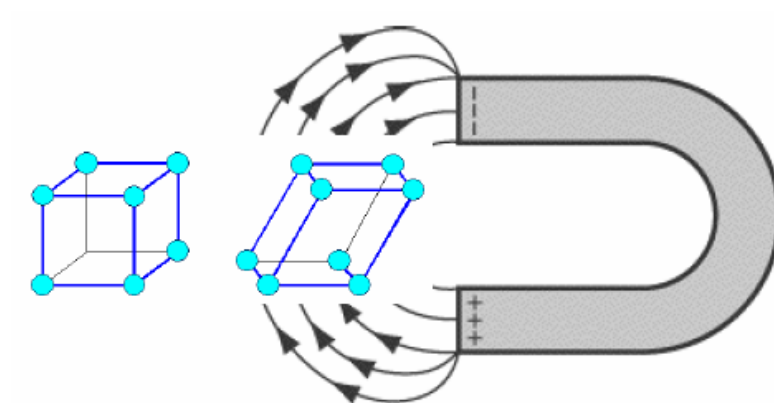

Figure 4.1.: The shape of a solid body changes as a result of an applied magnetic field.

When any magnetic solid acquires a magnetization M under the application of a magnetic field H at the same time its crystalline lattice is deformed [1, 2]. Due to the dependence of the magnetic interactions on the distance between the interacting atoms, an elastic and magnetic body exhibits magnetoelastic phenomena: its dimensions and its elastic properties depend on its magnetic state (direct magnetoelastic effects), and its magnetic properties [3–10] are influenced by the external and internal mechanical stresses (inverse magnetoelastic effects).

These phenomena are quite general, and have been observed obviously in ferromagnets, but also in ferrimagnets, antiferromagnets, paramagnets and even diamagnets and

superconductors. It does not matter if the solid is a metal or an insulator, what only matters is, if the atoms either acquire an induced magnetic moment or they have a permanent one. By Hooke´s law [1, 11, 12] the deformation suffered is proportional to the material size, say l, and therefore it is convenient to express the deformation by the relative variation $\lambda = \Delta l/l = (l(H, T) - l(H = 0, T))/l(H = 0, T)$, called the linear magnetostriction [2, 13, 14].

For the measurement of magnetostriction no special physical unit is needed because λ is just the ratio of $\Delta l/l$. To denote the measured proportions dimensionless quantities like parts per million, 1 ppm = 10^{-6} , are used.

4.2. Magnetoelastic interactions

The difference in energy which is necessary to magnetize a material in different directions is called magnetic anisotropy [15,16]. It is easily possible to connect the magnetostriction by the help of thermodynamics to other fundamental macroscopic properties [2, 12, 17]. Therefore the Euler equation is needed to write the Helmholtz free energy F as a function of temperature T, (anisotropic) strain ϵ_{ij} and magnetic field H_k as

$$dF(T, V, H) = -SdT\text{-}\,pdV - MdH \tag{4.1}$$

$$dF(T, V, H) = -SdT + \sum_{ij} V\sigma_{ij}d\epsilon_{ij} - \sum_{k} M_k dH_k \tag{4.2}$$

where the indices i, j, k denote the components in x, y, z direction. S represents the entropy, σ_{ij} the external stress (= the negative pressure in isotropic case) and M_k the magnetization. So, theoretical thermodynamic offers a complex picture of relations between mechanical, thermal and magnetic properties of solids. All of them correspond to each other. For further and more detailed information on the thermodynamic interactions in an anisotropic solid, the paper [17] is recommended. Figure 4.2 shows the physical connections of the magnetostriction which are based in the equation of the Helmholtz free energy F.

The interactions of strain ϵ_{ij}, magnetization M_k and entropy S open the way to transpose material parameters into each other and to look at the behaviour of magnetic systems from different points of view [14,17]. In most of the applications of this thermodynamical scheme, experimental as well as theoretical, only the direct connections are considered. For example, the influence of a magnetic field H_k on the magnetization M_k is studied in ac- or dc- susceptibility measurements. Other basic experiments deal with the stress σ_{ij} or pressure influence on the strain ϵ_{ij}, and with the effect of temperature T changes - via specific heat measurements - on the entropy S. But only the indirect (or coupled) effects bring the picture to a complete one. The influence of external magnetic field H_k on the strain ϵ_{ij}, which is the magnetostriction, and of temperature T on
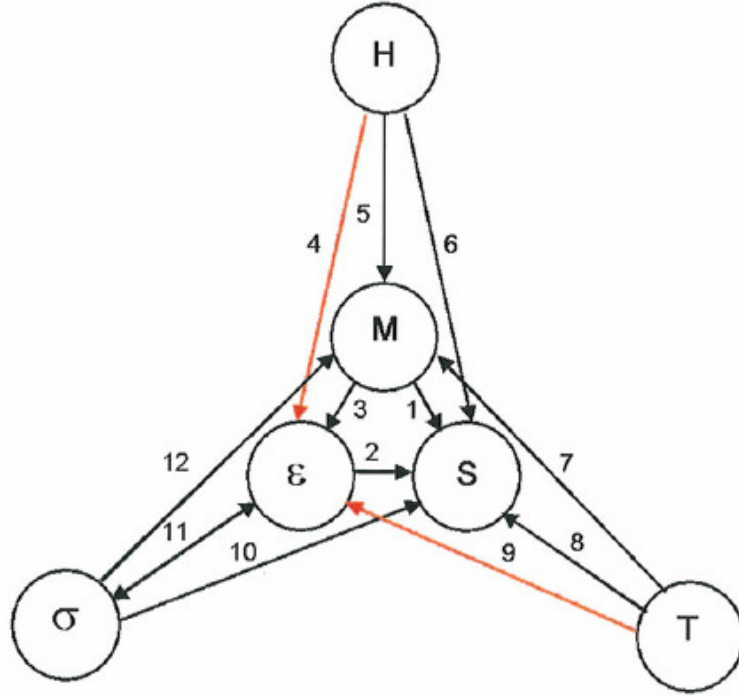
Figure 4.2.: The magnetic, thermal and mechanical properties of solids [2, 14, 17] as a direct or indirect interplay of the external parameters H (magnetic field), σ(external stress or pressure), T (temperature) and the internal response M (magnetization or magnetic moment), ϵ (strain) and S (Entropie). The physical influences of those interactions are: 1...heat of magnetization; 2...heat of deformation; 3...magnetoelasticity; 4...magnetostriction; 5...susceptibility; 6...magnetocaloric effect; 7...thermal remagnetization; 8...heat capacity; 9...thermal expansion; 10...piezocaloric effect; 11...elasticity; 12...converse magnetostriction;

strain ϵ_{ij}, which is the thermal expansion are probably the most important "indirect" phenomena. These facts illustrate the importance of magnetostriction measurements for the discussion of experiments in the frame of thermodynamics.

4.3. The physical mechanism of magnetostriction

There are two types of origins of magnetostriction: the spin-orbit coupling (exchange interaction) and the crystal electric field (CEF) that splits the energy levels of the "magnetic electrons". The lattice distortion occurs in order to minimize the free energy [2,14,17] including the magnetic exchange.

The spin-orbit coupling is very important for the specification of the magnetic ma-

terial, which depends on the orientation of the spins [3, 4, 7, 8, 10, 18]. Ferromagnetic or antiferromagnetic order in solids is the result of the exchange interaction between electrons. The exchange interaction is an isotropic exchange with volume distortion but without symmetry changes.

In magnetic solids there exists a strongly inhomogeneous electric field due to the charge distribution of ions, called the crystal electric field, CEF, whose gradients interact with the ion magnetic electrons, consisting of the sum of magnetic moments of the orbit m_l and the spin m_s. The CEF causes the deformation or distortion of the lattice symmetry.

We consider the simple model system shown in figure 4.3 to explain the physical mechanism of magnetostriction in an antiferromagnetic material [1,3,5,17]. An antiferromagnetic crystal allows the most general description of this mechanism. Above the Neel temperature T_N [3–6,9,10,18], an antiferromagnetic solid gets paramagnetic and only below the Neel temperature T_N it shows its antiferromagnetic behaviour. Therefore figures 4.3 a and 4.3 d take place in a paramagnetic crystal while figures 4.3 b, c and 4.3 e, f show the system ordered antiferromagnetically.
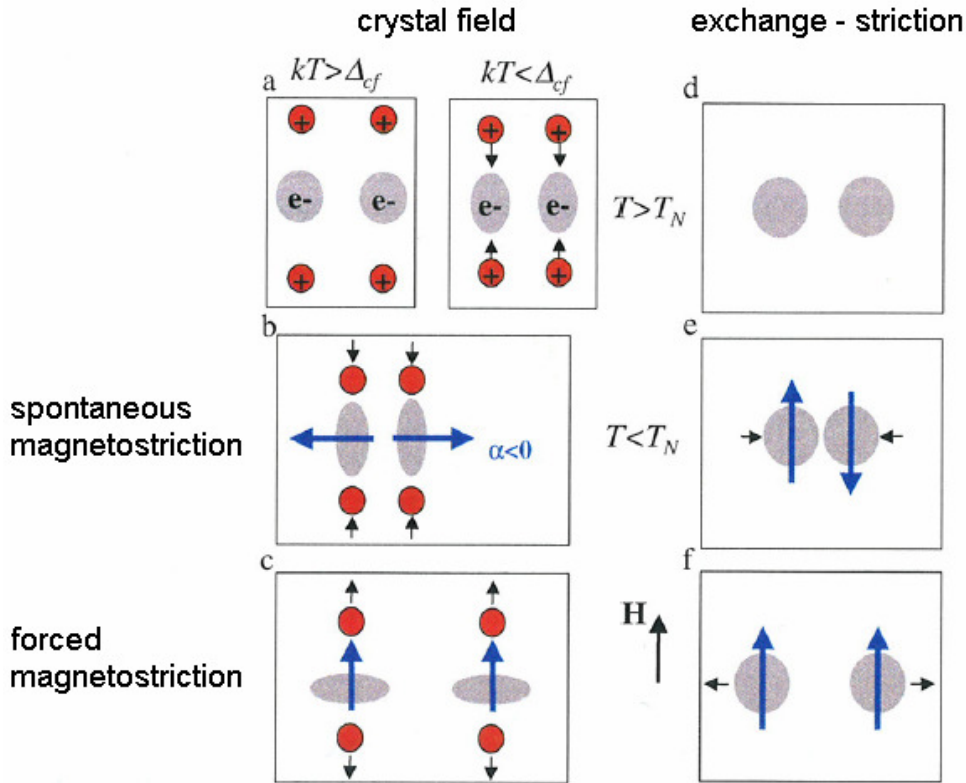

Figure 4.3.: Magnetostriction has two physical origins: the spin-orbit coupling of the atoms (exchange striction) and the interaction between the lattice of a solid and the atomic orbits. Both mechanism are dependent on the temperature T and the magnetic field H.

4.3.1. The crystal electric field

On the left hand side of figure 4.3 the crystal field mechanism is shown for a crystal field produced according to Coulomb´s law [3, 10] by two positive charges. For temperatures higher than the crystal field splitting energy $kT > \Delta_{cf}$, with the Boltzmann constant k and the temperature T, the electron charge density is spherical symmetric, because the thermal energy does not allow any bonding between the electron charge densities and the two positive charges (figure 4.3 a left).

When the temperature is lower than the crystal field splitting energy $kT < \Delta_{cf}$ (figure 4.3 a right), only the low energy crystal field states are thermally populated. This leads to a continuous deformation of the electron charge density with decreasing temperature. The shape of the deformation resembles the geometry of the crystal field, in our example the two positive charges produce an ellipsoidal (cigar) shape. The crystal field striction arises from the fact, that a thermally (or magnetic field induced) change of the electron charge density shape changes the force between the free electrons of the electron charge density and the positive charges which produce the crystal field. A magnetostrictive strain of the crystal lattice results as indicated by the small arrows in the right figure of 4.3 a. For this magnetostrictive effect no long range order is necessary and it is called crystal field influence on the thermal expansion [1, 17]. As assumed for a paramagnet the magnetic moments are randomly distributed (no blue arrows in figure 4.3 a).

If the temperature gets lower than the Neel temperature T_N, the system orders anti-ferromagnetically (figure 4.3 b). The shape and, because of the spin-orbit coupling, the magnetic moment (blue arrow) of the electron charge density is closely associated with magnetic anisotropy, which is governed in crystal field theory by Stevens factors [4]. For our example we take the vertical ellipsoidal shape with a horizontal magnetic moment (blue arrow). The direction of the magnetic moment is defined by the right-hand-rule. Below the Neel temperature T_N the magnetic moments (blue arrows) are ordered antifer-romagnetically, as shown in figure 4.3 b. The deformation of the electron charge density already incipient above T_N is increased by the appearance of the magnetic moment and consequently leads to a spontaneous magnetostrictive effect below T_N as indicated by the small black arrows.

The application of a magnetic field H in vertical direction reduces the ellipsoidal deformation of the electron charge density and reverses the spontaneous magnetostrictive effect because the magnetic moments now tend to point in the same direction as the applied magnetic field H. If the magnetic field $H > H_{critical}$ is strong enough, the charge density may even turn from a cigar shape into a pancake (forced magnetostriction) as shown in figure 4.3 c. Otherwise for status of figure 4.3 b remains.

4.3.2. The exchange interaction

When the crystal field can be neglected, the spin-orbit coupling will be the dominant mechanism for magnetostriction (right hand side of figure 4.3). Now the direction of the magnetic moments is not determined by the crystal field anymore, but by small anisotropies such as the dipolar interaction [15, 16, 19]. The explanation of this mechanism is equal to the description, how an antiferromagnetic interaction works. We use a spherical electron charge density (orbital momentum $\vec{L} = \vec{0}$) to explain the exchange interaction by the help of figures 4.3 d, e and f.

For temperatures higher than the Neel temperature T_N the antiferromagnet behaves like a paramagnet and the magnetic moments of the electron charge densities are randomly distributed (no blue arrows) in figure 4.3 d. In contrast to the crystal field mechanism, the exchange striction may lead to magnetoelastic effects only for non-zero magnetic moments. Therefore in the paramagnetic state $T > T_N$ with no applied magnetic field ($H = 0$) no exchange striction is expected.

Below the Neel temperature T_N the neighbouring magnetic moments of an antiferromagnetic solid point in opposite directions figure 4.3 e. The two ion interaction depends on the distance between the electron charge densities, and therefore below the Neel temperature T_N the two ion interaction energy may be lowered by a change of distance. Therefore two opposite directed neighbouring magnetic moments adduct each other, lower the distance between them (figure 4.3 e) and induce a magnetoelastic strain (spontaneous magnetostriction), which is called exchange striction.

Similar to the crystal field mechanism the spontaneous exchange striction may be reversed by the application of a magnetic field (figure 4.3 f. For an applied field $H > H_{critical}$ all magnetic moments of an antiferromagnetic material are adjusted in the same direction. Because two neighbouring rectified magnetic moments push off each other, the distance between the electron charge densities get taller and a forced exchange striction is the result (figure 4.3 f). When $H < H_{critical}$ the antiferromagnetic order of figure 4.3 e is retained.

4.4. Fundamental types of magnetostriction

Magnetostriction can be divided into spontaneous magnetostriction and forced magnetostriction. The deformation caused by magnetic interactions within a sample ($H_{ext} = 0$) is called spontaneous magnetostriction (figure 4.3) while the strain induced by an external magnetic field ($H_{ext} \neq 0$) is called forced magnetostriction (figure 4.3). Both of them have an isotropic component, the so called volume magnetostriction (figure 4.4), and anisotropic components which are of dipolar origin (form effect) or arise from short-range interactions and are named linear or Joule magnetostriction [1, 13, 17].
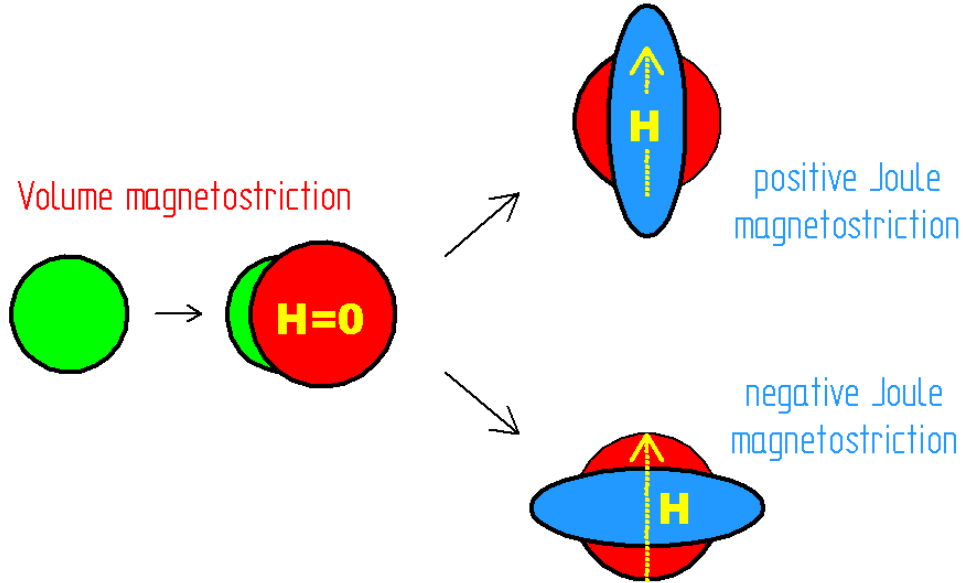
Figure 4.4.: The effect of magnetostriction consists of the isotropic volume magnetostriction and the anisotropic and magnet field dependent linear Joule magnetostriction. By a spherical sample the shape invariant change of volume magnetostriction can be demonstrated. An additional magnetic field $H \neq 0$ causes a volume conserving, anisotropic deformation that stretches or shrinks the sample in the direction of the magnetic field H.

4.4.1. Volume magnetostriction

When a material is cooled down from high temperature through its Curie temperature T_C [3–7, 9, 10, 18], an anomalous isotropic thermal expansion is observed near the Curie temperature. In figures 4.5 this anomalous thermal expansion can be viewed because ω is not equal zero at the Curie temperature T_C. This slightly magnetic field-dependent anomaly associated with the magnetic ordering of magnetic substances is called volume magnetostriction ω [1, 2, 13]. The volume magnetostriction is a shape invariant change and a material undergoes an isotropic expansion (or contraction) of the lattice caused by the onset of magnetic order for spontaneous magnetostriction or upon the application of magnetic field (forced magnetostriction) [20]. The volume anomaly is also slightly field dependent: at lower magnetic fields, ω varies linearly with the applied field, since this one remains a small perturbation of the exchange field. This effect is the main origin of the forced magnetostriction [1]. Volume magnetostriction is a high-field phenomenon [20] and is about 10-100 times smaller than the Joule magnetostriction. Therefore it can

often be neglected for measurements with lower magnetic fields.
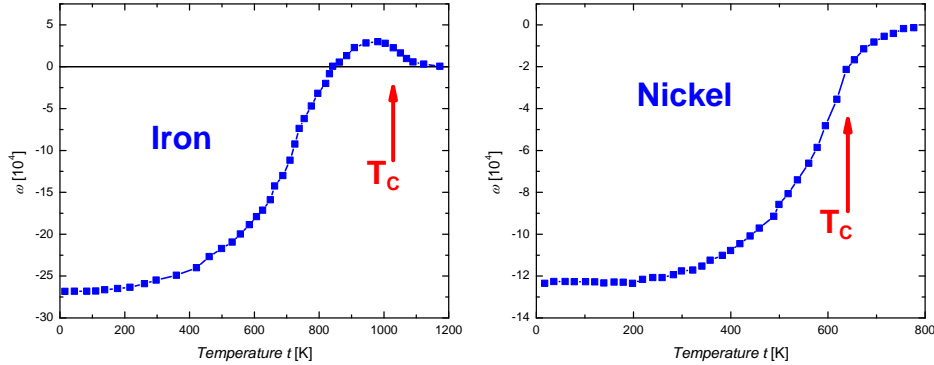
Figure 4.5.: The anomalous isotropic thermal expansion near the Curie temperature T_C is the reason for volume magnetostriction ω. Therefore $\omega \neq 0$ at Curie temperature T_C. The two curves of iron [21] and nickel [22] represent this behaviour.

4.4.2. Linear Joule magnetostriction

If a magnetic field is applied to the magnetically ordered sample, an additional anisotropic deformation that stretches or shrinks the sample in the direction of the magnetic field H is observed. This field-dependent phenomenon is called Joule or linear magnetostriction [1,2,13] and arises from spin-orbit coupling, which links the direction of the magnetic moment to the crystal lattice. The process of magnetostriction can then be viewed as the transition from a demagnetized multi domain state to a single domain state, which is aligned with the applied magnetic field. It is a volume conserving process in which one axis expands (contracts) while the other two axes contract (expand). The anisotropic strain depends strongly on the field strength, and reaches a limiting value (figure 4.6) when the magnetic technical saturation is achieved [1, 20, 23–25].

The interaction of a solid and an applied magnetic field H causes reactions, as already learned in section 4.2, inside the crystals. It may be worthwhile to study the relationship between some of those physical processes. As an example the relationship between the linear Joule magnetostriction $\lambda = \Delta l/l$ and the magnetization M [27] is able to provide information about the condition of the material. Therefore the proportionality of the two functions is significant. The Joule magnetostriction is an even function and in some cases it is approximated as being proportional to the square of magnetization at low fields [20]. To exemplify the implied behaviour, in figure 4.7 a typical magnetization M [28] and magnetostriction $\lambda = \Delta l/l$ are plotted against the applied magnetic field H.

The highest Joule magnetostriction which has ever been observed at room temperature is that of the $Tb_{0.3}Dy_{0.7}Fe_2$ alloy, called Terfenol-D, with about $\lambda_S \approx 10^{-3}$. Magne-
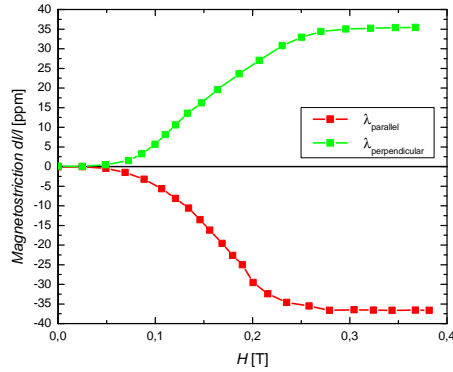
Figure 4.6.: A typical field dependent Joule magnetostriction λ at 4.2K, here for a nickel sample [26], measured parallel $\lambda_{\parallel}$ and perpendicular $\lambda_{\perp}$ to the direction of the applied magnetic field H.

tostrictive materials with large Joule magnetostriction are currently an object of intense study [1, 4, 20, 23–25, 29]. Because this effect is such important and technically used for sensors and actuators, table 4.1 shows a short comparison of the magnetostriction values of different materials:

Crystals	λ_{100} [ppm]	λ_{111} [ppm]	λ_S [ppm]
Fe	20.7	-21.2	-4.4
Ni	-45.9	-24.3	-33
$85\% \ Ni - Fe$	-3	-3	-3
$40\% \ Co - Fe$	146.8	8.7	64
$19\% \ Ga - Fe$	265	28	123
$19\% \ Al - Fe$	106	5	45.4
Fe_3O_4	-20	78	39
$Mn_{1.05}Fe_{1.95}O_4$	-28	4	-8.8
$Mn_{0.4}Zn_{0.1}Fe_{2.1}O_4$	-14	14	3
$Ni_{0.8}Fe_{2.2}O_4$	-36	-4	-17
$Ni_{0.3}Zn_{0.45}Fe_{2.25}O_4$	-15	11	0.6
$Co_{0.8}Fe_{2.2}O_4$	-590	120	164
$Co_{0.8}Zn_{0.2}Fe_{2.2}O_4$	-210	110	-18
$Tb_{0.3}Dy_{0.7}Fe_2$		1200	

Table 4.1.: A short overview of values [19] for different magnetostrictive crystals demonstrates the wide range of magnetostriction.

The Joule magnetostriction depends also on the temperature (figure 4.8) and mechanical stresses. This is a result of the theoretical formula of the Helmholtz free energy F
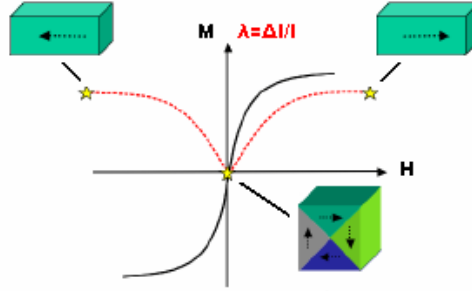
Figure 4.7.: magnetization M (black curve) and magnetostriction $\lambda = \frac{\Delta l}{l}$ (red curve) in comparison. The hysteresis of magnetic materials can be studied in [3–10, 18].

(section 4.2) and can be proved by measurements. This stress dependence of the magnetostriction consists mainly of the modification of the shape of the $\lambda(H)$ curves, while the value of the magnetostriction coefficient λ_S is usually nearly stress-independent.
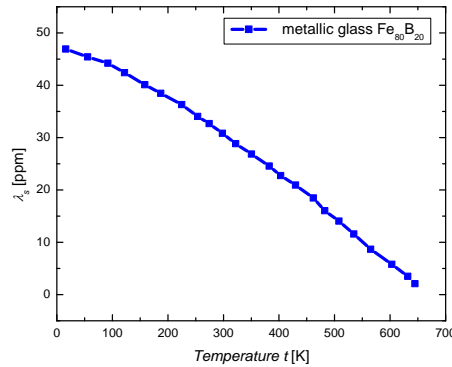

Figure 4.8.: Joule magnetostriction depends not only on the applied magnetic field H (section 4.2 and figure 4.2), but also on various other external parameters, like external stress or pressure σ, temperature T. As an example, this curve [30, 31] represents the temperature T dependence of the saturation magnetostriction λ_S of $Fe_{80}B_{20}$ glass.

4.5. Magnetostrictive Effects

Magnetostriction links thermodynamical units with magnetic ones. It is a reversible exchange between magnetic and mechanical energies. Several effects are recognized as a

consequence of magnetostriction [1, 2]:

Direct effects	Inverse effects
Volume magnetostriction (section 4.4.1)	Pressure dependence of stress σ_{ij} and temperature T
Joule magnetostriction (section 4.4.2)	Villari effect [1, 2, 5, 14]: is inverse of the Joule magnetostriction and therefore the change of susceptibility and magnetization of a magnetostrictive material when subjected to a mechanical stress.
Direct Wiedemann effect [1, 2, 5, 14]: a current carrying ferromagnetic wire will produce a circular magnetic field in a plane perpendicular to the wire (direction by the right-hand-rule) and the moments will align predominantly in the circumferential direction. When an axial magnetic field is applied, some of the moments align in a helical fashion creating a helical magnetic field. The twist observed in the wire is called the Wiedemann effect [figure].	Inverse Wiedemann effect or Matteuci effect [1, 2, 5, 14]: is the change in axial magnetization of a current carrying wire when it is twisted [figure].
ΔE effect [1,2,5,14]: is a magnetoelastic contribution to elastic properties and is quantified by $(E_S - E_0)/E_0$. The Young´s modulus E of materials changes as a result of the applied field. The elasticity of magnetostrictive materials is composed of conventional stress-strain elasticity (E_0) arising from inter atomic forces and the magnetoelastic (E_S) contribution due to the rotation of magnetic moments and resulting strains which occur when a stress is applied.	Magnetoelastic contribution to magnetocrystalline anisotropy [1,2,5,14, 15]
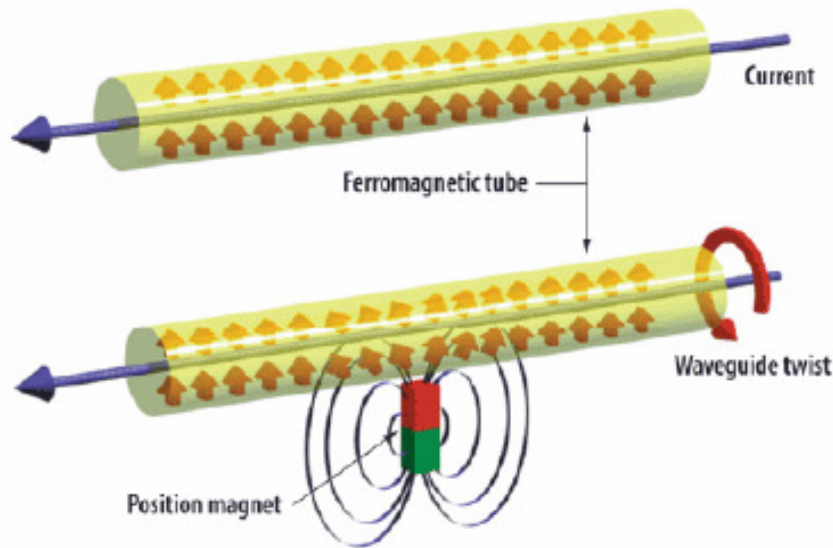
Figure 4.9.: The Wiedemann effect and the inverse Matteuci effect are a result of the interaction between a current carrying ferromagnetic wire, an axial applied magnetic field and the mechanical twisting of the wire.

4.6. Measurement of magnetostriction in solids

In solids λ is doubly anisotropic: it depends on the crystallographic direction of measurement and on the direction along which the magnetization M is oriented by the applied magnetic field H [1, 13]. Therefore the magnetostriction has different values in different crystallographic directions. Those directions and planes of the crystal are defined by the help of the notation of the Miller indices [3, 4, 6, 7, 9, 32].

4.6.1. Magnetostriction in an isotropic cubic single crystal

Inside a crystal atoms and molecules are not randomly distributed but regular arranged. There exist 32 crystal classes which differ in symmetry. The number of independent directions and areas which define the symmetry of the crystal are studied by so called Miller indices.

In an isotropic cubic single crystal [19, 24, 25], it is possible to measure magnetostriction along the from Miller indices 100 and 111 selected directions (figure 4.10). The more complex the structures get the more independent areas of the crystal are necessary to define it. Then the magnetostriction has to be measured along more directions than the from Miller indices 100 and 111 selected areas of a cubic crystal.
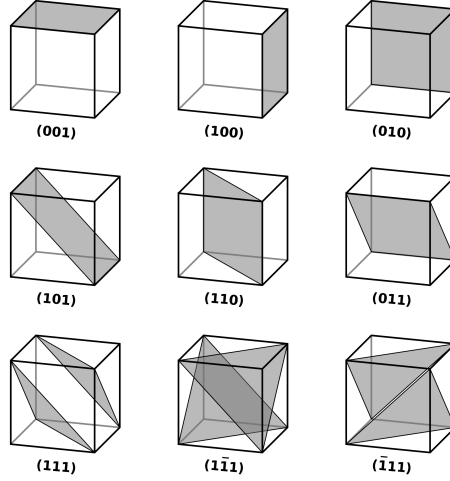
Figure 4.10.: Miller indices are a notation system in crystallography for planes and directions in crystal (Bravais) lattices [15, 19, 32].

4.6.2. Magnetostriction in a polycrystalline material

The situation gets more complex in polycrystalline materials than in single crystals, because the whole piece of material consists of individual grains, which show different magnetoelastic and elastic properties and therefore different values for magnetostriction [5, 15, 18, 33]. This problem cannot be solved by an averaging procedure. If the polycrystalline solid is isotropic, it is assumed that the material is composed of a large number of domains with the strain uniform in all directions. Therefore isotropic crystals imply homogeneity in all directions. Anisotropic materials contrariwise have arbitrary distributed domains and exhibit differences in a material's physical property, like stresses, strains and other magnetoelastic effects, when measured along different axes.

It can be shown that for an isotropic cubic polycrystalline material, in which no preferred grain orientation exists, the following expression for the saturation magnetostriction λ_S can be found [1, 33]:

$$\lambda_S = \frac{1}{5}(2\lambda_{100} + 3\lambda_{111}) \qquad (4.3)$$

For an isotropic amorphous or polycrystalline, but not necessary cubic, body the saturation magnetostriction $\lambda_S(\theta)$ at an angle θ from the field is [1, 33]:

$$\lambda_S(\theta) = \frac{3}{2}\lambda_S(\cos 2\theta - \frac{1}{3}) \tag{4.4}$$

where λ_S is the saturation value in an ideal demagnetized state and it is calculated from the difference between the maximum magnetostriction with field applied parallel to a certain direction $\lambda_{\parallel}$ and field applied perpendicular to the given direction $\lambda_{\perp}$. Substituting $\theta = 0^{\circ}$ and $\theta = 90^{\circ}$ in equation 4.4, a very general relation for magnetostriction is given [1,33]:

$$\lambda_{\parallel} - \lambda_{\perp} = \lambda_S + \frac{1}{2}\lambda_S = \frac{3}{2}\lambda_S \tag{4.5}$$

In a more general anisotropic polycrystalline material, maybe even with stresses and strains, formed by small crystallites more or less randomly distributed the parallel magnetostriction $\lambda_{\parallel}$, measured along H, and the perpendicular magnetostriction $\lambda_{\perp}$, oriented perpendicular to H, are the basic units of measurement. From the measurements of $\lambda_{\perp}$ and $\lambda_{\parallel}$ the magnetic quantities saturation magnetostriction λ_S and volume magnetostriction ω can be determined [1,33]:

$$\lambda_S = \frac{2}{3}(\lambda_{\parallel} - \lambda_{\perp}) \tag{4.6}$$

$$\omega = \Delta V/V = \lambda_{\parallel} + 2\lambda_{\perp} \tag{4.7}$$

Additionally there are some more useful definitions for an isotropic polycrystalline material. From a phenomenological approach it follows that saturation magnetostriction λ_S is in the limiting case equal to the value of $\lambda_{\parallel}$ when the demagnetized state of the sample before the application of the field is isotropic and the corresponding $\lambda_{\perp}$ equals $-\lambda_S/2$. The value $\lambda_{\parallel}/2\lambda_{\perp} \neq 1$ indicates the existence of anisotropy of the demagnetized state [1,33].

4.7. Methods of measurement

There is a huge number of different methods for magnetostriction to be measured. All of them with advantages and disadvantages in handling, operation and interpretation. This table is just a short comparison of the methods without explicit analysis of their strong points and their debilities.

Microscopic methods	Sensitivity	Temperature T	External magnetic field H
X-ray diffraction	10^{-5}	1.5 - $2000K$	0 - $7T$
Neutron diffraction	10^{-5}	0.01 - $600K$	0 - $15T$
Macroscopic methods	Sensitivity	Temperature T	External magnetic field H
Capacitance dilatometry	10^{-9}	0.01 - $1000K$	0 - $50T$
Strain Gauge	10^{-6}	1.5 - $700K$	0 - $50T$
Twin Microscope	10^{-6}	300 - $2000K$	$0T$
Extensometers	10^{-7}	1.5 - $700K$	0 - $30T$
Tunnel Tip Transducer	10^{-9}	$300K$	0 - $3T$
Interferometry	10^{-8}	4 - $2000K$	$0T$

For the knowledge of the magnetostrictive characteristics (interconnection to the external magnetic field H, temperature T and external stress or pressure σ) of a material, in dependence on section 4.2, a combination of some of those methods is necessary to get best results. In this thesis we concentrate on capacitance dilatometers which have an advantage over strain gauges (figure 4.11) in resolution. Furthermore the effect of magnetoresistance doesn´t occur for capacitance dilatometers.
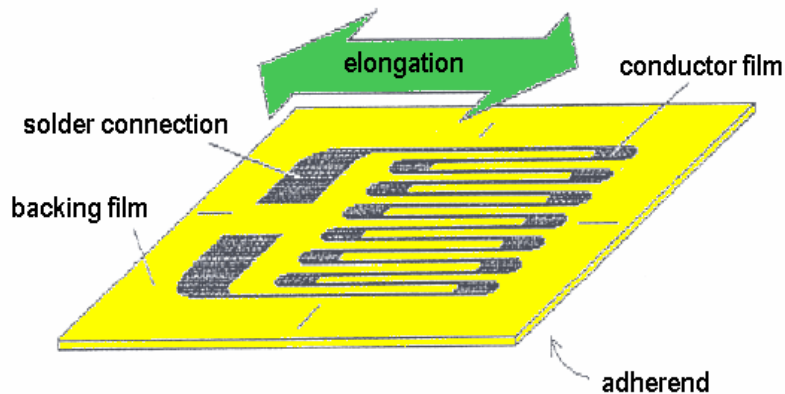
Figure 4.11.: The easy assembling of a cheap and tiny strain gauge.

4.7.1. Capacitance dilatometers

4.7.1.1. Historic development

The capacitive method for small displacements has been widely used for magnetostriction measurements in magnetic fields. One of the first capacitance cells for measuring small length changes was described by White [34]. Its high sensitivity has often been used for magnetostriction measurements of diamagnetic and paramagnetic materials [35–38]. The advantage of this capacitance method was a high resolution of 10^{-10} in strain. But refinements to the early simple dilatometer of White [34] which has the disadvantage, that it had to be specifically constructed for each sample´s length, got needful. New capacitance dilatometers afforded to use different shapes and dimensions of samples or to adjust the gap between the capacitance plates. In [39] two specific capacitive dilatometers, a push rod dilatometer and a tilted plate dilatometer were introduced. Generally they were made in beryllium-copper alloy or in OFHC copper [40].

The push rod dilatometer consists of three essential parts: a sensor, the push rod and the sample. The used kind of sensor doesn´t need to be necessarily a capacitance. For example pressure sensitive sensors, inductive sensors or strain gauges could also be realized for the measurement of magnetostriction in combination with push rod dilatometry. If a capacitive sensor is utilized the most common way is a fixed capacitance plate and the second one moveable. Push rod dilatometers work excellent at high temperature and have a moderate resolution and reproducibility. But it is difficult to adapt them to high magnetic fields.

In tilted plate capacitance sensors the two capacitance plates are not parallel to each other but angle shifted [41]. No sample screws are necessary and therefore they are operated for high magnetic fields. Silver is used as dilatometer material because its heat capacity per volume is 50% smaller than that of copper. Because glues have often an higher expansion than silver they should be avoided.

All these types of cells, have been successfully used in steady or slowly varying magnetic fields, mainly produced by superconductive coils, where the mechanical noise which can affect the capacitance cell, is small and the electrical noise can be inhibited by a high resolution capacitance bridge.

The basic idea for most kind of capacitance dilatometers is attached to the measurement of C [27,33,42]. Using the example of a perfect plate capacitance (figure 4.13), the alternating of the capacitance C can be studied by the equation for the capacitance C

$$C = \epsilon_0 \epsilon \frac{A}{d} \tag{4.8}$$

with the non-dimensional relative permittivity ϵ, the permittivity $\epsilon_0 = 8.8542 \cdot 10^{-12} F/m$ of vacuum, the gap d between the capacitance plates and the area A of the overlapping capacitance plates. During the measurement of magnetostriction the capacitance C alters with the change of the sample length l. Thus the change of the gap d between the plates or the varying area A of them are the reason for the modifying C. Depending
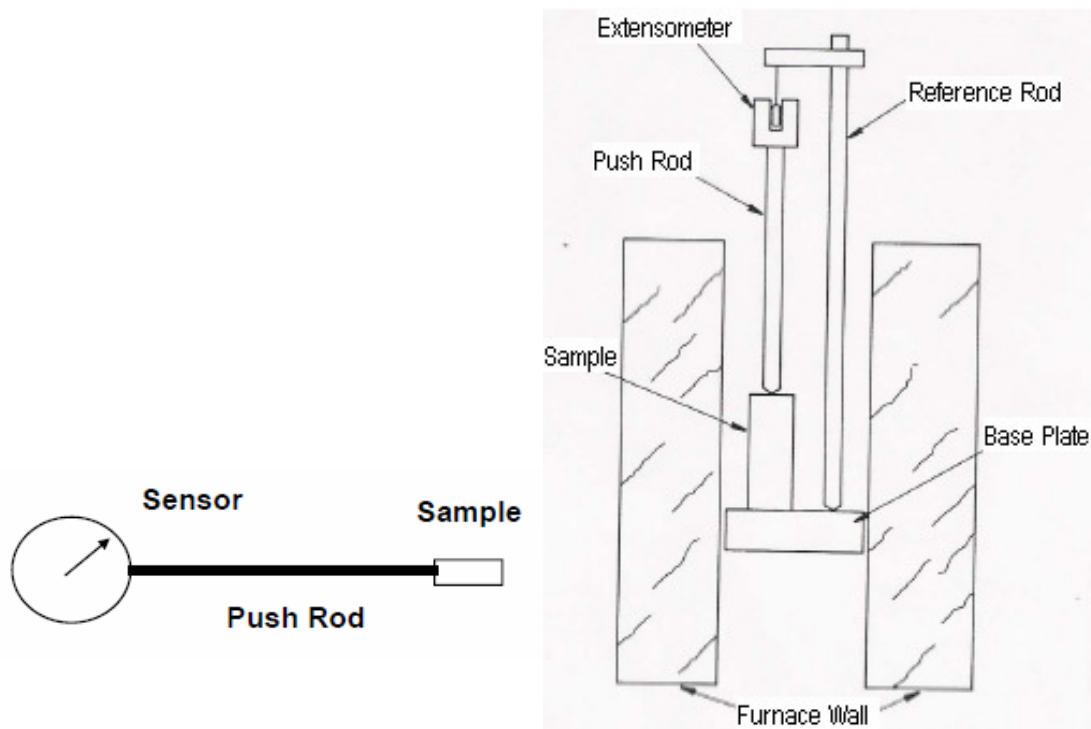
(a) The basic concept of a push rod dilatometer.
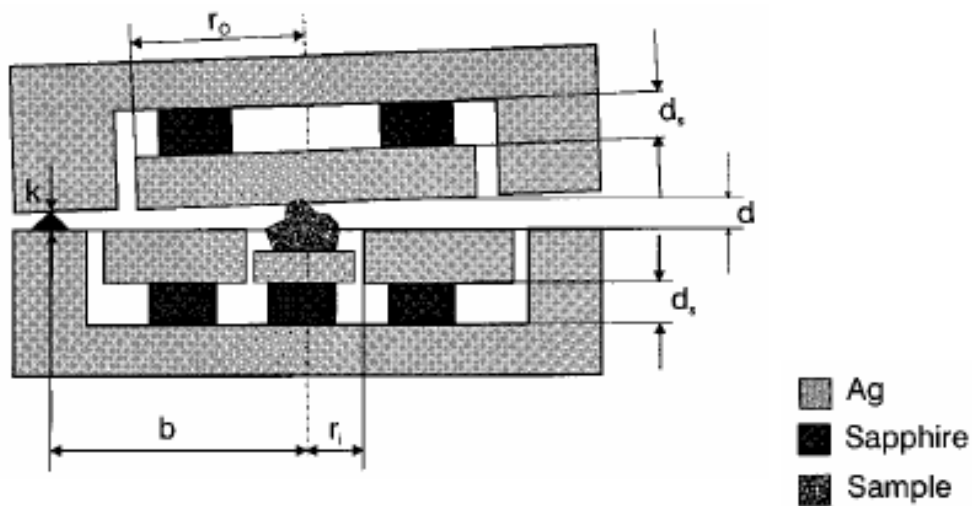
(b) A diagram of a tilted plate capacitance dilatometer [41] with its defining quantities: r_0 ... the outer plate radius, r_i ... the inner plate radius, d ... gap, d_s ... the thickness of the sapphire washers, k ... pivot distance, b ... distance between the center of the capacitor and the pivot;

Figure 4.12.

on the specific adjustment of the dilatometers some additional geometric relations are useful.
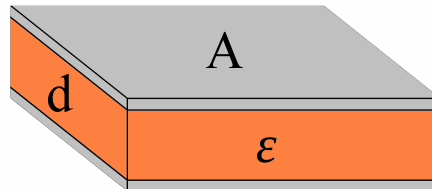
Figure 4.13.: For a plate capacitor its capacitance C is defined by the area A of the plates (grey), the distance d (orange) between these plates and the permittivities ϵ (orange) and ϵ_0.

4.7.1.2. How to apply magnetic fields

Historical magnetostriction was often studied by the help of superconducting coils. But the maximum field of available superconductive magnets is around 15T. Therefore for very high field magnetostriction Bitter or pulsed magnets are used [27, 42]. In table 4.3 several magnet types are registered with their properties, advantages and disadvantages [40].

Magnet type	Maximum magnetic field [T]	Sweeping time to the maximum field	Advantages	Disadvantages	Special precautions
Electromagnet	2	minutes	fast	limited field, temperature drift	few
Small superconductor	5	minutes	fast, quiet	limited field	few
Large superconductor	15	hours	quiet	slow	minimise thermal drift (very difficult)
Bitter electromagnet	20 - 22	minutes	fast	mechanical noise (small cold bore)	independent suspension
Pulsed magnet	40	ms	very fast, any temperature	mechanical noise, electromechanical coupling, inapplicable to samples with high electrical conductivity	independent suspension, shielding of metallic parts of the cell

Table 4.3.: Summary of properties of several magnet types used for magnetostriction measurements [40].

5. Capacitance cell at RT

Based on the ideas of the capacitance dilatometer in [27, 42] a capacitance cell for the measurement of magnetostriction at room temperature (RT) is engineered. Later with the help of this knowledge, construction and magnetostriction results at high temperatures are aspired. The basics for such measurements is the development of a capacitance cell (used materials and layout) and a measurement system which consists of a computer program (software) and a magnet with its activation (e.g. measurement card, capacitance bridge, hall probe etc.).

5.1. Design and development of a capacitance cell for RT

5.1.1. The basic idea of this capacitance cell

Historical magnetostriction was studied by many different capacitance dilatometer (section 4.7.1.1). Nevertheless the plans for such dilatometers should be kept as simple as feasible with the highest possible resolution. As already shortly mentioned in section 4.7.1 the most elementary concept of a capacitance cell is a plate capacitor with the capacitance C

$$C = \epsilon\epsilon_0 \frac{A}{d} \tag{5.1}$$

with the dimensionless relative permittivity ϵ, the permittivity $\epsilon_0 = 8.8542 \cdot 10^{-12} F/m$ of vacuum, the gap d between the capacitance plates and the area A of the overlapping capacitance plates. If the relative permittivity ϵ is assumed for vacuum, $\epsilon = 1$ and formula 5.1 changes to:

$$C = \epsilon_0 \frac{A}{d} \tag{5.2}$$

By studying equation 5.2 it is no problem to comprehend that an increase of the capacitance C requires an enhancement of A or a decrease of the gap d. Due to the fact that d can be adjusted during the later assembling of the cell it is more important for the designing of the cell to concentrate on the area A. Therefore the parallel horizontal plates of the capacitor are changed to angular parallel plates. Then the shape of the plates alters from a circle to an ellipse with the relation $a = b/\cos\alpha$ (figure 5.1).
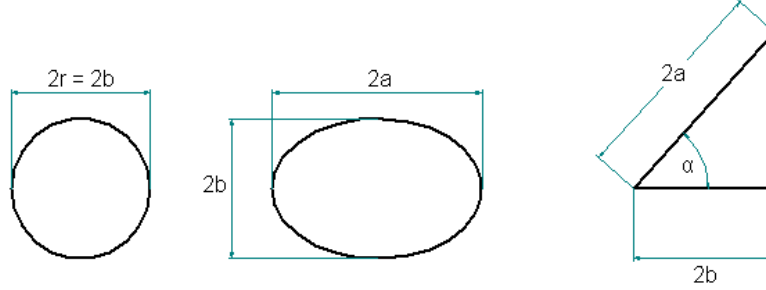
Figure 5.1.: The change from parallel horizontal capacitor plates to angular parallel plates increases the capacitance C.

Comparing equations 5.3 and 5.4 for the area of a circle and an ellipse it is self-explanatory that the area A changes with the factor $1/\cos\alpha$.

$$A_c = r^2\pi = b^2\pi \tag{5.3}$$

$$
\begin{aligned}
A_{ell} &= ab\pi = \\
&= b^2\frac{1}{\cos\alpha}\pi = \\
&= A_c\frac{1}{\cos\alpha} \tag{5.4}
\end{aligned}
$$

A short example demonstrates how the factor $1/\cos\alpha$ similarly alters the capacitance C. $\alpha = 0°$ simulates an horizontal parallel plate capacitor whereas $\alpha = 45°$ and $\alpha = 60°$ mean angled capacitor plates. As dimensions for the radius $r = b$ and d we use $b = 3$mm and $d = 100$µm.

$$
\begin{aligned}
C_{0°} &= 2.5\text{pF} \\
C_{45°} &= 3.5\text{pF} \\
C_{60°} &= 5\text{pF}
\end{aligned}
$$

A more detailed study of an angled parallel plate capacitor exhibits the up to now not embraced fact that two opposite angled capacitor plates feature capacitance deficits

(figure 5.2). The reason for it are not totally comprehensive lying upon another capacitor plates. Figure 5.2 demonstrates the effective used capacitance C_{eff} as the space between the two blue marked areas. In contrast to that homogeneous electrical field the red denoted areas offer ineffective an inhomogeneous boundary effects.
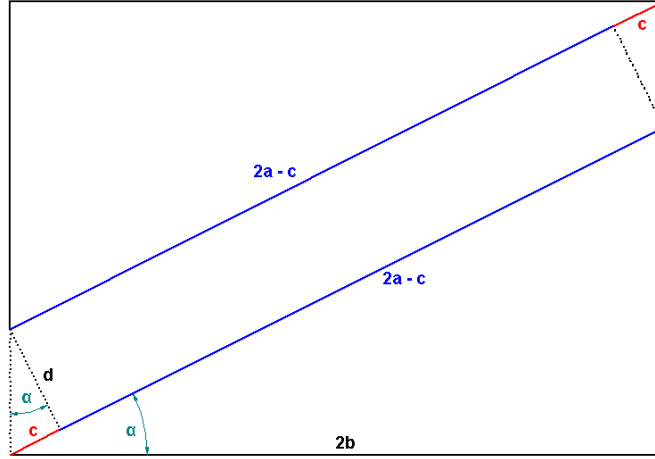
Figure 5.2.: Between the blue marked comprehensive parts of the capacitor plates a homogeneous electrical field persists. On the other hand the red marked areas show marginal problems and boundary effects. Therefore the blue area is called effective capacitance area whereas the red one is ineffective.

In consideration of this capacitance loss the simple equation 5.4 for angled capacitor plates gets more sophisticated. By means of sectionA.1 the equation for the effective capacitance area A_{eff} is obtained (figure A.1).

$$
\begin{aligned}
A_{eff} \;=\; & ab\left[2\arcsin\left(\frac{2a-c}{2a}\right) + \sin\left(2\arcsin\left(\frac{2a-c}{2a}\right)\right)\right] \\
& -ab\left[2\arcsin\left(\frac{c}{2a}\right) + \sin\left(2\arcsin\left(\frac{c}{2a}\right)\right)\right]
\end{aligned}
\tag{5.5}
$$

With the relations $a = b/\cos\alpha$ and $c = d \cdot \tan\alpha$ (figure 5.2) and the dimensions for $b = 3\text{mm}$ and $d = 100\mu\text{m}$ the capacitance results for $\alpha = 0°$, $\alpha = 45°$ and $\alpha = 60°$ are:

$$
C_{0°_{eff}} = 2.5\text{pF} = C_{0°}
$$
$$
C_{45°_{eff}} = 3.482\text{pF}
$$
$$
C_{60°_{eff}} = 4.905\text{pF}
$$

These results ensure that angled capacitance plates are even though the ineffective losses still reasonable. Another positive side effect of these angled capacitor plates in comparison to horizontal ones is a reduction of eddy-currents.

5.1.2. Dimensions and material of the cell

For the body parts of the capacitance cell a polymer plastic called PEEK (Polyether Ether Ketone) lends itself to be a distinguished choice. PEEK offers a good machinability and concerning magnetostriction an evanescent answer to an applied magnetic field. Practically this is equal to the declaration that its magnetostriction is $\lambda_S = 0$ ppm. Its melting point is about 350°C. Furthermore this capacitance cell for room temperature is abbreviatory also called PEEK cell regarding to the used material.

5.1.3. Dimensions and first design of the capacitance cell

The design of the capacitance cell consists of seven parts (figure 5.3). From top to bottom these seven parts are called:
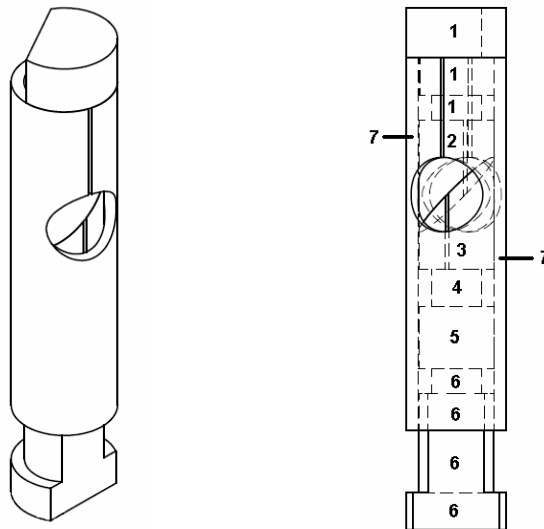
Figure 5.3.: The figure on the left demonstrates the assembled PEEK cell. The first design of the PEEK cell is made up of seven single parts as exhibited on the right hand picture. Their notations are: 1) the upper PEEK cell plunger, 2) the upper capacitance plunger, 3) the lower capacitance plunger, 4) the sample, 5) the sample plunger, 6) the lower PEEK cell plunger, 7) the PEEK body around them

1. the upper PEEK cell plunger

2. the upper capacitance plunger

3. the lower capacitance plunger

4. the sample

5. the sample plunger

6. the lower PEEK cell plunger

7. the PEEK body around them

These parts are conglutinated with the aid of "Loctite super glue gel" without need of any screws in the following way: The bottom of the sample (4) gets glued on the sample plunger (5). After a few minutes the lower capactiance plunger (3) is sticked on the top of the sample. The side surfaces of the sample has to be retained clean without any glue. As next step of the connection the three already assembled parts (3, 4 and 5) are attached into the PEEK body (7). Before another part is bonded all pieces of the PEEK cell are put together as shown in the left hand picture of figure 5.3. Furthermore the upper (1) and lower (6) PEEK cell plungers are removed again. Carefully a small drop of glue is placed on the bottom of the sample plunger (5) to connect it with the lower PEEK cell plunger (6) and the PEEK body around (7). The same procedure occurs between the upper capacitance plunger (2), the upper PEEK cell plunger (1) and the PEEK body (7). Because of this approach the upper capacitance plunger (2) is fixed whereas the lower capacitance plunger (3) stays without bonding to the PEEK body (7) and therefore moveable. If the sample below the lower capacitance plunger (3) expands the gap d between the capacitance plates alters and change the capacitance C. For a closer and more realistic description of the assembling of the PEEK cell view section 6.4.

The capacitance plates can be designed in two possible ways. Either the capacitance surfaces of the upper (2) and lower (3) capacitance plunger are coated with a thin layer (for example 10nm chrome and on it 200nm gold) or thin plates (100µm) made of copper are bonded with glue on the PEEK surface of the capacitance plungers (2 and 3). The disadvantage of the film of gold as capacitor plates is its insufficient mechanical strength. During the preparation process of the cell partial areas of the evaporated gold disappeared. Thus the variant of thin plates (100µm copper) as plate capacitors was further used.

The dimensions of the capacitance cell are kept as small as possible to allow its assembly into the limited space in magnets. Thus the radius of the capacitance plungers is 3mm and the radius of the PEEK body around is 4mm. For more detailed information about the dimensions of the different pieces of the PEEK cell, a look to the detailed construction plans in the appendix section A.2 is recommended.

5.2. Equipment for the measurement of magnetostriction at RT

As briefly mentioned in section 4.7.1, the assembly for the measurement of magnetostriction is composed of more components than just the PEEK cell. The entire needed installation consists of six main components:

1. An electro magnet which is essential for the generation of the applied magnetic field to a sample.

2. A hall probe to have acquirement about the magnitude of the applied magnetic field.

3. A capacitance cell which responds sensitively to the applied magnetic field and the associated magnetostriction.

4. The "AH 2500A" capacitance bridge with high resolution for the gauging of the capacitance changes ΔC (for more details about the conversion of Δl to ΔC see subsection 5.3.2) of the capacitance cell according to the length changes of the sample caused by magnetostriction. For the wiring between the "AH 2500A" and the capacitance cell a coaxial cable of the type "LakeShore SC" is used. It is extremely important to pay attention that the inner conductor of the coax has to be sheltered as far as possible. For good results the unshielded part of the inner conductor that is bonded to the capacitance plates has to be smaller than 10mm. Otherwise the noise gets determinative.

5. Computer software (section 7.3) to pilot the attachments and which later helps to evaluate the data.

6. The "NI 6211" measuring card for the communication and messaging between the computer and the instruments (electro magnet and hall probe).

In figure 5.4 these six essential devices with its accordant wiring for magnetostriction measurement are yellow deposited. As an assistance the blue coloured parts of figure 5.4 are used:

- A constant current source with 10.15mA is essential for the operation of the hall probe (2). Its supply voltage is +9V dc.

- The dual low power operational amplifier ("LM258N") is indispensable because the output current of the "NI 6211" measuring card is ± 2mA. Thus the power for the controlling of the electro magnet would be to low and the "LM258N" is needed. Its supply voltage is +15V dc.

5.3. The computer software

For the regulation and communication between advanced equipments computer software is essential. Comparably analysis of measurements is supported by programs. The software package "Labview" of "National Instruments" is one possible way to interact with measurement equipments.
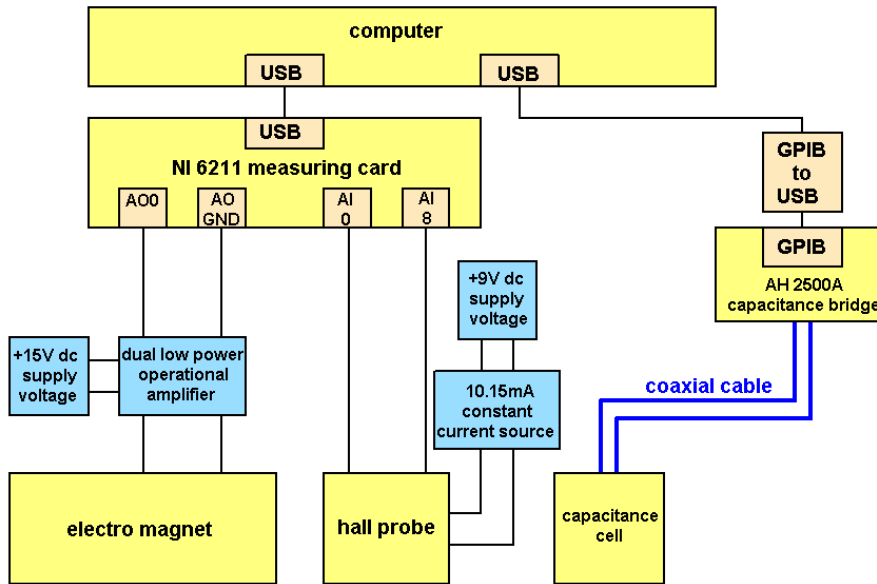
Figure 5.4.: An overview of the equipment needed for the measurement of magnetostriction at room temperature demonstrates coexistently the schematic circuit of them. The main components are yellow deposited whereas the ones with a blue background are just of supporting use for them.

For the measurement of magnetostriction a "Labview" program was written to control the used hardware (electro magnet, hall probe, measurement card etc.) and afford the automatic interpretation of data. After starting the "Labview" program it is possible to press four buttons. In figure 5.5 these four buttons on the left hand side of the program are indicated illustratively with red numbers 1 to 4. The corresponding parts of the program which are activated after one of the four buttons was pressed, are also counted by these numbers. A short explanation of the operations which hide behind the four buttons exhibits how simple this measuring software is to use.
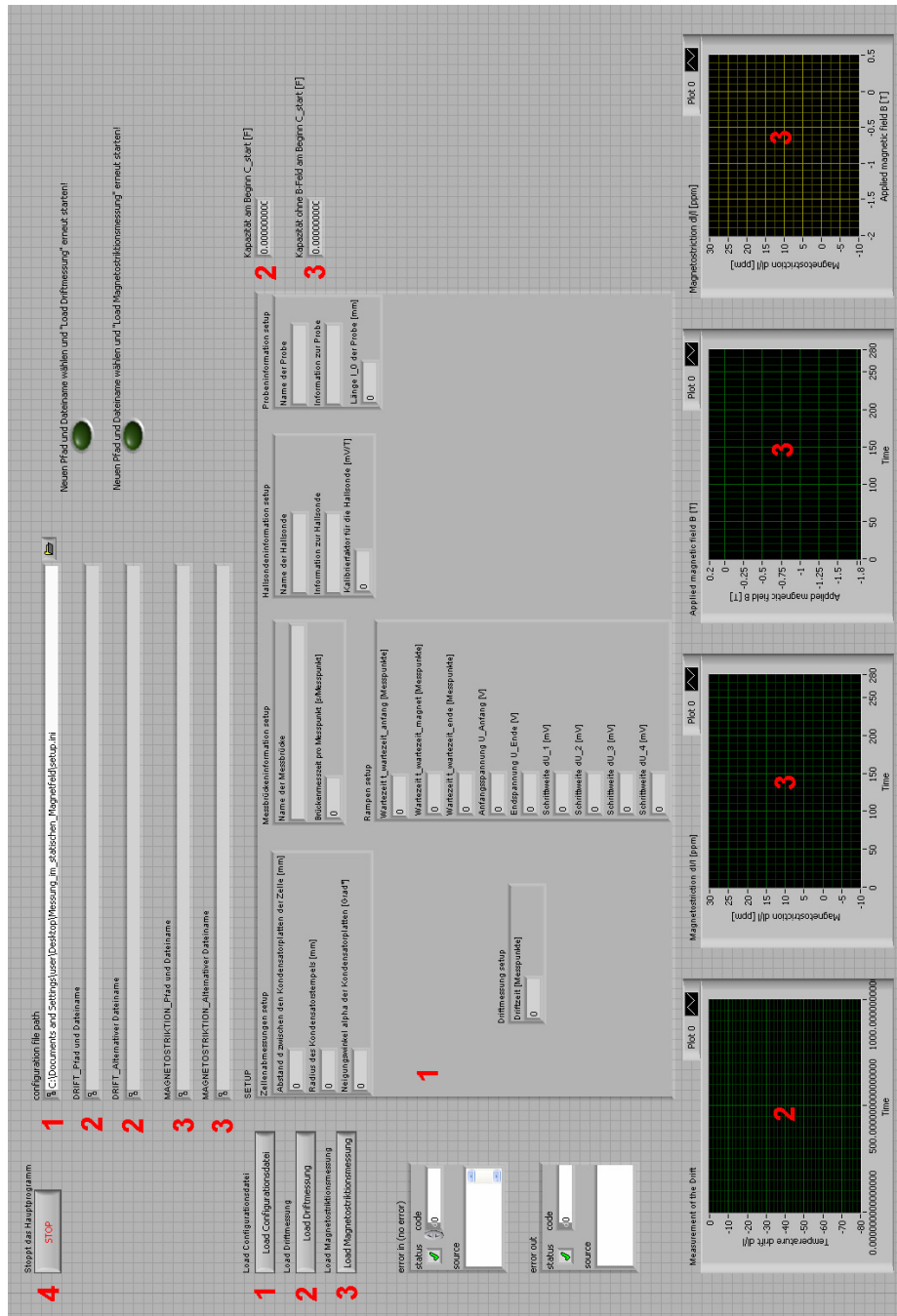
Figure 5.5.: The front panel of the "Labview" program which is used to regulate and analyze the measurement of magnetostriction. The red numbers 1 to 3 symbolize the three facilities of the program. By pressing the adequate (red numbered) button the (to this number in the picture) corresponding operations are accomplished.

5.3.1. The application of the "Labview" program

1) Load configuration file path

By pressing the "Load Configurationsdatei" button (figure 5.5) the user can change the parameters of the setup. If the "setup.ini" file path has been entered in the "configuration file path" bar the old settings are loaded and viewed in "SETUP" display window. Otherwise the setting parameters of table 5.1 have to be entered.

2) Load drift measurement

If the "Load Driftmessung" button (figure 5.5) is pressed a window pops up for entering a path and file name where the data of the measurement are saved. In case that the entered file name already exists, an alternative file name is generated to ensure that old data are not lost. If this alternative file name similarly can be found yet in the path, the drift measurement does not start and the "Load Driftmessung" button has to be pushed again for starting the gauging. Otherwise after the file name was agreed the program starts measuring.

For the drift measurement no applied magnetic field is used. In section 4.2 the magnetoelastic interactions and the external influence of a magnetic field H, external stress or pressure σ and temperature T to the expansion of the sample were mentioned. During the drift measurement the thermal behaviour of the sample is studied. With the aid of the parameter "measuring time for the drift" (table 5.1) the required time for the observance of the drift is adjusted. The unit of this "measuring time for the drift" is given in "data points" and the realistic needed time in seconds for the measurement depends on the used capacitance bridge (see parameter "estimated measuring time of the bridge for each data point" in table 5.1). For instance the "AH 2500A" bridge needs about 1s to get a data point. Thus, if the "measuring time for the drift" is set to 300 data points, the drift measurement lasts 300s.

Every capacitance C which the capacitance bridge obtains is saved. After the measurement the first preserved capacitance C_0 (the indicator value is marked in figure 5.5 with a red 2) is used as point of origin. To get the changes in capacitance ΔC the "Labview" program automatically calculates the difference between the later capacitance C_i and C_0 to get $\Delta C_i = C_i - C_0$. The transformation from $\frac{\Delta C}{C}$ to $\frac{\Delta l}{l}$ (for more details see section 5.3.2) in order to get the thermal expansion of the sample is saved combined with the raw data in the before declared file.

For the first analysis of the data the graph in the "Labview" program, marked with a red 2 (figure 5.5) plots the course of the drift after finishing the program. Now the program is ready for another measurement and the buttons 1 to 4 can be pressed again.

setup mode	possible settings	unit
"Zellenabmessungen setup"	gap between the capacitor plates d	mm
	radius b of the capacitor plates	mm
	angle α of the capacitor plates	°
"Messbrückeninformation setup"	name of the capacitance bridge	
	estimated measuring time of the bridge for each data point	s / data point
"Hallsondeninformation setup"	notation of the used hall probe	
	information about the hall probe	
	calibration coefficient for the hall probe	mV / T
"Probeninformation setup"	denomination of the sample	
	information about the sample	
	length l of the sample	mm
"Driftmessung setup"	measuring time for the drift	data points
"Rampen setup"	initial holding time t_i	data points
	holding time at the highest voltage value t_{magnet}	data points
	final holding time t_f	data points
	initial voltage U_i	V
	final voltage U_f	V
	increment dU_1	mV
	increment dU_2	mV
	increment dU_3	mV
	increment dU_4	mV

Table 5.1.: The setup settings of the "Labview" program for the measurement of magnetostriction in the electro magnet can be entered or changed after the "Load Configurationsdatei" button was pressed.

3) Load magnetostriction measurement

After the "Load Magnetostriktionsmessung" button (figure 5.5) is pressed a separate window appears like for the drift measurement (2). The path and file name where the data are saved has to be entered to start measuring. If the file name already exists an alternative file name is created instead of overwriting the preexisting data. In case that the alternative file name just as well resides in the declared folder the magnetostriction measurement does not start and the "Load Magnetostriktionsmessung" has to be pressed again. On the other hand magnetostriction gauging starts after accepting the file name.
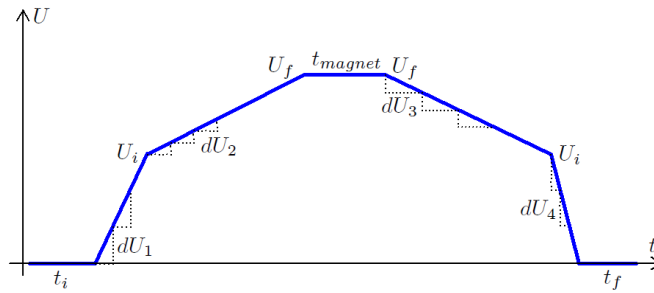
Figure 5.6.: The voltage ramp for the magnetostriction measurement is defined by the parameters of table 5.1.

On the contrary to drift measurements (2) for gauging magnetostriction an applied magnetic field H is essential for the length elongation. Even though the influence of variation in temperature T is not negligible and can manipulate the results. Therefore the variability of temperature T and the corresponding drift should stay minimal.

For applying a magnetic field H to a sample, that was inserted into the capacitance cell, the electro magnet is activated via a voltage ramp (figure 5.6). Therefore the "NI 6211" measurement card actuates the power supply of the electro magnet with voltages between $0 - 10$V. Then the power supply of the electro magnet converts this voltage to an accordant current between $0 - 200$A which further is responsible for the magnetic field between the pole shoes of the electro magnet. The parameters for the voltage ramp of table 5.1 cause its shape. The maximal allowed voltage for the ramp is 10V, caused by the limit of the "NI 6211" measuring card.

The "to prevenient time" for the measurement is compounded by the three holding times t_i, t_{magnet} and t_f and how often the four increments dU_1, dU_2, dU_3 and dU_4 are used to reach the initial U_i or final voltage U_f. For example dividing $U_f - U_1$ by dU_2 tells how many data points are produced by dU_2 to reach U_f from U_i. Multiplying

this result with the "estimated measuring time of the bridge for each data point" of the measuring bridge setup (table 5.1) the operation time for this part of the voltage ramp is calculated. The initial t_i and final holding time t_f of the voltage ramp (figure 5.6) allow furthermore a manually correction of the drift after the magnetostriction measurement has been finished.

The computer sends the accordant present signal of the voltage ramp over the "NI 6211" measuring card to the electro magnet (see also figure 5.4). The voltage ramp controls the power supply of the electro magnet which generates a magnetic field. Further the applied magnetic field is measured with the hall probe and affects the magnetostriction of the sample. The raw data of the hall probe are read by the "NI 6211" measuring card and saved as well as the capacitance signal by the "AH 2500A" capacitance bridge (see also figure 5.4). Then the next step of the voltage ramp supplies the electro magnet and the new data of the hall probe and the "AH 2500A" capacitance bridge are received. Finally when the voltage ramp has finished and all raw data are connected the program translates them. With the aid of the calibration factor of the hall probe its raw data are converted from voltage V values to tesla T ones. Similarly the conversion from $\frac{\Delta C}{C}$ to $\frac{\Delta l}{l}$ of the "AH 2500A" results is performed as calculated in section 5.3.2. Therefore the first preserved capacitance C_0 (the indicator of it is marked in figure 5.5 with a red 3) is used as point of origin in order to get $\Delta C_i = C_i - C_0$. Raw data are saved as well as the translated data in the file specified before.

After the raw data were translated the three graphs in the "Labview" program, marked with a red 3 (figure 5.5) plot the converted results for the first analysis. Afterwards the program is ready for other measurements and one of the buttons 1 to 4 can be pressed again.

4) STOP

As the name implies pressing the "STOP" button (figure 5.5) quits the complete "Labview" program.

5.3.2. Conversion from $\frac{\Delta C}{C}$ to $\frac{\Delta l}{l}$

The "AH 2500A" measurement bridge determines the changes of the capacitance C of the capacitance cell. For a better analysis of the magnetoelastic elongations these capacitances ΔC are converted to length changes Δl of the sample.

First the changes of capacitance ΔC and of the gap Δd have to be defined similar. The indices 0 symbolize the first unmodified values whereas the indices i characterize the altered ones:

$$\Delta C = C_i - C_0 \tag{5.6}$$
$$\Delta d = d_i - d_0 \tag{5.7}$$

Based on the formula for the capacitance C of a plate capacitor in vacuum (equation 5.2) with the dimensionless relative permittivity $\epsilon = 1$, the permittivity $\epsilon_0 = 8.8542 \cdot 10^{-12} F/m$ of vacuum, the gap d between the capacitance plates and the area A of the overlapping capacitance plates:

$$C = \epsilon_0 \frac{A}{d} \tag{5.8}$$

the relation between ΔC and Δd is transformed:

$$
\begin{aligned}
\Delta d &= d_i - d_0 = \\
&= \epsilon_0 A \left(\frac{1}{C_i} - \frac{1}{C_0} \right) = \\
&= \epsilon_0 A \left(\frac{C_0 - C_i}{C_0 C_i} \right) = \\
&= \epsilon_0 A \left(\frac{-\Delta C}{C_0 C_i} \right) = \\
&= \epsilon_0 \frac{A}{C_0} \left(-\frac{\Delta C}{C_i} \right) = \\
&= d_0 \left(-\frac{\Delta C}{C_i} \right)
\end{aligned}
$$

Equation 5.9 reflects the ratio between Δd and ΔC. Especial attention has to be paid to the different indices of d and C. Contrary to the index 0 which distinguishes an unvaried value, the index i emblematizes a modified one.

$$\frac{\Delta d}{d_0} = -\frac{\Delta C}{C_i} \tag{5.9}$$

By means of geometrical considerations exhibited in figure 5.7 the relation between Δd and Δl is derived. If the sample l expands the gap d contracts. The minus in the equation 5.10 is a result of that fact.

$$\Delta l = -\frac{\Delta d}{\cos \alpha} \tag{5.10}$$

Combining equations 5.9 and 5.10 leads to the direct values of the sample elongations Δl. The relation $\frac{\Delta l}{l}$ expresses the thermal expansion for the drift measurement or the magnetostriction for the magnetostriction gauging. Multiplying $\frac{\Delta l}{l}$ with the factor 10^6 ensures to get the result in ppm.

$$\Delta l = \frac{\Delta C}{C_i} \frac{d_0}{\cos \alpha} \tag{5.11}$$
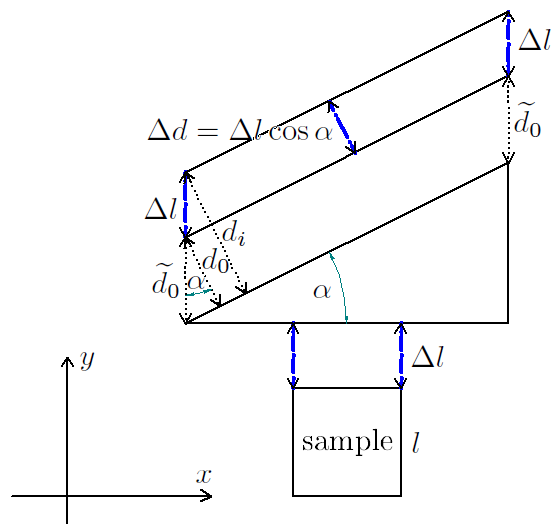
Figure 5.7.: The relation between Δl and Δd is geometrically derivated.

6. Magnetostriction measurements at RT

After introducing the basics of our capacitance cell measurements prove if the system works as wanted. Therefore the results of the PEEK cell at room temperature are compared to literature. Based on these researches magnetostriction is then developed for high temperatures in chapters 7 and 8.

6.1. The temperature drift

The thermal influence to a capacitance dilatometer as mentioned in section 4.2 is not negligible. Therefore the action of temperature in our system is studied and the PEEK cell is cooled down from room temperature to $\sim 0°$C in ice water. Thereby a plastic bag surrounds the capacitance cell in order to protect it from water. The "drift program" described in 5.3.1 controls the gauging.

   The drift effect is exhibited in figure 6.1 and demonstrates a high dependence of the capacitance C on the temperature t. In the refrigeration phase of the first 500 seconds the capacitance decreases linear as a first approximation. After acclimating in the ice water the temperature varies less and the drift is dispositively smaller. The slowly reheating of the ice water goes hand in hand with a slight, nearly linear increase of the capacitance C in figure 6.1.

   As a conclusion of this measurement we learn how sensitive the PEEK cell reacts on temperature gradiants. As long as the temperature gradiant does not change, the drift seems to be linear as a first approximation. Thus, in order to get the "true" magnetostriction curves this (nearly) linear drift effect can be removed with the aid of a linear fit (figures 6.2a and 6.2b).

6.2. First measurement of magnetostriction

For the calibration of the system well known and documented values for magnetostriction λ of literature are necessary. Polycrystalline nickel (subsection 4.6.2) is best qualified for first measurements and the comparison to former experimental studies (table 4.1). The dimension of the used nickel sample with 2.93mm is secondary for the relative magnetostriction measurement $\lambda = \frac{\Delta l}{l}$, but important for a later comparison in section 6.5.2.
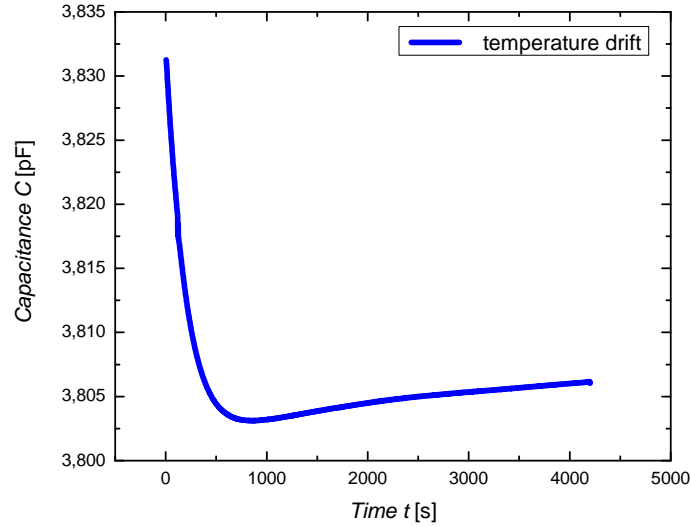
Figure 6.1.: The PEEK cell is put into ice water and cooled down. In the first 500
seconds the capacitance dilatometer chills from room temperature to $\sim 0°$C
of the ice water. After the PEEK cell has acclimated in the ice water the
temperature drift is significant smaller. The increasing of the temperature
drift after 500 seconds is a fault of the slowly warm up of the ice water. As
a first approximation the temperature drift seems to be linear as long as the
temperature gradation does not change.

If a longitudinal magnetic field (LF) is applied on the nickel sample $\lambda_\parallel$ is measured.
Otherwise for a transversal magnetic field (TF), $\lambda_\perp$ is detected. The values of $\lambda_\parallel$ and
$\lambda_\perp$ in literature are $\lambda_\parallel \approx -36$ppm and $\lambda_\perp \approx 18$ppm at room temperature.

Every measurement of magnetostriction is superposed with a thermal drift (section
6.1) of the capacitance C, which is subducted for pure magnetostriction curves by a
linear line described by a fit $y = kx + d$ as a first approximation. There are two possible
ways to plot magnetostriction graphes. Either it can be drafted over the time t axis
(figures 6.2a and 6.2b) or over the applied magnetic field B (figure 6.3). The second one
is more common but with the aid of the first one the superposed drift influence is better
illustrated (figures 6.2a and 6.2b). It seems plausible that the longer the magnetostriction
gauging lasts the larger the additional drift effect gets.

The "Labview" program, described in section 5.3.1 measures the first 5 (t_i of table 5.1)
and the last 9 data points (t_f in table 5.1), which are marked red in figures 6.2a and
6.2b, without applying a magnetic field on the sample. Due to removing the linear drift
effect through these points a linear fit is placed. After this drift correction the "true"
magnetostriction values remain.

After the magnetostriction of nickel was drift-corrected (figure 6.2b) it is plotted over
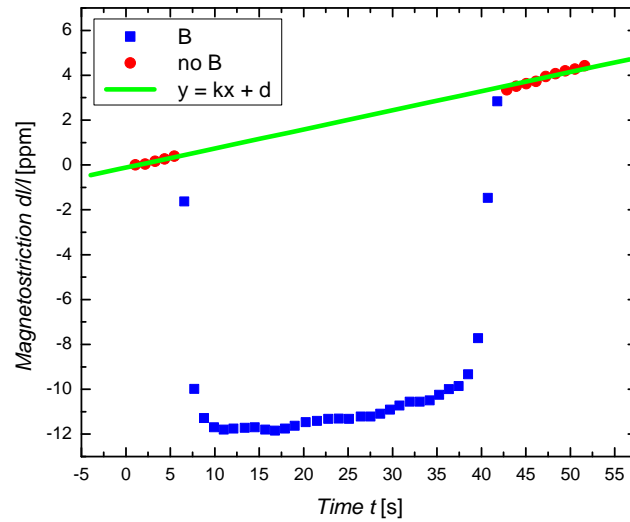
(a) A magnetostriction over time graph is overlayed with temperature drift. By subtracting this thermal drift with a linear fit straight line $y = kx + d$, a driftless curve 6.2b is achieved. For the creation of this best-fit line the "Labview" program (section 5.3.1) measures the first 5 (t_i of table 5.1) and the last 9 data points (t_f in table 5.1), which are marked red, without applying a magnetic field on the sample.
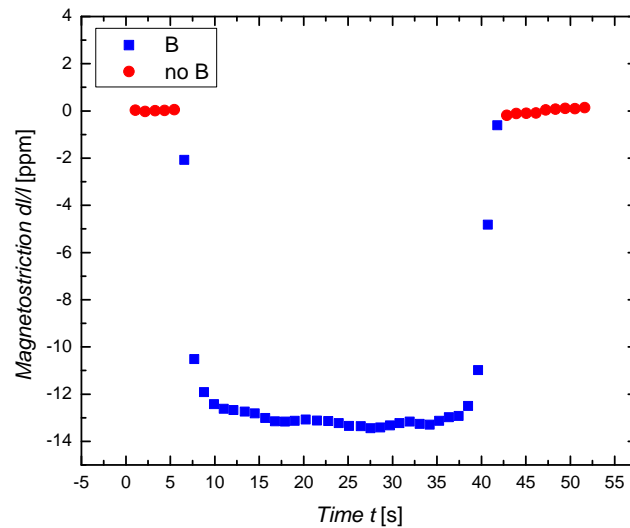
(b) The "true" magnetostriction curve after subducting the linear thermal drift by $y = kx + d$.

Figure 6.2.
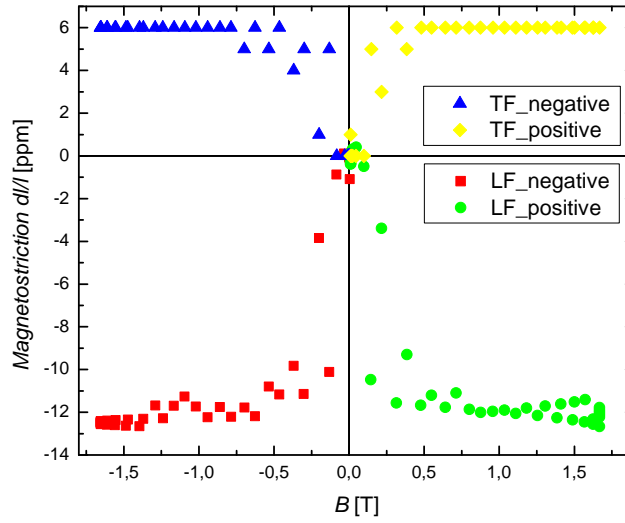
Figure 6.3.: The magnetostriction dl/l over applied magnetic field B graph of a poly-crystalline nickel sample do not agree with the well documented λ values of literature. By applying a longitudinal magnetic field (LF) on the sample we get $\lambda_{\parallel}$. Otherwise, if the magnetic field is transversal (TF) to the sample, $\lambda_{\perp}$ is detected.

the applied magnetic field B in figure 6.3. Comparing its results to literature exhibits too low values for $\lambda_{\parallel}$ and $\lambda_{\perp}$. After proving that the nickel sample has no texture (anisotropically ordered) by the measurement of the two other cube sides and receiving the same too small results for $\lambda_{\parallel}$ and $\lambda_{\perp}$, improving our system is unavoidable (section 6.3).

6.3. Improvements

Till the start of the magnetostriction measurements the system was improved. For example the coax links the capacitance bridge "AH 2500A" with the PEEK cell. The reproducibility of the magnetostriction curves disappears if the unshielded inner conductor of the coax, which is bonded to the capacitance plate, is longer than 10mm. But the result of figure 6.3 demonstrates that some additional advancements have to be accomplished.

6.3.1. Improvement of the PEEK cell

Further studies indicated the main problem for wrong results. The lower capacitance plate plunger (subsection 5.1.3) which is coated with a thin layer (for example 10nm

chrome and on it 200nm gold) or thin plates (100µm) made of copper are bonded with glue on its PEEK surface has to move according to the magnetoelastic expansion of the sample. It seems that there is a mechanical resistance between this plunger and the PEEK body around which prevents the change of capacitance ΔC.

Figure 6.4.: In the redesigned capacitance PEEK cell the (red marked) capacitor plates are horizontal and parallel to each other. The lower one is placed directly on the (blue coloured) sample. Contrary to the upper capacitor plate it has to stay movable to detect the changes of the capacitance C according to the magnetoelastic expansion or contraction of the sample.

Therefore the PEEK cell was redesigned (figures 6.4 and 6.7 and section A.3 with its construction plans). The dimensions of the plungers are altered and new thicker capacitance plates with an altitude of $\approx$ 1mm and a diameter of 5.7mm were made of copper. One plate is glued on the upper capacitance plunger as up to now, but the second one gets stuck directly on the top of the sample. For an easier handling the plates are not angled but horizontal from now on. One has to pay attention that the glue just coats the top surface of the sample which is bonded to the capacitor plate (see reason in subsection 6.5.2). The side faces of the cube have to stay clean and glueless. The thicker capacitance plates ensure that do not start to oscillate when a magnetic field is applied. A thin copper wire is soldered or welded on the capacitance plate before the plate gets adhered on the sample. Otherwise it is possible that the glue evaporates between the sample and the capacitance plate when the copper wire is soldered. Before the PEEK cell is assembled into the magnet the copper wire is connected to the inner conductor of the coax (for more details see figure 6.7).

6.3.2. Dependence of the gap d and introduction of a pretended gap $d_{pretended}$

The formula for the capacitance C of a plate capacitor $C = \epsilon_0 \frac{A}{d}$ in vacuum depends on the the area A and the gap d. The "Labview" program for magnetostriction of section 5.3.1 automatically converts the raw data C of magnetostriction of the sample to λ after the measurement. Thus the user has to enter the gap d, the radius b and the angle α of the capacitance plates into the configuration setup of the "Labview" program (section 5.3.1 and table 5.1). With the aid of b and α the effective area A_{eff} is evaluated.

But it is possible, that the calculated capacitance $C_{calculation}$ using the two values for d and A_{eff} do not correspond with the capacitance $C_{measurement}$ of the "AH 2500A". The reasons are:

- The gap d of the PEEK cell is adjusted with a 100µm thin PTFE (polytetrafluoroethylene) foil (more details in section 6.4). This PTFE foil can easily be crushed and as a result the gap d would change to another value.

- The capacitance plates do not overlap comprehensively and features boundary value problem.

- The capacitance plates are not perfectly parallel.

- The capacitance plates exhibit small irregularities in thickness.

Figures 6.5a and 6.5b demonstrate the influence of $\lambda_\perp$ and $\lambda_\parallel$ of the gap d. Thus a wrong gap d manipulates the results. Because of the reason that it is hardly possible to know the correct gap d and the precise area A_{eff} a pretended gap $d_{pretended}$ is introduced in the "Labview" magnetostriction measurement program (section 5.3.1). The program saves the first capacitance $C_{measurement}$ and calculates $d_{pretended}$:

$$d_{pretended} = \epsilon_0 \frac{A_{eff}}{C_{measurement}} \tag{6.1}$$

This pretended gap $d_{pretended}$ is then used in the program to convert the raw data of the "AH 2500A" measurement bridge to λ.

6.3.3. Angle dependent measurement of magnetostriction

In a polycrystalline, maybe anisotropic sample with randomly distributed crstallites, magnetostriction is measured along B and perpendicular to B. The associated units are $\lambda_\parallel$ and $\lambda_\perp$. As an example for polycrystalline nickel in figure 6.6 the values for $\lambda_{\parallel nickel}$ and $\lambda_{\perp nickel}$ are shown. If the angle between the applied magnetic field B and the sample alters, the value vor the magnetostriction λ varies. As a consequence the capacitance cell has to be attached exactly in the desired direction to the applied magnetic field B.
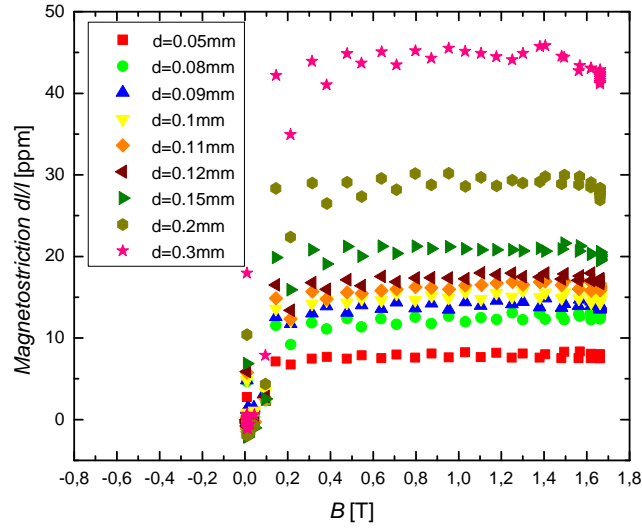
(a) The perpendicular magnetostriction $\lambda_\perp$ depends on the gap d (equations 5.9 and 5.10).
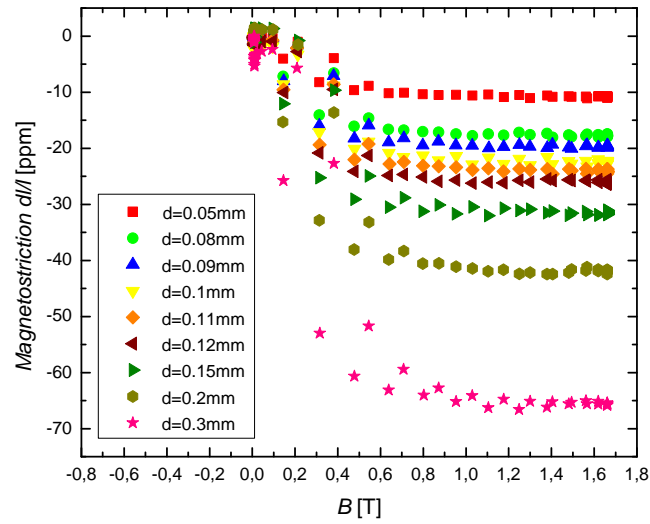
(b) As $\lambda_\perp$ the parallel magnetostriction $\lambda_\parallel$ similarly is affected by the gap d (equations 5.9 and 5.10).

Figure 6.5.

48
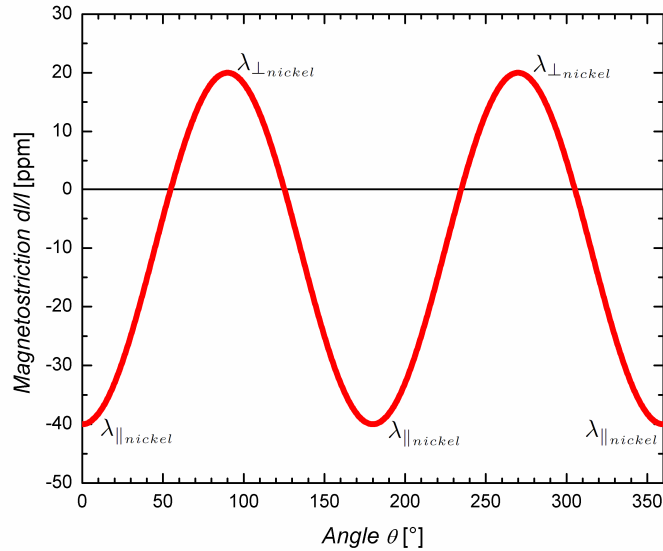
Figure 6.6.: Magnetostriction λ varies according to the angle between a cubic sample and the applied magnetic field B.

6.4. Preparation of the improved PEEK cell

A basic procedure of the measurements is the assembly of the capacitance PEEK cell. The results for the capacitance changes ΔC which go hand in hand with the magnetostriction λ would be incorrect, if the cell were not carefully assembled. The complete construction set of the PEEK cell is displayed in 6.7a and 6.7b. A thin copper wire is soldered on the capacitor plates which are similarly made of copper. Later these copper wires are bonded with the inner conductors of the coax that measures the changes of capacitance ΔC via the "AH 2500A" capacitance bridge.

As a first step the sample gets stuck on the "sample plunger" with the aid of "Loctite super glue gel" (figure 6.7c). After a few minutes of waiting to ensure that the glue has hardened the lower capacitance plate is fixed on the top surface of the cubic sample. The plate is placed in a central position of the PEEK cell to protect the mobility (figure 6.7d). On the side faces of the cubic sample no glue should be coated. This would put stress on the sample and prevent its magnetoelastic deformation.

Then the adhered construction is put into the PEEK body as demonstrated in picture 6.7d. Carefully the upper capacitance plate is positioned above the lower one. For adjusting the gap d between them a 100µm PTFE foil is used. The "upper capacitance plunger" is glued on the upper copper capacitor plate. Contrary to the lower capacitance plate the upper one is bonded with the PEEK body around.

Finally "Loctite super glue gel" is put on the upper and on the the lower PEEK

(a)   (b)   (c)

(d)   (e)   (f)

(g)
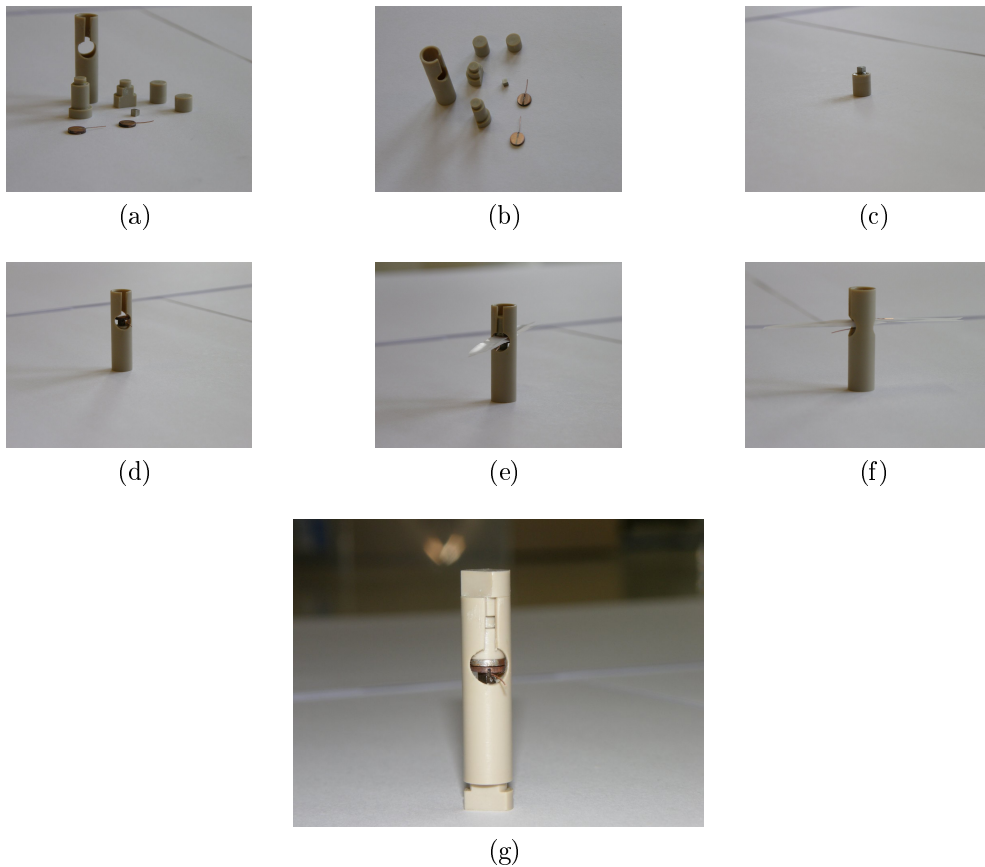
Figure 6.7.: A step by step declaration about the preparation of the redesigned final PEEK cell.

plunger. As fast as possible they are positioned as shown in pictures 6.7e and 6.7f. By pressing the upper and the lower PEEK plunger with the fingers together ensures that capacitor plates are parallel and the gap d between them is not taller than 100µm.

The hardening of the "Loctite super glue" lasts about 60 minutes after the assembly of the PEEK cell. In this period no useful gauging is possible (section 6.4.1). After this time the PTFE foil between the capacitor plates can be removed and the PEEK cell is ready for measuring (figure 6.7g).

6.4.1. The "Loctite super glue gel" test

Because of the fact that the PEEK cell reacts extremely sensitive on capacitance variations ΔC, generated by an applied magnetic field H, stresses σ and temperature T, it is possible to detect the effect of the "Loctite super glue gel" on the capacitance during the hardening phase. A drift measurement (figure 6.8) right away after the assembling of the capacitance PEEK cell with "Loctite super glue gel" has been finished demonstrates,

why magnetostriction gauging will lead to no needful results for this term. The graph 6.8 of the capacitance drift is not authentic linear in the first minutes after the preparation of the cell. After this time duration the drift shows the normal temperature dependence and the system is ready to gauge magnetostriction.

In the period of hardening the "Loctite super glue gel" causes mechanical stresses σ on the sample and on the other parts of the capacitance PEEK cell. As a result the capacitance C changes as long as the "Loctite super glue gel" curing process quits. After this time the normal thermal influences on the PEEK cell take place.
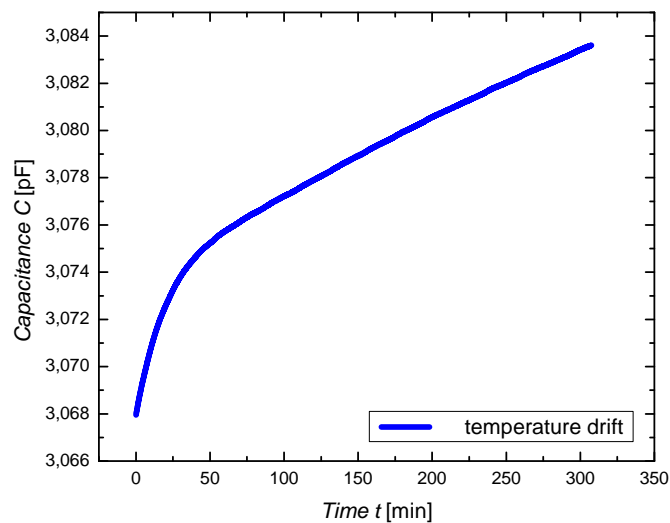
Figure 6.8.: A drift measurement, immediately after the PEEK cell was assembled, demonstrates the desiccation of the "Loctite super glue gel". For the first 60 minutes after the preparation no gauging with the capacitance cell should be arranged because the desiccating causes nonlinear drift effects. Therefore it is supposed that the "Loctite super glue gel" needs these 60 minutes for hardening.

6.5. Magnetostriction measurements at RT

Experimental magnetostriction measurements are always linked to temperature effects as discussed in section 4.2. This in most cases objectionable thermal interactions can be subtracted as demonstrated for the figures 6.2a and 6.2b.

6.5.1. Polycrystalline nickel sample

The measurement of a 2.93mm in altitude polycrystalline nickel sample with the improved PEEK cell with the lower capacitor plate directly on the sample features the correct values for the parallel $\lambda_\parallel = -40$ppm and perpendicular magnetostriction $\lambda_\perp = 20$ppm (figure 6.9). The dimension of the used nickel sample with 2.93mm is unimportant for the relative magnetostriction gauging $\lambda = \frac{\Delta l}{l}$, but a comparative value for a later comparison in section 6.5.2.
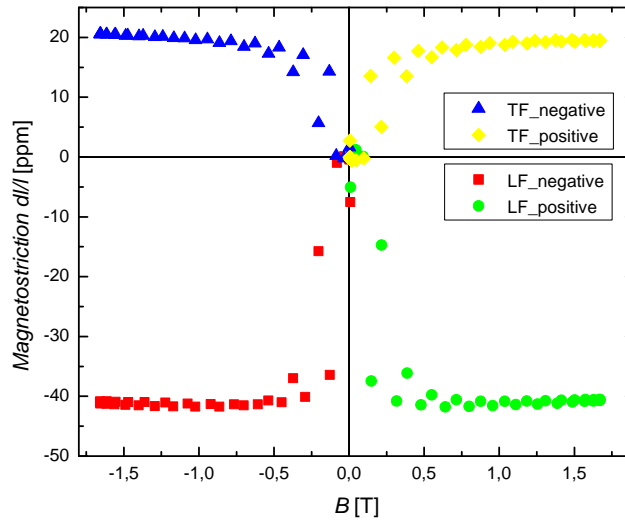
Figure 6.9.: Magnetostriction of polycrystalline nickel measured longitudinal (LF) and transversal (TF) to the applied magnetic field B results in $\lambda_\parallel = -40$ppm and $\lambda_\perp = 20$ppm.

Thus the basic principles of the magnetostriction measurement at room temperature are found. The studies on the nickel sample which are exactly documented in literature agree with these results. After calibrating the system with the well known polycrystalline nickel sample further measurements can be achieved.

6.5.2. The problem of small samples

Further studies with polycrystalline cubic nickel samples of the same material but different dimensions present varying $\lambda_\parallel$ and $\lambda_\perp$. It seems that the values decrease with smaller samples (figure 6.10a). Especially $\lambda_\parallel$ seems to be dependent on the length l of the sample. Multiple repeats of the measurements lead to same results.

A plausible explanation for this behaviour is given in figure 6.11. The "Loctite super glue gel" and its damps cause stresses on the surface of the sample if they are in contact.
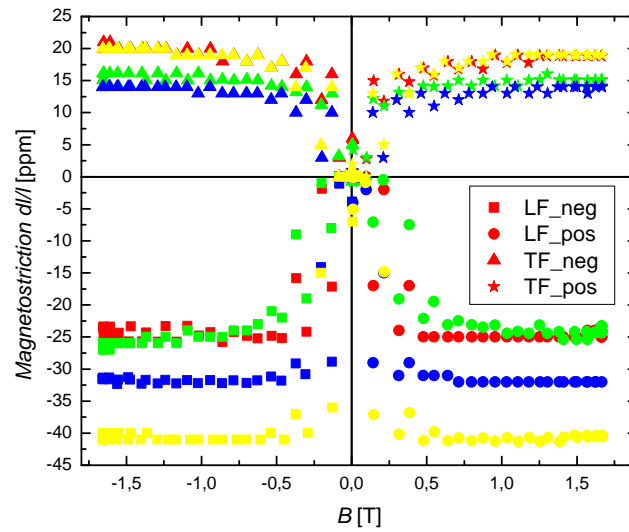
(a) The results for $\lambda_{\parallel}$ and $\lambda_{\perp}$ decrease for smaller samples. A comparison of four polycrystalline nickel samples of the same material with different dimensions distinguish this tendency. The corresponding lengths l of the different coloured curves are: 2.93mm (yellow), 2.04mm (blue), 1.00mm (green) and 0.91mm (red). The two directions of $\lambda_{\parallel}$ and $\lambda_{\perp}$ for the positive and the negative applied magnetic field are indicated by different symbols.
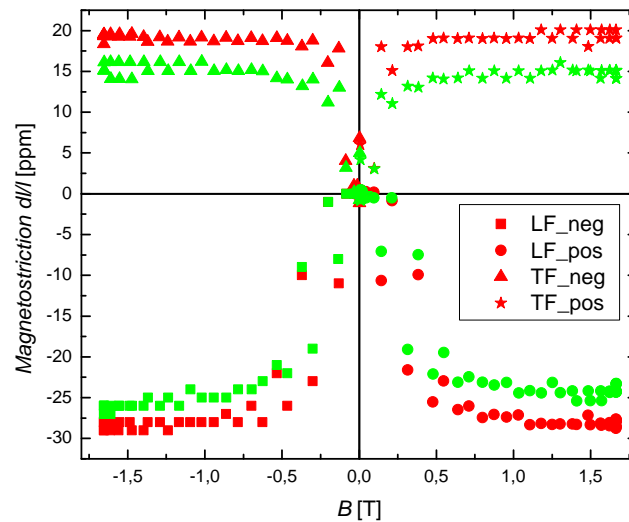
(b) Coating the four side faces of a 1.00mm cubic nickel sample with oil increases the values of $\lambda_{\parallel}$ and $\lambda_{\perp}$. The red coloured curve exhibits the magnetostriction of the 1.00mm cubic polycrystalline nickel sample whereas the green one shows the same sample but not oil treated.

Figure 6.10.

The glue seems to manipulate and prevent the elongations of the sample. This would similarly explain why samples with higher altitudes suffer less under this influence because the ratio of the glue polluted piece of the side face to the clean part is taller than for smaller samples. Coating the side faces with oil avoids the contact with the glue. If this theory is correct, the magnetostriction of small samples should advance and the oil film allows them to change their lengths.
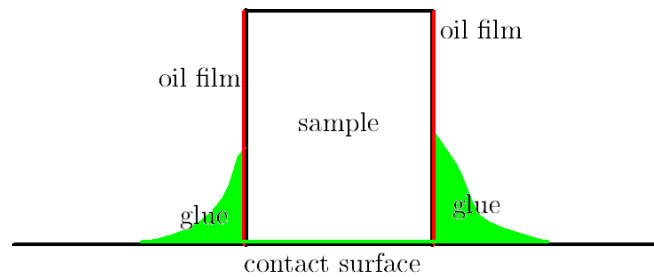
Figure 6.11.: If the side faces of the cubic sample is coated with oil (red coloured) the "Loctite super glue gel" (green marked) and its exhalation are not able to contact its surfaces.

A comparison of a 1.00mm cubic polycrystalline nickel sample with an oil film on its side faces (red marked in figure 6.10b) with the same nickel sample, but unoiled (green graphes of figure 6.10b) demonstrates the positive effect of the oil. Thus the theory is underlined by these results.

Even if these studies told how to treat small samples it is rather recommended to use larger dimensions of samples because the oiling process of such small samples proves itself to be not easy. One has to pay attention to coat the four side faces of a cubic sample but not to coat its top and bottom surface because for the preparation of the cell they have to be glued. Therefore small samples should rather be avoided. From experience the ideal sample length turns out to be between 3mm and 4mm.

6.5.3. Silver sample

In literature silver is documented to exhibit nearly no magnetostrictive effect. As a consequence magnetostriction measurements could give information about the resolution and the sensitivity of our system.

Figure 6.12 is not able to declare the precise magnetoelastic elongation of the used 2.58mm silver sample. Anyway a close study of this curve confirms how sensitively the
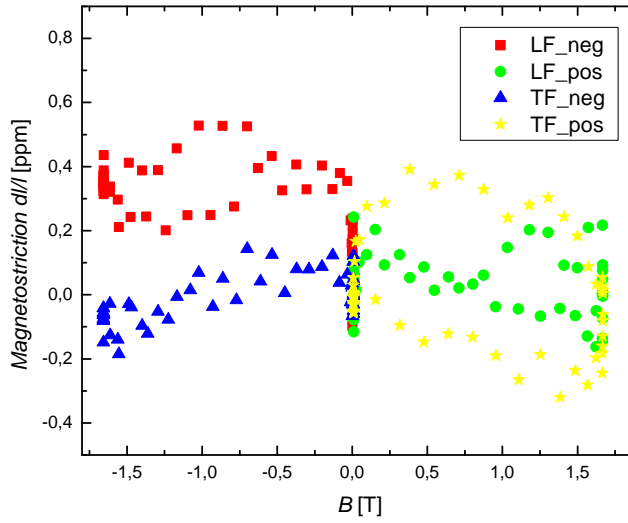
Figure 6.12.: The magnetostriction of silver is known to be very low. The received graphes display how sensitive system measures. Its resolution is very high.

system behaves and gives an idea of its high resolution.

6.5.4. $Fe_{81}Ga_{19}$ sample

As mentioned in section 4.6.2 anisotropic polycrystalline samples are often crossed with textures and stresses. In that case the magnetostrition $\lambda_\parallel$ and $\lambda_\perp$ have different values in the three spatial directions of a sample.

For example magnetostriction of an anisotropic polycrystalline $Fe_{81}Ga_{19}$ sample with textures and stresses is plotted in figure 6.13. Every colour emblematises a direction in space. The three gauged sample dimensions are 2.34mm, 2.00mm and 1.88mm. The different symbols of figure 6.13 explain the directions of λ and the sign of the applied magnetic field B. In comparison to nickel the signs of $\lambda_\parallel$ and $\lambda_\perp$ of $Fe_{81}Ga_{19}$ are converse.

As a solution for such anisotropic samples with textures and stresses they have to be heated up to T_C or T_N in order to get isotropic reordered. After that the magnetostriction values for $\lambda_\parallel$ and $\lambda_\perp$ are similar in the three spatial directions of the cubic.
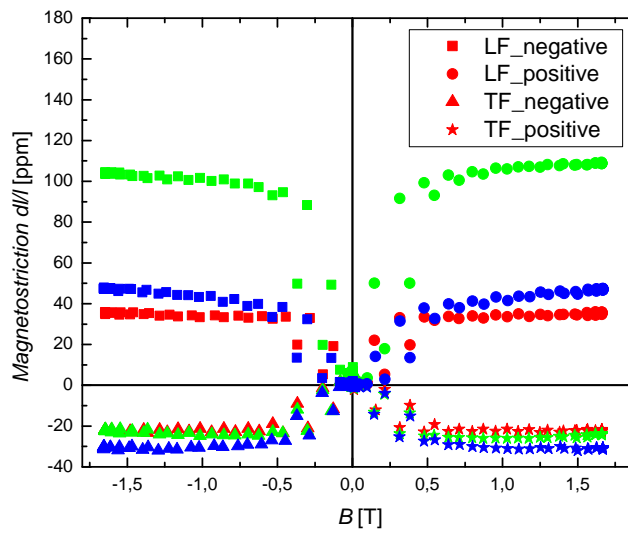
Figure 6.13.: Anisotropic samples with textures and stresses exhibit different values of magnetostriction $\lambda_\parallel$ and $\lambda_\perp$ in all three directions in space. The studied $Fe_{81}Ga_{19}$ sample demonstrates this effect. Every colour of the figure illustrates another spatial direction. Contrary to nickel the magnetostriction values $\lambda_\parallel$ and $\lambda_\perp$ of $Fe_{81}Ga_{19}$ are conversely signed.

7. Capacitance cell for high temperature

High temperature measurements for temperatures over 600K make great demands on material and limit the choice of them. The functionality of the gauging systems depends on more parameters than those for room temperature or cryogenic temperatures which feature other difficulties. Also the measurement of magnetostriction is not excluded. Thus by trend more (experimental) researches into lower temperatures physics were accomplished up to now. Nevertheless this is an interesting challenge and first knowledge and experience for magnetostriction measurements at high temperatures are achieved. The finite assortment of materials is reflected in the equipment of the measurement system (section 7.1), the design and the materials of the capacitance dilatometer (section 7.2).

7.1. Equipment for the measurement of magnetostriction at high temperatures

As a first consequence of the achievement of high temperatures over 600K the equipment used for room temperature (section 5.2) expands and alters. What comes first to mind as an additional part for the magnetostriction measurement at high temperatures is a heating furnace (subsection 7.2.3) to achieve these high temperatures.

But the introduction of the heating furnace leads to temperature gradients inside the capacitance dilatometer. A basic information of the results for magnetostriction at room temperature 6 was the enormous proportion of the thermal drift in magnetostriction gauging. Even small temperature fluctuations lead to manipulated magnetostriction results. Thus temperature gradients have to be avoided. Especially this know-how emerges as the highest demand for magnetostriction at high temperatures.

Best suitable to keep thermal fluctuations as low as possible is a proximity in vacuo. Therefore the used electro magnet at room temperature (section 5.2) is replaced by the superconducting "OXFORD" teslatron which is able to come up to magnetic fields of 14T. Inside the cryostat a variable temperature insert (VTI) is provided in which a high temperature insert (HTI) with the capacitance dilatometer is placed. Inside this HTI vacuum will be produced which should keep the variations in temperature low.

The further configuration is adapted to these two main divergences to the setup at
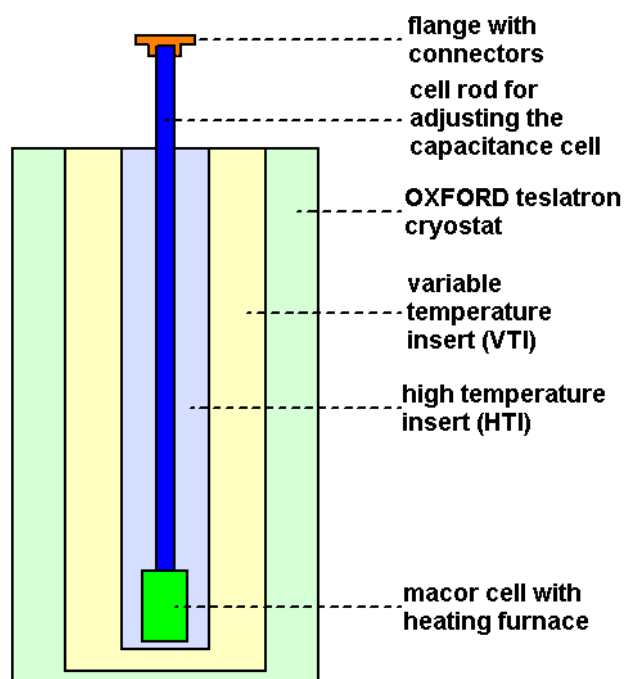
Figure 7.1.: The structural assembly of the "Oxford" teslatron with its variable temperature insert (VTI) and an installed high temperature (HTI) which is evacuated and keeps therefore thermal fluctuations low. Such fluctuations in temperature are the main fraction to affect magnetostriction measurements and should be avoided.

room temperature, that is described in section 5.2. The main components of the system are:

1. The "OXFORD" teslatron superconducting magnet generates magnetic fields up to 14T. Contrary to the room temperature measurement with the electro magnet of section 5.2, that was triggered with voltage, the teslatron is driven directly with a magnetic field (section 7.3.1). Thus neither a hall probe has to be attached nor a measuring card like the type "NI 6211" is necessary for the superconducting "OXFORD" teslatron. Instead of the "NI 6211" measurement card four "OXFORD" operating instruments are actuating the system (figure 7.3). The "OXFORD IPS" is the power supply for the magnet and assigns the achieved magnetic field to the teslatron. Additionally the three "OXFORD" instruments "ITC 503", "ILM" and the "Lambda Controller" control the temperature of the variable temperature insert (VTI), the helium level, the pressure and the temperature of the "OXFORD" teslatron. For a further and more detailed information about the communication between the computer and the "OXFORD" teslatron a view on figure 7.3 is recommended.
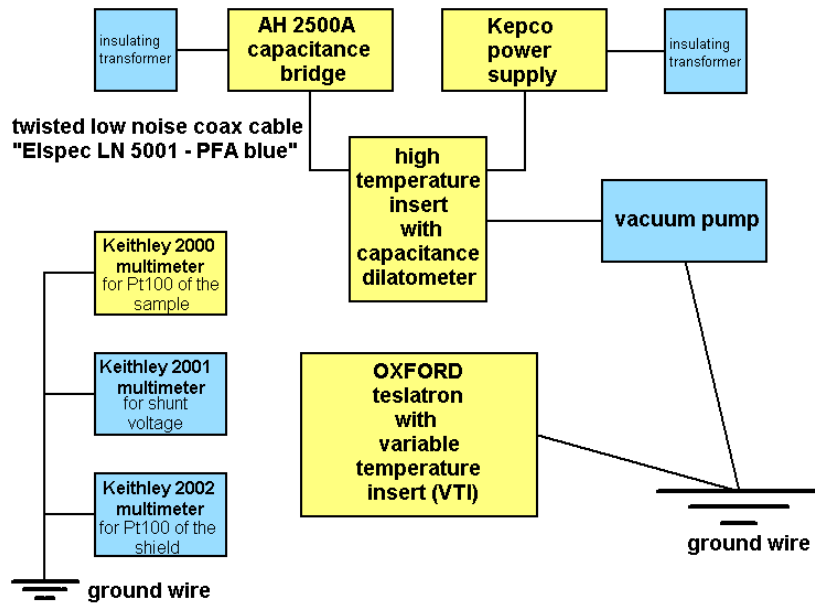
Figure 7.2.: A diagram of the setup for high temperature magnetostriction. The yellow coloured instruments are the cornerstones of the equipment whereas the blue ones are in support of them. In order to create no ground loops isolating transformers are applied.

2. The high temperature insert (HTI) is evacuated in order to keep the thermal fluctuations for the high temperature measurements as low as possible. During the magnetostriction gauging at a regulated high temperature T the temperature should be steady. Inside the insert HTI the capacitance dilatometer and a heating furnace are positioned in the centre of the superconducting coils to ensure homogeneity of the applied magnetic field B.

3. The "AH 2500A" capacitance bridge with its high resolution gauges the altering of the capacitance C of the dilatometer. Later these capacitance changes ΔC are converted to length changes Δl of the measured sample as described in subsection 5.3.2. A twisted low noise "Elspec LN 5001 - PFA blue" coaxial cable connects the "AH 2500A" capacitance bridge with the flange with connectors (figure 7.1) of the cell rod, on which the capacitance cell is placed. This low noise coax ensures that no additional unwanted capacitances between the "AH 2500 A" and the capacitance cell are measured.

4. With the aid of a "Kepco power supply" the heating furnace (subsection 7.2.3) around the capacitance dilatometer is actuated.

5. A Pt100 detects the temperature of the sample during the magnetostriction measurement. Every specific resistance R of the Pt100 corresponds to a temperature T (figure 7.4). Thus the "Keithley 2000" multimeter displays the actual temperature of the Pt100. In connection with a small computer software the graph of this temperature T over the time t is plotted.

In figure 7.2 these five apparats are yellow deposited and the concerning ground wires are plotted. The blue coloured attachments support these basic parts:

- The vacuum pump evacuates the high temperature insert (HTI).

- The isolating transformers avoid ground loops which produce high noises and eliminate reproducible results.

- Both, the "Keithley 2001" as well as the "Keithley 2002" multimeters are additional controls. The first one detects the shunt voltage of the heating furnace. Over the equation $P = UI$ the heating power is recorded. The second one observes the Pt100 which is bonded outside on the bottom of the HTI.

7.2. Design and development of a capacitance cell for high temperatures

The developed and elaborately studied concept of the PEEK capacitance (figure 6.4) cell is the point of origin for the design of high temperature magnetostriction dilatometer. Notwithstanding caused by the achieved high temperatures this capacitance cell differs in material and dimensions. The major challenge is the replacement of the "Loctite super glue gel" which does not qualify for temperatures over 100°C because the complete design of the PEEK cell is based on glueing. If no adequate high temperature adhesive is found the screwless PEEK cell concept has to be reconsidered.

7.2.1. Material of the cell

A basic prerequisite in the analysis of problems is to find a list of possible reasons and try to enhance them. Adapting the concept of the PEEK cell to temperatures over 300°C depends on the solution of three weak points:

1. The non magnetostrictive material PEEK, which was successfully used at room temperature, has a melting point of about 350°C and should therefore be exchanged with a material with a higher fusing point.

2. The "Loctite super glue gel" resists temperatures up to 100°C. Maybe all other well known organic adhesives and silicone are similarly not suitable for temperatures over 300°C.
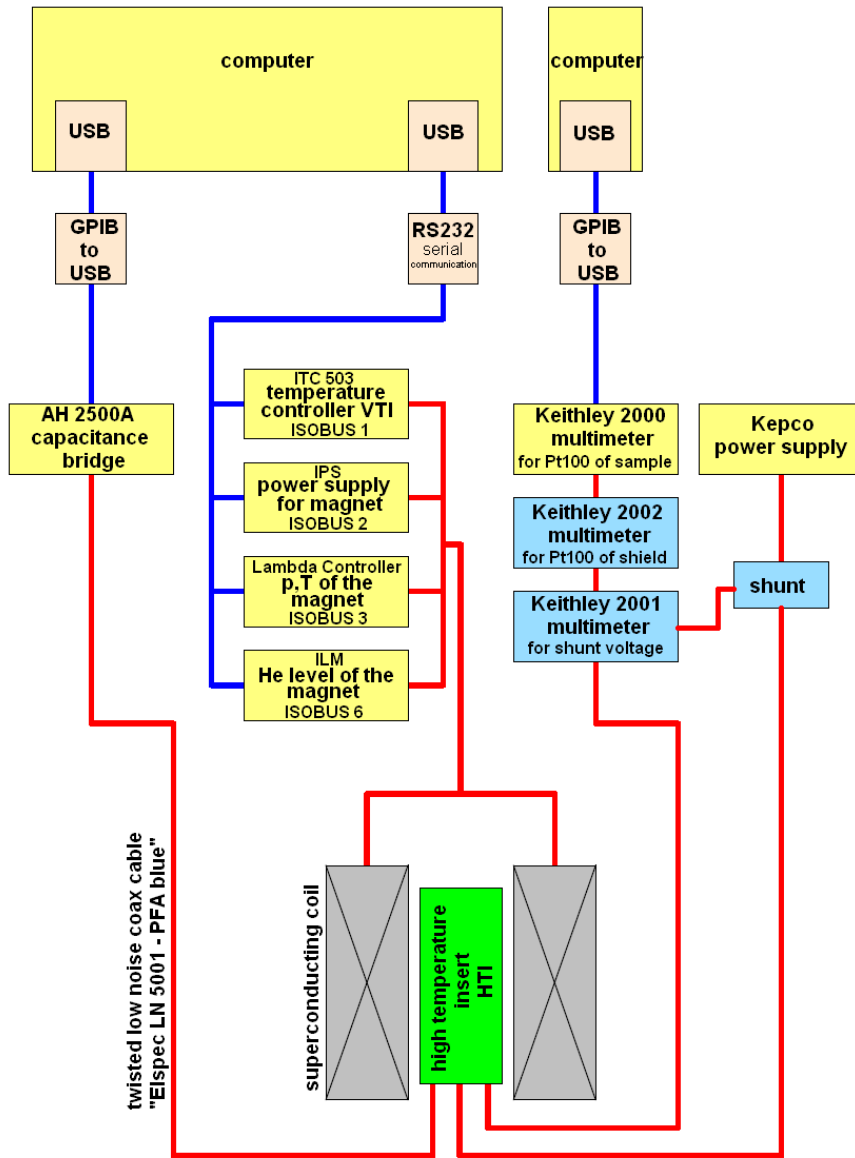
Figure 7.3.: The communication and messaging between the computer and the different instruments is divided into two paths. The right path marks the interaction with the "OXFORD" teslatron in order to apply a magnetic field. The left one controls the different capacitances C of the capacitance dilatometer via the "AH 2500A" capacitance bridge. Blue wires symbolize the information, the computer transfers to (gets from) "AH 2500A" and the "OXFORD" operating equipment that forward it on (receive it from) the red wires to the direct experiment.
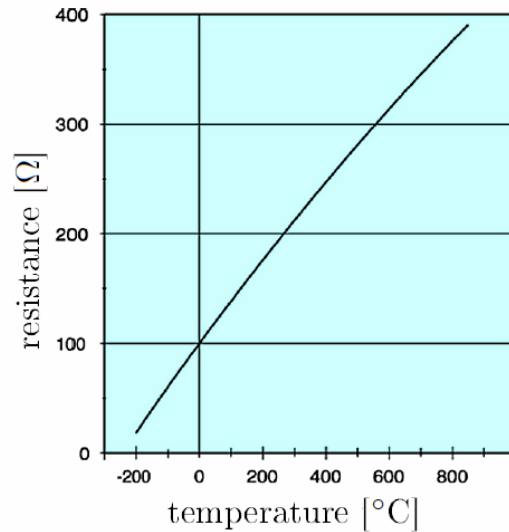
Figure 7.4.: The characteristic line of a Pt100 is displayed as a function of the resistance [Ω] over the temperature [°C].

3. Also the soft-soldering of copper wires on the capacitance plates depends on the softening point of the solder. Most of them have maximal melting points of about 300°C.

Therefore the demand on the used materials is a combination of a high temperature resistance and non or extremely low magnetostrictive characteristics. Substances which come into consideration are well explored before used. With the aid of the best qualified ones the capacitance dilatometer for high temperature dilatometer is constructed.

1. Instead of the polymer plastic PEEK a non magnetostrictive glass ceramics named MACOR is used for the body and plungers of the capacitance cell. Due to the used glass ceramics MACOR this capacitance cell is shortly called MACOR cell.

2. As three alternatives to the "Loctite super glue gel" ceramic cements of the company "Omega" are a possibility. "Omegabond 600", "Omegabond 700" and "Omegabond CC" are high temperature adhesives which work at least up to 800°C. "Omegabond 600" even stands temperatures up to 1427°C. Nevertheless the "Omegabond CC" is chosen because of some advantages in comparison to the two other high temperature glues. Contrary to them the "Omegabond CC" is not prepared with water. It consists of a solid powder part and a liquid solution (for the accurate mixing proportions see section 8.1). Thus the precipitation hardening is constitutively faster than those of the other two ones. After 30 minutes at room temperature the curing process is insofar finished that the part on is not moveable any more without high mechanical pressure. But the final hardening lasts 4 hours at 105°C.

Not only the cure time of the "Omegabond CC" let it appear unique, also the temperature range between $-200°C$ and $843°C$ is optimally suitable for a large region of measurements. The "Omegabond" adhesives can be completely removed with NaOH base.

3. By welding instead of soldering the copper wires are bonded on tantal capacitor plates which replace the copper plates because of the fact that it is much easier to weld copper with tantal than with itself. Similar to copper tantal is known in literature as an extremely low magnetostrictive material.

With these adaptions the design of the MACOR cell can be constructed on the basis of the PEEK cell.

7.2.2. Dimensions and design of the capacitance cell

In the style of the PEEK cell which is introduced in subsection 6.3.1 the MACOR cell is structured with two horizontal parallel capacitor plates (figure 7.5). The capacitor plates made of tantal are placed directly on the sample on which magnetostriction has to be measured. The diameter of the capacitor plate discs is with 7mm larger than the copper capacitor plates of the PEEK cell with 5.7mm. Based on equation 5.1 the capacitance C_{macor} of the MACOR cell is also higher than C_{peek}. The explicit construction plans of the MACOR cell can be found in the appendix section B.1.

The MACOR cell consists of six parts. From top to bottom of figure 7.5 these pieces are called:

1. the upper MACOR cell plunger

2. the upper tantal capacitor plate

3. the lower tantal capacitor plate

4. the sample

5. the MACOR body around them

6. the lower MACOR cell plunger

These six components are glued together with the aid of "Omegabond CC" as described in section 8.1. The construction of the MACOR cell is similar to the PEEK cell screwless.

The dimensions of the MACOR cell are modulated to the superconducting coil length of the "OXFORD" teslatron. Only if the MACOR cell is positioned in the centre of those superconducting coil the homogeneity of the applied magnetic field B guaranteed. For adjusting the MACOR cell in this part of the "OXFORD" teslatron the MACOR cell is assembled on a cell rod (figures 7.1 and 7.6). The correct dimensions of this cell rod can be found in drawings of the appendix section B.2.
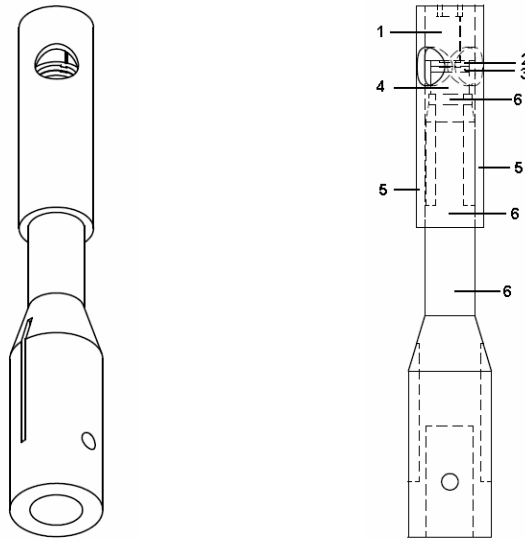
Figure 7.5.: The figure on the left demonstrates the assembled MACOR cell. The first design of the MACOR cell is made up of six single parts as exhibited on the right hand picture. Their notations are: 1) the upper MACOR cell plunger, 2) the upper tantal capacitor plate, 3) the lower tantal capacitor plate, 4) the sample, 5) the MACOR body around them, 6) the lower MACOR cell plunger

Of course the MACOR cell is able to measure magnetostriction parallel $\lambda_\parallel$ as well as the component perpendicular $\lambda_\perp$ to the applied magnetic field. But the assembling of the MACOR cell with the aid of the cell rod inside the "OXFORD" teslatron allows only the measurement of $\lambda_\parallel$. By studying figure 7.6 and viewing that the cell rod always stays parallel to the superconducting coil makes this fact comprehensible. For measuring $\lambda_\perp$ a second MACOR cell would be needed which is orthogonally installed on the cell rod. For first researches however the parallel component $\lambda_\parallel$ is enough.

7.2.3. The heating furnace

The cornerstone for the heating of the sample is a heating furnace. It consists of a copper body and a bifilar winded non magnetic $NiCr$ heating wire with 35Ω around. Bifilar spooling reduces the inductance and the after Lenz´s rule therewith associated generated magnetic field is zero because the magnetic field created by one winding is therefore equal and opposite to that created by the other, resulting in a net magnetic field of zero. The heating furnace is coated with a thin insulating film of "Omegabond CC". A detailed plan of the copper body of the heating furnace is plotted in section B.3.

The heat output of the heating furnace is defined by Ohm´s law $U = RI$ and the equation for the wattage $P = UI$, with the current I, the voltage U and the resistance
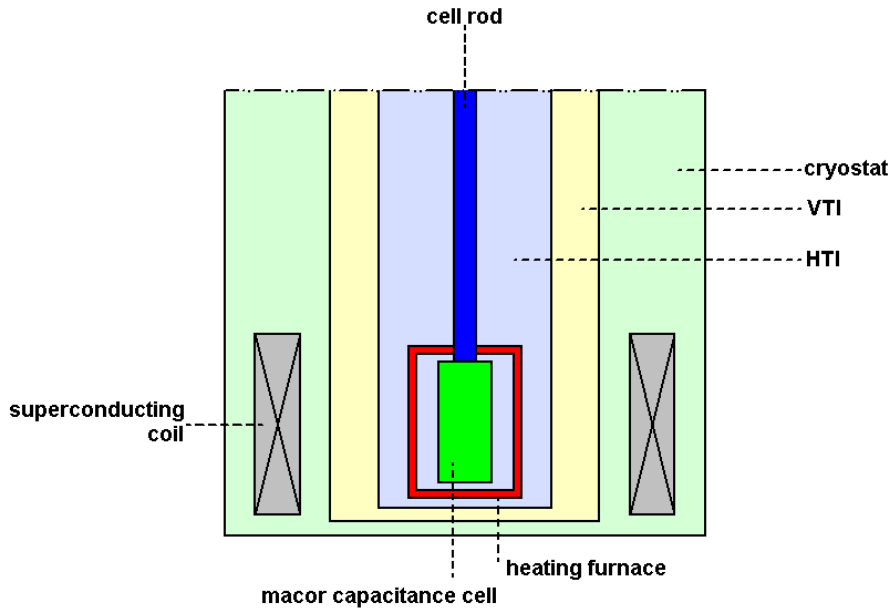
Figure 7.6.: The MACOR cell is mounted on a cell rod that sites it in the centre of the superconducting coil in order to apply an homogeneous magnetic field B. With the heating furnace around the cell the sample is heated.
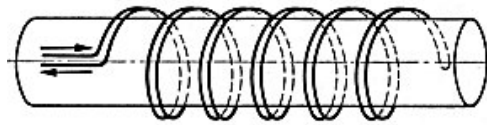
Figure 7.7.: The heating furnace consists of a body made of copper and a bifilar coiled heating resistor around.

R. For instance the used heating resistor with 35Ω and a current of 1A enable a filament power of 35W. Tests exhibit temperatures over 400°C for this heating capacity and so the made demands are satisfied.

The heating furnace surrounds the MACOR cell and is placed on the cell rod together with the MACOR cell (figure 7.6). Therefore the lower MACOR cell plunger (figure 7.5) exhibits a 8.5mm in diameter big opening in longitudinal direction of the cell, in which the cell rod gets inserted. Through the two small holes on the side of the lower MACOR cell plunger screws connect the MACOR cell with the cell rod. These two screws are rotated in threads inside the cell rod. In this way the MACOR cell gets deep-seated with the cell rod. In an analogous manner the heating furnace is added closely around the MACOR cell. So these three components form a compact construct.

Figure 7.8 exhibits the wiring of the MACOR cell and the heating furnace. The capacitor plates of the MACOR cell are bonded with a thermocoax which resists high

65
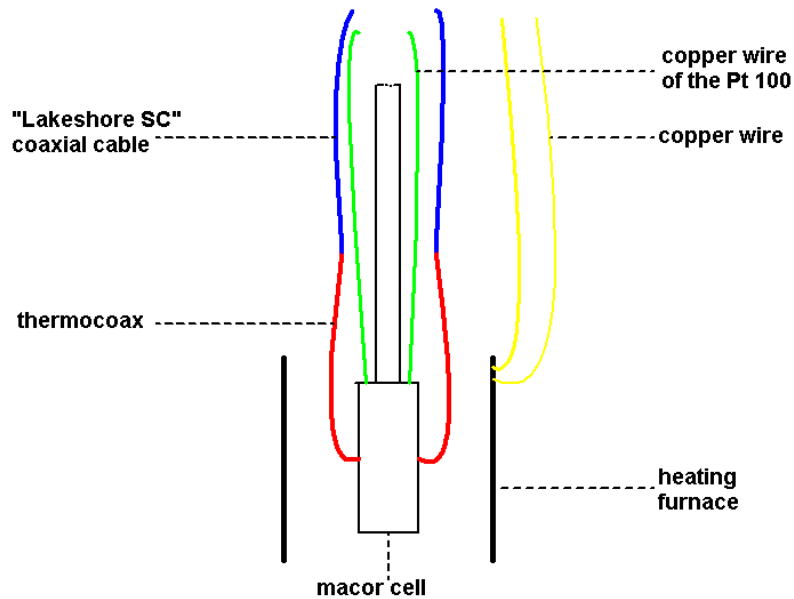
Figure 7.8.: Inside the high temperature insert (HTI) the capacitor plates of the MA-
COR cell are bonded with a (red) thermocoax which is in a cooler area
connected with a "Lakeshore SC" coaxial cable (blue). The copper wires of
a Pt100, which is positioned as close as possible to the sample in order to
measure the real temperature of the sample, are green coloured. The yellow
marked copper wires are hard-soldered with the bifilar heated filaments of
the heating furnace. All eight wires lead to the flange with connectors on
the top of the cell rod (figure 7.1).

temperatures up to 700°C. In a cooler space the thermocoax gets connected with the
"Lakeshore SC" coax, which has already been used for the measurements at room tem-
perature. As close as possible to the sample a Pt100 is placed in order to measure the
temperature of the sample. The heating resistor of the heating furnace is hard soldered
with copper wires which is connected, similar to the other wires, with the flange with
connectors on the top of the cell rod (figure 7.1). Further the flange with connectors
is cabled with the corresponding "Kepco power supply", the "AH 2500A" capacitance
bridge and the "Keithley 2000" multimeter as exhibited in figure 7.2.

7.3. The computer software for the "OXFORD" teslatron

The "Labview" program controls the used instruments ("OXFORD" teslatron and "AH
2500A" capacitance bridge) as demonstrated in figure 7.3 and safes and processes the

received data. The software features many similarities with the "Labview" program for the electro magnet (section 5.5). When the "Labview" program is started the user can choose between three different buttons. In figure 7.9 these three buttons on the left hand side of the "Labview" front panel are distinguished with red numbers 1 to 3. The corresponding activities of the program which start running after one of the buttons was pressed are similarly symbolized with the same numbers 1 to 3. A short description of the operations behind the three buttons demonstrates how easy the program can be handled.

7.3.1. The application of the "Labview" program for the "OXFORD" teslatron

1) Load configuration file path

As soon as the button "Load Configurationsdatei" is pressed the parameters can be set. If a "setup.ini" file path is entered in the "configuration file path" bar the old settings are loaded and appear in the "SETUP" display window (figure 7.9). Otherwise the parameters have to be typed by hand.

2) Load magnetostriction measurement

Before the magnetostriction measurement starts the temperature of the sample is regulated with the aid of the heating furnace. For first experiments the thermal control of the sample is carefully adjusted by hand. The "Keithley 2000" multimeter displays by means of the Pt100 close to the sample when the temperature is steady. Before this stable temperature is not guaranteed, no rational magnetostriction measurement is accomplished.

   Immediately when the temperature gets steady the button "Load Magnetostriktionsmessung" should be pressed. Then a new window pops out for entering the file name in which the data of the measurement should be safed. If the inserted file name already exists an alternative file name is created. In case that this alternative file name is likewise already available in this path, the magnetostriction measurement does not start and the button "Load Magnetostriktionsmessung" has to be pressed again. Otherwise the measurement starts after a correct and not existing file name was entered.
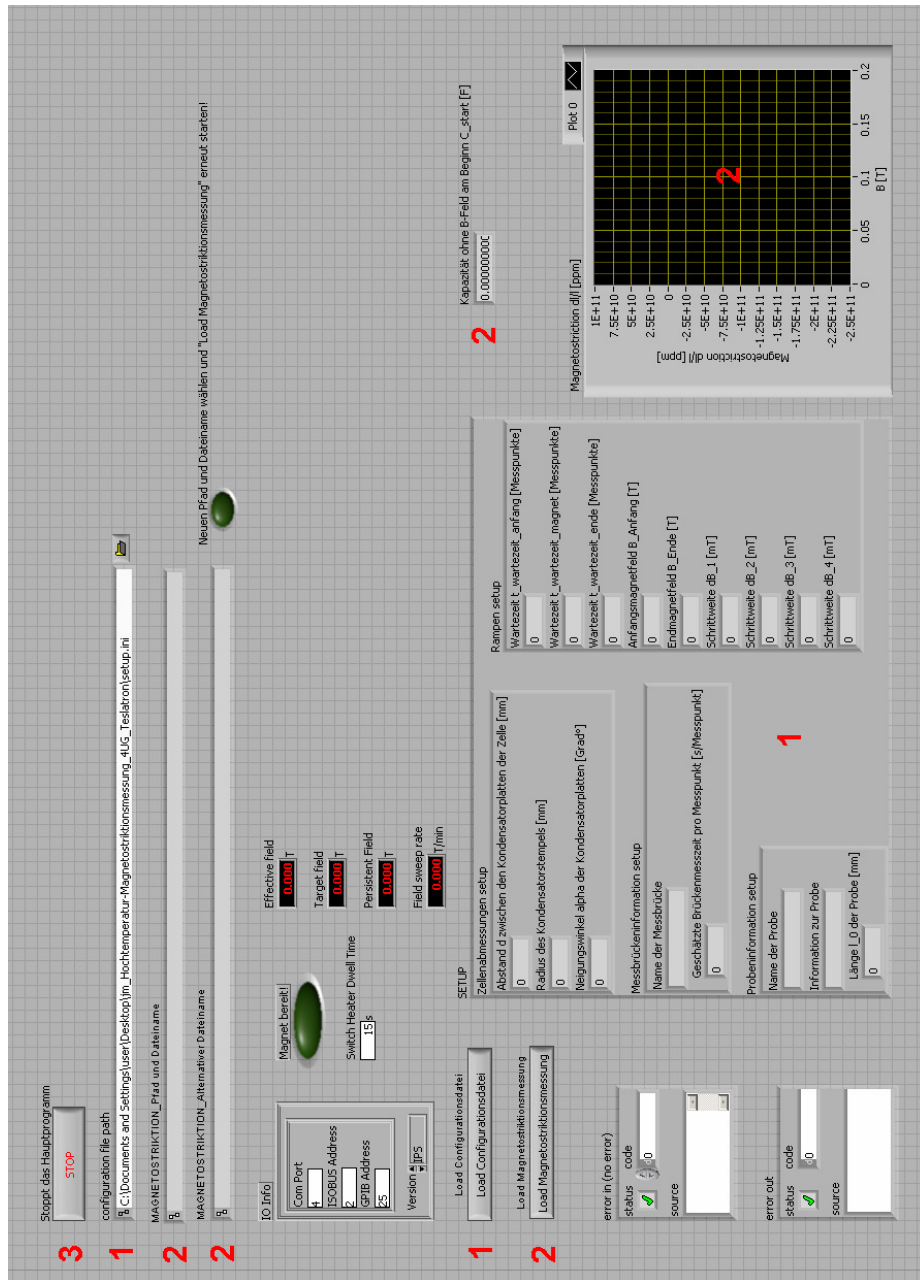
Figure 7.9.: The "Labview" program regulates and analyzes the measurement of magnetostriction. In the "Labview" front panel of the software for the control of the teslatron the red numbers 1 and 2 symbolize the two options of the program. When the adequate (red numbered) button is pressed, the (to this number in the picture) corresponding operations are accomplished. If the "STOP" button, marked with a red 3, is pressed as the name implies the "Labview" program quits.

setup mode	possible settings	unit
"Zellenabmessungen setup"	gap between the capacitor plates d	mm
	radius b of the capacitor plates	mm
	angle α of the capacitor plates	°
"Messbrückeninformation setup"	name of the capacitance bridge	
	estimated measuring time of the bridge for each data point	s / data point
"Probeninformation setup"	denomination of the sample	
	information about the sample	
	length l of the sample	mm
"Rampen setup"	initial holding time t_i	data points
	holding time at the highest voltage value t_{magnet}	data points
	final holding time t_f	data points
	initial voltage B_i	T
	final voltage B_f	T
	increment dB_1	mT
	increment dB_2	mT
	increment dB_3	mT
	increment dB_4	mT

Table 7.1.: After the "Load Configurationsdatei" button was pressed the setup settings of the "Labview" program for the measurement of magnetostriction in the "OXFORD" teslatron can be entered or altered.
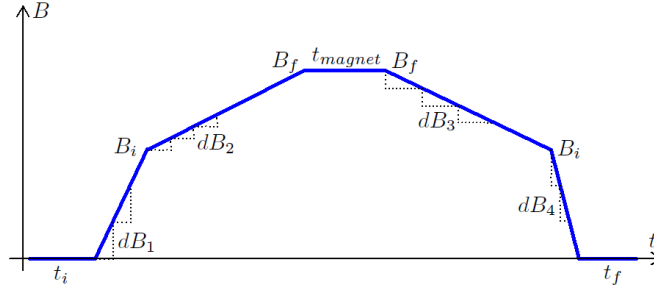
Figure 7.10.: The parameters of table 7.1 define the magnet ramp and control the magnetic field of the "OXFORD" teslatron.

Contrary to the "Labview" program of the electro magnet this program deals directly with magnetic fields B instead of voltages U which have to be converted. The "Labview" program therefore sends a pulse to the "OXFORD IPS" power supply which induces then a current inside the superconducting coils. With the aid of the coil constant $7.264285\frac{\text{A}}{\text{T}}$ of the "OXFORD" teslatron this current I is converted in a magnetic field B. Nevertheless the components of the magnet ramp (figure 7.10) influence its shape. The initial t_i and the final holding time t_f of the magnet ramp alleviate a later manually drift correction of the magnetostriction measurement.

Thus the parameters of the magnet ramp order the "OXFORD" teslatron over the "OXFORD IPS" power supply the magnetic field which it has to apply on the sample. Right away when the desired magnetic field is achieved the "AH 2500A" capacitance bridge detects the capacitance C of the MACOR cell. Then the next value of the magnet ramp is driven and the associated capacitance C is saved. Step by step, dB the magnet ramp is perambulated.

During the complete gauging time of this "Labview" program the temperature T of the sample is controlled over the "Keithley 2000" multimeter (figure 7.3). A small computer software for the "Keithley 2000" multimeter can be used as an additional support to display the temperature control of the Pt100 in real time.

Finally when the magnet ramp has quit and all raw data are connected the program translates them. For the conversion from $\frac{\Delta C}{C}$ of the "AH 2500A" capacitance bridge to $\frac{\Delta l}{l}$ the equations of 5.3.2 are used. Thus the first preserved capacitance C_0 (the indicator of it is marked in figure 7.9 with a red 2) of the "AH 2500A" capacitance bridge, which is gauged with $B = 0$, is used as point of origin in order to get $\Delta C_i = C_i - C_0$. Raw data are saved as well as the edited data in the file declared before.

After saving the data the program exhibits the translated magnetostriction data $\frac{\Delta l}{l}$ over the applied magnetic field B in the graph of the "Labview" front panel (figure 7.9).

Then the program is ready for further measurements and one of the three buttons has to be pressed again.

3) STOP

By pressing the "STOP" button as the name implies the "Labview" program for the high temperature magnetostriction quits and has to be reloaded if further magnetostriction gaugings are aimed.

8. Magnetostriction measurements at high temperatures

The final proof of principle completes the work and provides information about the functionality. The MACOR capacitance cell is mounted (subsection 8.1) with the identical polycrystalline nickel sample as discussed in subsection 6.5.1 and is attached between the pole shoes of the electromagnet like the PEEK cell. Then drift measurements and magnetostriction gaugings shed light on the success of the researches.

8.1. Preparation of the MACOR cell

A correct preparation of the capacitance cells shapes up as a cornerstone for rational and reproducable gaugings and pristine results. Even if the remaining test setup works extremely accurately a minor defect of the capacitance dilatometer avoids an outstanding performance. It seems only reasonable to turn the attention to it and devote the assembling (figure 8.1) an own section.

The complete accessory kit of the the MACOR cell except for the capacitor plates and the Pt100 temperature sensor are represented in figure 8.1a and 8.1b. As a first step thin copper wires get spot-welded into the chamfer of the tantal capacitor plates. A thin film of "Omegabond CC" adhesive stabilizes the bonding of the copper wire on the tantal plates. The look of the finished capacitor plates can be viewed in picture 8.1e. Later these copper wires of the capacitor plates are welded together with the inner conductor of the thermocoax (figure 7.8). A Pt100 sensor is as well prepared and spot-welded with copper wires.

After the dimensions of the sample are determined with a micrometer screw it is cemented with a thin coat of "Omegabond CC" on the lower MACOR cell plunger (picture 8.1c). This occours cautiously with the knowledge of section 6.5.2 about the influence of glues on the side faces of cubic samples. Glue on the side faces of the sample puts stress on it and prevents its magnetoelastic deformations.

The proportion of the solid powder and the fluid component of the "Omegabond CC" emerges to be optimal with 40 : 60. As a result of the evaporating solvent it is recommended to compound only small portions of the high temperature glue. As soon as the "Omegabond CC" film between the sample and the lower MACOR cell plunger has dried and the sample is fixed the next work step is made. At least this curing process lasts about 30 minutes. If the duration is not observed the bonded parts can detach.
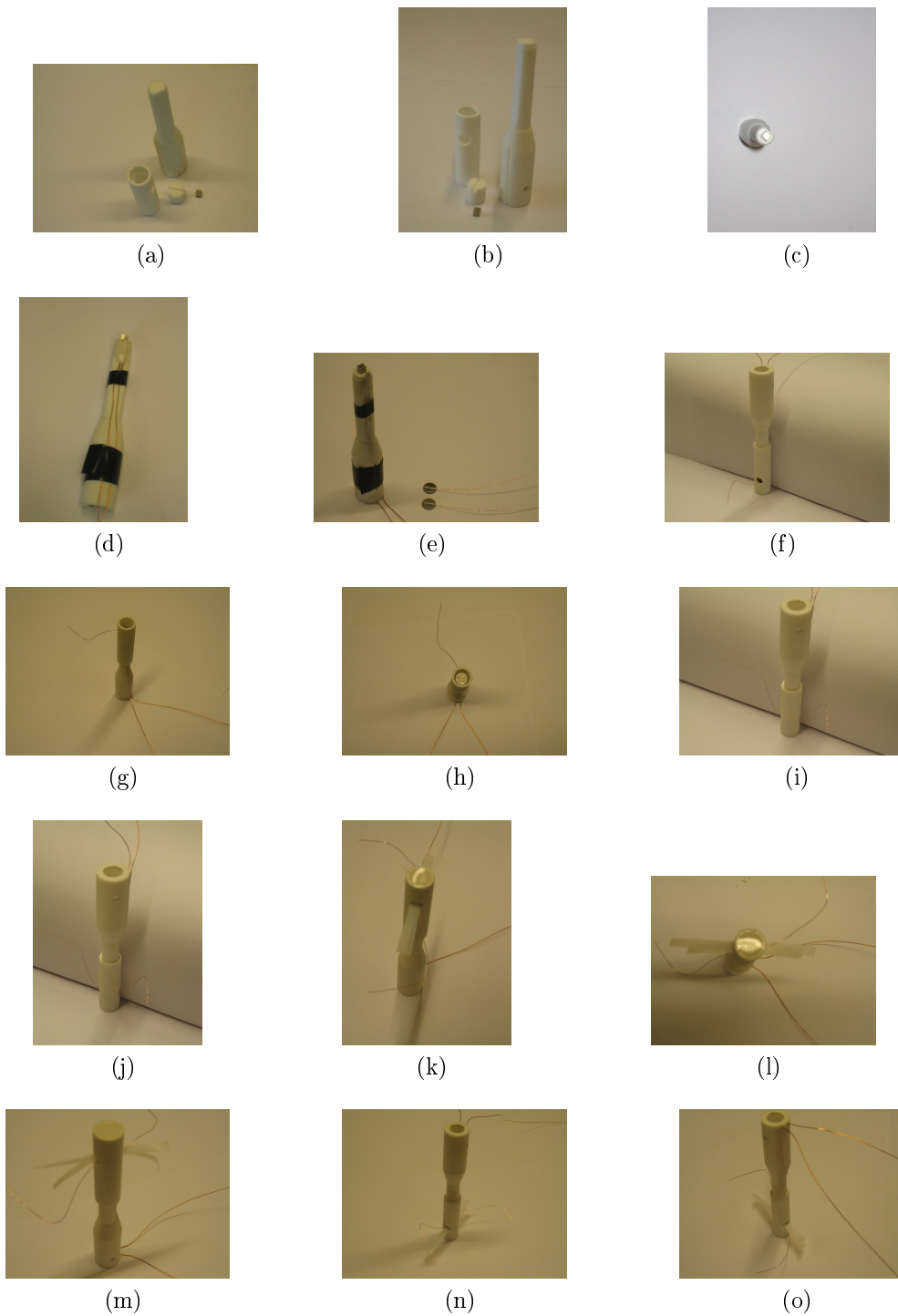
Figure 8.1.: A step by step declaration about the preparation of the MACOR cell.

Then the Pt100 sensor is placed as close as possible to the sample in order to detect the exact temperature of it. With the aid of a tape the copper wires of the Pt100 are fixed on the lower MACOR cell plunger and the Pt100 itself is adhered with "Omegabond CC" (figure 8.1d and 8.1e). A thin film of the high temperature cement covers the copper wires of the Pt100 sensor. Once the "Omegabond CC" has hardened the helpful tape is carefully removed again.

After the sample and the Pt100 are bonded on the lower MACOR cell plunger the lower tantal capacitor plate gets glued on the top surface of the sample (figure 8.1e). Therefore the wire is threaded through the hole of the MACOR body and pressed on the sample which is coated with a thin "Omegabond CC" film. For the hardening process the upper MACOR cell plunger is put on the lower capacitor plate and after that the complete construction is turned through 180° as demonstrated in picture 8.1f. In this position the upper MACOR cell plunger stabilizes the capacitor plate and the glue between the sample and the tantal disc cures.

When the lower capacitor plate is fixed on the sample (pictures 8.1g and 8.1h) the upper plate has to be assembled as well in the centre of the MACOR cell above it. Thus a "Omegabond CC" is put on the upper MACOR cell plunger which is then bonded with the upper tantal disc. The copper wire of the upper capacitor plate is first threaded through the window of the MACOR body as presented in the figures 8.1i and 8.1j. For the curing process the MACOR cell is put in the position shown in these two pictures.

Up to now the upper capacitor plate with the upper MACOR cell plunger are still moveable inside the MACOR cell body. Carefully the two capacitor plates are spreaded and a 100µm PTFE foil is placed between them in order to get a well defined gap d between the plates. Then "Omegabond CC" is poured in the space between the upper MACOR cell plunger and the MACOR cell body in order to fix the upper capacitor plate which has to stay unmoveable. This procedure is figured in 8.1k to 8.1m.

Finally the lower MACOR cell plunger is similarly bonded with the MACOR cell body (pictures 8.1n and 8.1o). But inside the lower tantal plate which was directly connected with the sample stays moveable. Therefore the changes of capacitance ΔC according to the magnetoelastic elongation of the sample can be detected by the "AH 2500A" capacitance bridge.

The complete preparation progress lasts about four hours according to the hardening of the "Omegabond CC". As a last step the heating of the MACOR cell exhibited in figure 8.1o with 105°C for four hours is indispensable for the purpose of a complete curing process. After that the 100µm PTFE foil is removed and the capacitance cell is ready for magnetostriction measurements at high temperatures.

8.2. First perpendicular magnetostriction measurement in the electromagnet

After the preparation of the MACOR cell with a polycrystalline nickel sample the MA-COR cell is positioned between the pole shoes of the electromagnet. Therefore the dimensions of the nickel sample are the same as already used for the PEEK cell in section 6.5.1. It seems only reasonable to use the already well known electromagnet for first measurements. Only if they agree with those of the PEEK cell it is useful to assemble the MACOR cell inside the "OXFORD" teslatron. The space between the pole shoes of the electromagnet is limited. Thus only the perpendicular direction of the magnetostriction is detected.
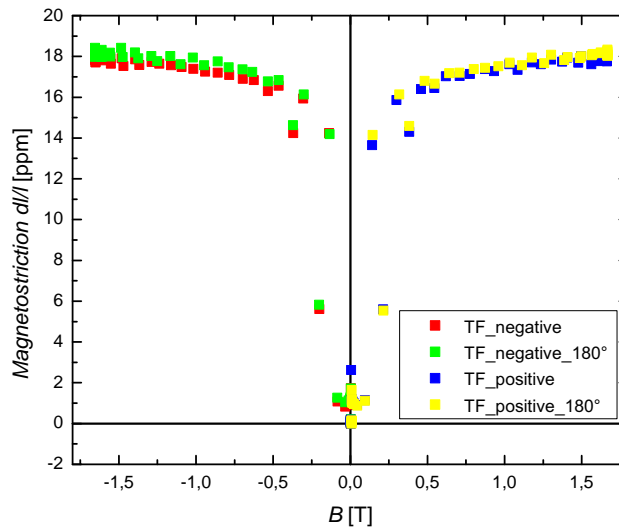
Figure 8.2.: Assembling the MACOR cell perpendicular into the electromagnet certifies if the MACOR cell works correct. The results for the perpendicular magnetostriction $\lambda_\perp$ at room temperature of the identical 2.93mm nickel sample agree with those of the PEEK cell of figure 6.9.

The values for $\lambda_\perp$ of figure 6.9 and 8.2 fit correctly together. Even the reproducibility for the results of the MACOR cell is ensured with rotations of the MACOR cell for 180 degrees. Insofar nothing militates against adapting the MACOR cell system inside the "OXFORD" teslatron.

8.3. Drift of the MACOR cell inside the "OXFORD" teslatron

Once the MACOR cell is attached in the teslatron the thermal influence is studied at 250K. First the pure temperature drift for the MACOR cell gets measured (figure8.3). Then the heating furnace is actuated with around 5W filament power in order to exhibit any unwanted induced signal compared to the drift measurement of the MACOR cell alone. Even though the heating furnace adds no high disturbing signals it attracts attention how strong the thermal drift responds to the increasing temperature of the heating furnace. For example the interval heating connects the two now discussed curves. Thereby the activating and deactivating of the heating furnace for each with 60 seconds is studied. Immediately it comes to mind that the thereby produced thermal gradients may affect the pure magnetostriction gauging of the sample. Thermal expansions and contractions could superpose the magnetostriction signal.
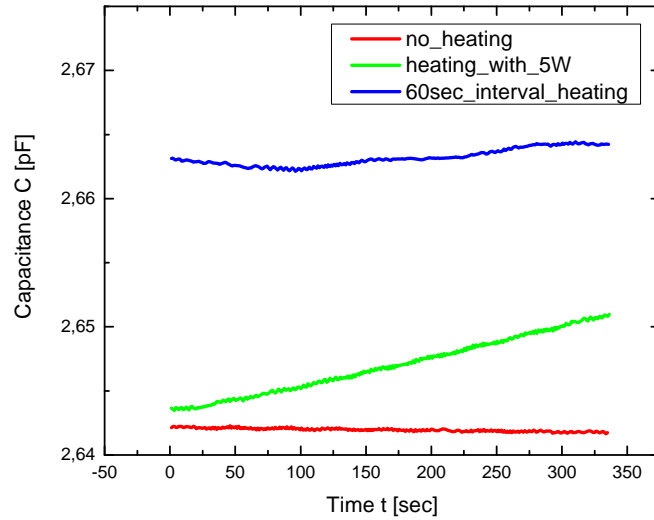
Figure 8.3.: A comparison between the three different drift measurements inside the "OXFORD" teslatron demonstrates the extreme thermal influence of magnetostriction. All three curves start at a temperature of 250K. The red line stands for the pure drift of the MACOR cell inside the VTI of the teslatron. Once the heating furnace was activated the drift follows the typical green line. The blue curve combines both. It is an interval heating and cooling process. Every 60 seconds the heating furnace is switched on therefore and turned off 60 seconds later again. The initial capacitance values vary according to small changes of the setup before the gauging starts because the capacitance is very low (pF). Even a short touch of a cable can affect this. But it does not matter at all because the measurement principle is a relative one ($\frac{\Delta C}{C}$).

8.4. High temperature magnetostriction measurements with nickel

No sample in literatures for magnetostriction is more detailed discussed than nickel. The forecasts for increasing temperatures predict a decreasing of $\lambda_\parallel$ and $\lambda_\perp$. This manner can be easily comprehended by remembering the correspondence between the magnetostriction λ and the magnetization M. Near the Curie temperature T_C the magnetization M of a solid goes to zero. As a result of the correspondence between λ and M, then λ similarly has to disappear.

Inside the "OXFORD" teslatron it is only possible to detect $\lambda_\parallel$ according to the longitudinal assembly of the MACOR cell on the cell rod (figure 7.6) and the parallel to

the cell rod positioned superconducting coils. Before the system measures the magnetostriction the temperature of the sample is set. The results of the drift measurements in figure 8.3 demonstrate arrestingly how important a steady temperature is for the magnetostriction gauging.

Carefully the heat output of the heating furnace is increased and after the temperature is stable in a range of at least about 200mK for the duration of the measurement the magnetostriction gauging gets started. The shorter the period of the detection is the more accurate are its results.
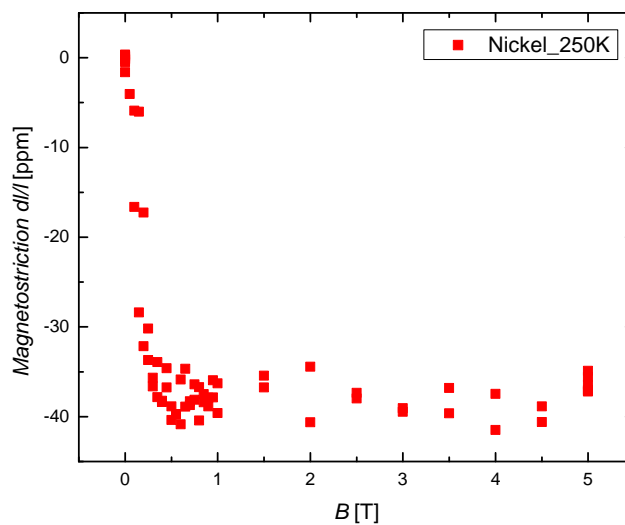
Figure 8.4.: Magnetostriction $\lambda_{\parallel}$ for a polycrystalline 2.93mm in length nickel sample at 250K.
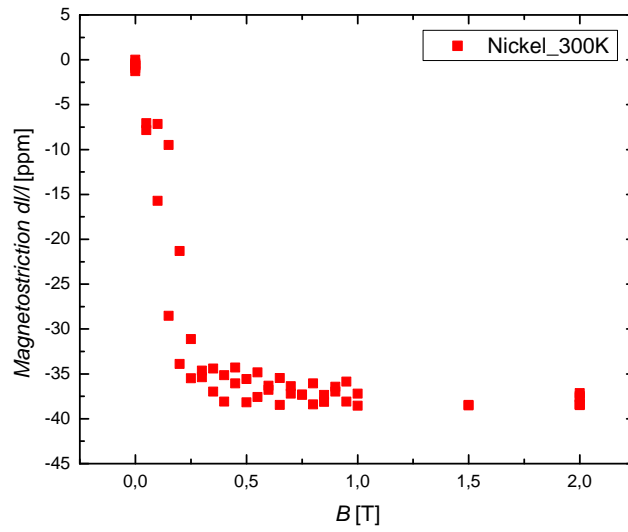
Figure 8.5.: Magnetostriction $\lambda_\parallel$ for a polycrystalline 2.93mm in length nickel sample at 300K.
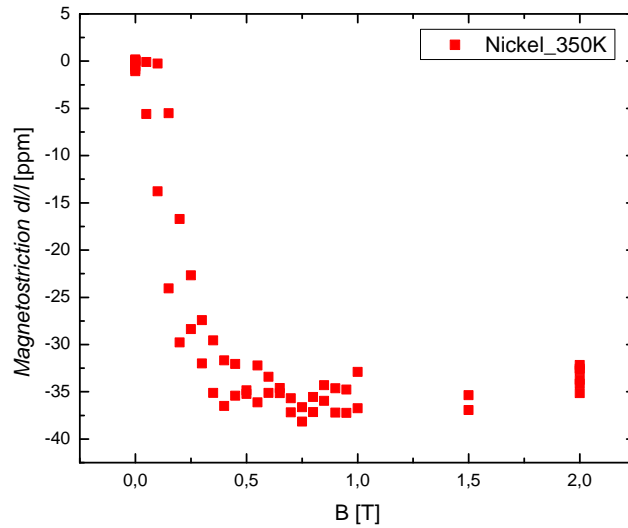
Figure 8.6.: Magnetostriction $\lambda_\parallel$ for a polycrystalline 2.93mm in length nickel sample at 350K.
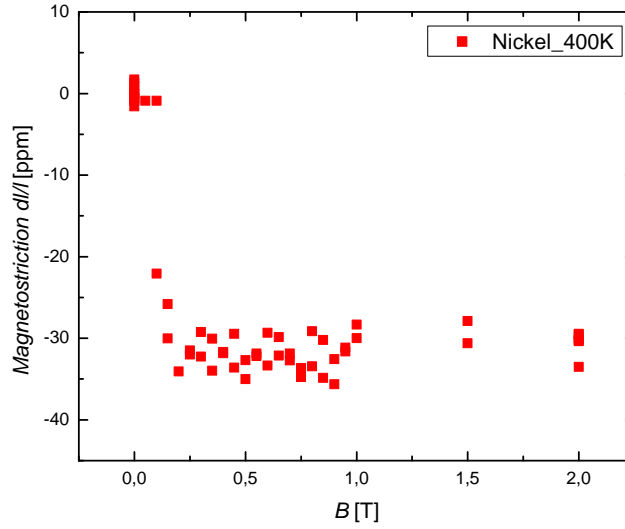
Figure 8.7.: Magnetostriction $\lambda_{\parallel}$ for a polycrystalline 2.93mm in length nickel sample at 400K.

Figures 8.4 to 8.7 represent magnetostriction measurements with a polycrystalline nickel sample at 250K, 300K, 350K and 400K. If these four graphes are viewed a bit closer it is possible to declare that the higher the temperatures get the lower gets the resolution of the curves. But this is no effect of the functionality of the system. It is simply the fault of the unsteady temperature on the sample because stabilizing the temperature around the sample with the aid of the "Kepco power supply", which controls the heating energy of the heating furnace, by hand is not the best solution. But for the proof of the functionality of the system and an analysis of its problems it is quite enough.

In figure 8.8 the four curves are plotted in one graph together. They are presented in different colours and symbols. This comparison of the nickel sample for those different temperatures in an thermal range of 150K exhibit how successful the high temperature system works. The parallel magnetostriction $\lambda_{\parallel}$ of the nickel sample converges slowly to zero and agrees therefore perfectly with the forecasts of literature. For higher temperatures magnetostriction converges faster to zero than the magnetization thus reaching the Curie temperature T_C.
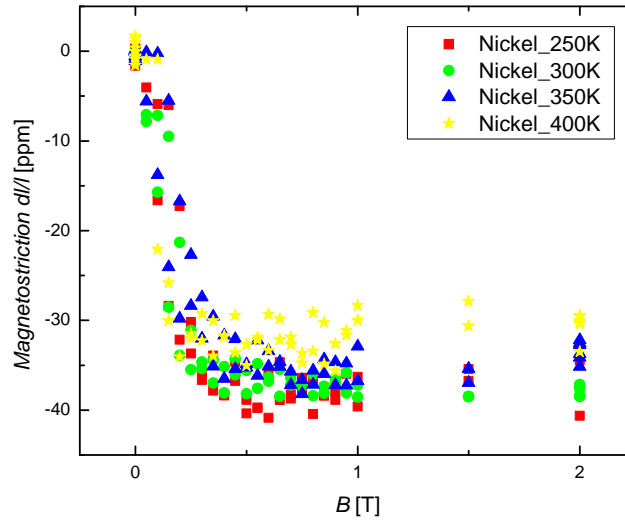
Figure 8.8.: A comparison of $\lambda_\parallel$ for these four temperatures exhibits the well documented trend that the length changes of polycrystalline nickel decrease with higher temperatures. A clear proof of the functionality of the system.

A comparison of the magnetostriction results of the MACOR cell with those of a strain gauge [43] is exhibited in figure 8.9. The magnetostriction values are detected at same temperatures. The differences of about 2ppm may even be a result of the not identical used polycrystalline nickel samples. But the adequate agreement of both curves ensure the functionality of the MACOR cell and the system at high temperatures.

The only deficit of the actual test setup is the missing uniformity of temperature. Higher temperatures cause enormous temperature gradients on the cell and adequate results are then not realizable any more as figure 8.10 displays. Temperature drifts often become troublesome when a measurement is made by use of a magnet with a long sweeping time. These drifts are cumbersome for magnetostriction measurements because of the differential thermal expansion between the cell and the sample, which can affect the capacitance gap. Even in the liquid helium range of temperature, typical thermal expansion coefficients are of the order of $10^{-6}K^{-1}$; thus a 10^{-8} stability in strain still requires a 10mK stability in temperature over the period of measurement [40].
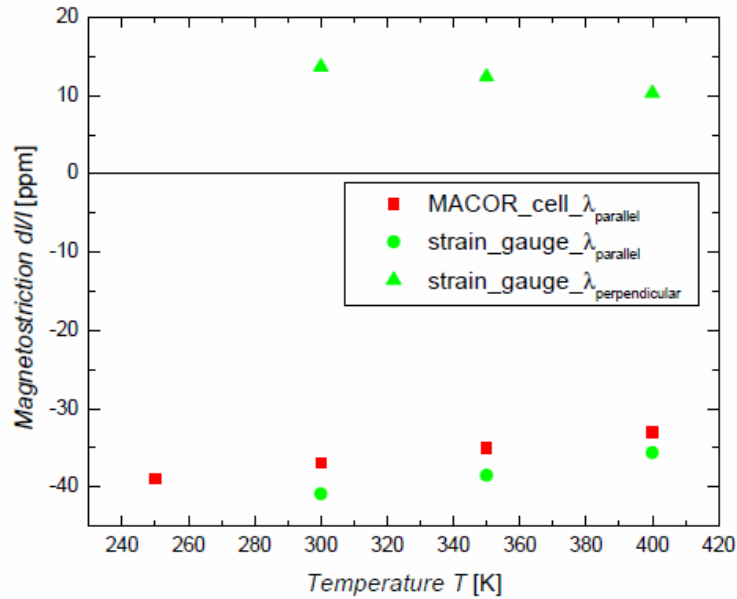
Figure 8.9.: The results for magnetostriction, detected at different temperatures with the MACOR cell (red coloured) are compared to those measured with a strain gauge [43] (green marked) at the same temperatures.
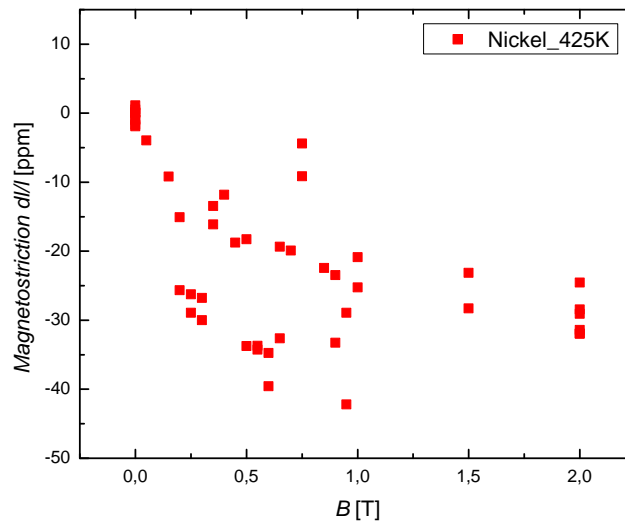
Figure 8.10.: The thermal gradients on the cell affect the results. During the measurement of approximately 3 to 5 minutes the thermal drift has to stay stable in a range of 200mK. If that is not guaranteed the resolution of the capacitance cell suffers enormous and reproducable results are impossible.

After all the introduction of a high temperature magnetostriction measurement coupled with the introduction of new materials which resist the high temperatures succeeded. The outstanding results of the system distinguish the functionality of it. As a final completion we want to give an outlook for a small addition to facilitate the thermal stability.

9. Outlook

As well as the high magnetostriction system itself worked an improved heating furnace with a higher thermal homogeneity in it would decrease the temperature gradient on the cell. As a consequence a higher temperature range for high temperature magentostriction measurements is possible.

It is recommended to guarantee an adequate temperature stability of a range of 100mK during the gauging process. There are two possibilities to achieve that. Either with a PID (proportional–integral–derivative) controller or by a change of the used superconductor to a pulsed magnet. Primarily the pulsed magnet presents practical advantages. The time required for measurements is very short. Pulsed fields can be operated at any temperatures and because of the short measurement durations no temperature gradients on the sample manipulate the results. Therefore temperature drifts are avoided. Furthermore the use of pulsed fields is much less expensive than Bitter magnets and, to a less extent, than superconductive coils. It is beyond all question that the adaption of the high temperature system to a pulsed magnet reflects in excellent results for high temperature magnetostriction. But it seems important to mention that therefore the measuring electonics has to be adapted again.

Bibliography

[1] Etienne du Trémolet de Lacheisserie. *MAGNETOSTRICTION THEORY and AP-PLICATIONS of MAGNETOELASTICITY*. CRC Press, 1993.

[2] E.W. Lee. Magnetostriction and Magnetomechanical Effects. *Reports on Progress in Physics*, 18(1):184–229, 1955.

[3] E.du.T.de Lacheisserie, D. Gignoux, and M. Schlenker. *Magnetism: Materials and Applications*. Springer (Grenoble Sciences), 2005.

[4] M.T. Hutchings. *Handbook of Magnetic Materials*, volume 16. Academic Press, New York, 1964.

[5] S. Chikazumi. *Physics of Magnetism*. John Wiley and Sons, Inc.,, 1964.

[6] D.C. Jiles. *Introduction to Magnetism and Magnetic Materials*. Chapman and Hall, 1991.

[7] E.W. Lee. *Experimental Magnetism*. John Wiley and Son, 1979.

[8] R. Grossinger, F. Keplinger, N. Mehmood, and R.Sato Turtelli. Magnetic characterization of soft and hard magnetic material. In *3rd International Conference on Magnetism and Metallurgy (WMM' 08) Ghent-Belgium*, 2008.

[9] M. Getzlaff. *Fundamentals of Magnetism*. Springer, 2007.

[10] Wolfgang Demtröder. *Experimentalphysik 2: Elektrizität und Optik*. Springer-Verlag GmbH, 2008.

[11] Wolfgang Demtröder. *Experimentalphysik 1: Mechanik und Wärme*. Springer-Verlag GmbH, 2005.

[12] Agustín del Moral. *Handbook of Magnetostriction and Magnetostrictive Materials*. Del Moral Publisher, 2008.

[13] A.del Moral. Magnetostriction: fundamental principles and novel magneto-strictive materials. *Europhysics*, 34:8, 2003.

[14] B.S. Chandrasekhar and E. Fawcett. Magnetostriction in Physics. *Advances in Physics*, 20:775, 1971.

[15] N.S. Akulov. Über die Anwendungen des Gesetzes ferromagnetischer Anisotropie zur Berechnung der Eigenschaften polykristallinischen Eisens, 1930.

[16] M. Rotter, M. Loewenhaupt, M. Doerr, A. Lindbaum, H. Sassik, K. Ziebeck, and B. Beuneu. Dipole interaction and magnetic anisotropy in gadolinium compounds. *Physical Review B*, 68:7, 2003.

[17] Dr. rer. nat. Mathias Dörr. *Magnetostriction of rare-earth based intermetallic compounds in very high magnetic fields.* PhD thesis, Technical University Dresden, 2007.

[18] K.H.J. Buschow and F.R. de Boer. *Physics of Magnetism and Magnetic Materials.* Kluwer Academic Publishers, 2004.

[19] Feiming Bai. *Structure Property Relationships of Multifeorric Materials: A nano Perspective.* PhD thesis, Virginia Polytechnic Institute and State University, 2006.

[20] Jason R. Hattrick-Simpers. *Combinatorial investigation of magnetostrictive materials.* PhD thesis, UNIVERSITY OF MARYLAND, COLLEGE PARK, 2008.

[21] R. Gersdorf. *On magnetostriction of single crystals of iron and some dilute iron alloys.* PhD thesis, University of Amsterdam, 1961.

[22] T.G. Kollie. Measurement of the thermal-expansion coefficient of nickel from 300 to 1000 K and determination of the power-law constants near the Curie temperature. *Physical Review B (Solid State)*, 16:10, 1977.

[23] R. Grössinger, R. Sato Turtelli, and N. Mehmood. Magnetostriction of Fe-X (X =Al,Ga,Si, Ge) Intermetallic Alloys. *IEEE Transactions on Magnetics*, 44(11):3001–3004, 2008.

[24] M.J. Dapino. *Magnetostrictive materials: their use in smart structure applications.* Encyclopedia of Smart Materials. John Wiley & Sons, Inc., New York, 2000.

[25] G. Engdahl. *Handbook of giant magnetostrictive materials.* Academic Press, 2000.

[26] V.I. Nizhankovskii. Classical magnetostriction of nickel in high magnetic field. *European Physical Journal B*, 53:4, 2006.

[27] M. Doerr, W. Lorenz, T. Neupert, M. Loewenhaupt, N.V. Kozlova, J. Freudenberger, M. Bartkowiak, E. Kampert, and M. Rotter. Simultaneous measurement of magnetization and magnetostriction in 50 T pulsed high magnetic fields. *Review of Scientific Instruments*, 79:5, 2008.

[28] Peter Oser. Ein Hysteresograph zur Charakterisierung weichmagnetischer Materialien. Master's thesis, TU Vienna, 2008.

[29] Nasir Mehmood. *Investigation of New High Magnetostrictive Materials*. PhD thesis, Technical University Vienna, 2009.

[30] R. C. O'Handley. Temperature dependence of magnetostriction in Fe80B20 glass. *Solid State Communications*, 22:4, 1977.

[31] R. C. O'Handley. Magnetostriction of transition-metal-metalloid glasses: Temperature dependence. *Physical Review B*, 18:9, 1978.

[32] Wolfgang Demtröder. *Experimentalphysik 3: Atome, Moleküle und Festkörper*. 2005.

[33] Gabriel Vlasák. Direct measurement of magnetostriction of rapidly quenched thin ribbons. *Journal of Magnetism and Magnetic Materials*, 215-216:3, 2000.

[34] G.K. White. Measurement of thermal expansion at low temperatures. *Cryogenics*, 1:151, 1961.

[35] B.A. Green and B.S. Chandrasekhar. Observation of oscillatory magnetostriction in bismuth. *Physical Review Letters*, 11:331, 1963.

[36] E. Fawcett. Magnetostriction of paramagnetic transition metals. *Physical Review B*, 2:1604, 1970.

[37] R. Griessen and R.S. Sorbello. Oscillatory magnetostriction and the stress dependence of the Fermi surface of aluminium. *Physical Review*, 6:2198, 1972.

[38] J.P. Michenaud, J. Heremans, J. Boxus, and C. Haumont. Longitudinal magnetostriction of bismuth above the last quantum limit. *Journal of Physics C: Solid State Physics*, 14:L13–6, 1981.

[39] G. Brändli and R. Griessen. Two capacitance dilatometers. *Cryogenics*, 13:3541, 1973.

[40] J. Heremans, J.P. Michenaud, Y. Iye, N. Miura, G. Kido, K. Nakamura, and S. Tanuma. A capacitive instrument for the measurement of magnetostriction in pulsed fields. *Journal of Physics E: Scientific Instruments*, 16:5, 1983.

[41] M. Rotter, H. Müller, E. Gratz, M. Doerr, and M. Loewenhaupt. A miniature capacitance dilatometer for thermal expansion and magnetostriction. *Review of Scientific Instruments*, 69(7):2742–2746, 1998. cited By (since 1996) 46.

[42] M. Doerr, W. Lorenz, M. Rotter, A. Barcza, M.D. Le, J. Brooks, E. Jobiliong, N.V. Kozlova, J. Freudenberger, and M. Loewenhaupt. Magnetostriction of 4f-electron compounds in high magnetic fields. *Journal of Physics: Conference Series*, 51:561–564, 2006.

[43] Martin Kriegisch. Phd thesis about magnetization and magnetostriction. is expected to be finished 2011.

[44] J. Heremans, J.P. Michenaud, M. Shayegan, and G. Dresselhaus. Magnetostriction and deformation potentials in graphite. *Journal of Physics C: Solid State Physics*, 14:3541, 1982.

[45] J.P. Michenaud, J. Heremans, M. Shayegan, and C. Haumont. Magnetostriction of bismuth in quantizing magnetic fields. *Physical Review B*, 26:2552, 1982.

[46] M. Rotter, M. Doerr, M. Loewenhaupt, W. Kockelmann, R.I. Bewley, R.S. Eccleston, A. Schneidewind, and G. Behr. Pressure dependence of the magnetic structures and excitations in the giant magnetostriction compound TbCu2. *Journal of Magnetism and Magnetic Materials*, 269:372–379, 2004.

List of Figures

List of Tables

A. Additional information about the PEEK cell

A.1. Derivation of the effective capacitance area

In section 5.1.1 the relations $a = b/\cos\alpha$ and $c = d\cdot\tan\alpha$ have already been introduced (figure 5.2). For the derivation of the effective capacitance area A_{eff} we study only the quarter of the ellipse in the first quadrant as shown in the right hand picture of figure A.1.

The general equation for an ellipse is known as:

$$\frac{x^2}{a^2} + \frac{y^2}{b^2} = 1 \tag{A.1}$$

which can also be formed to:

$$y^2 = \frac{b^2}{a^2} \cdot \left(a^2 - x^2\right)$$

and for the positive (the negative is not important because we are in the first quadrant of the ellipse) solution of this quadratic function we get for y:

$$y = f(x) = \frac{b}{a}\sqrt{(a^2 - x^2)} \tag{A.2}$$

By integrating the function A.2 with the integration limits $c/2$ and $a-c/2$ the effective capacitance area A_{eff} is conserved:

$$\frac{A_{eff}}{4} = \frac{b}{a}\int_{\frac{c}{2}}^{a-\frac{c}{2}} \sqrt{a^2 - x^2}dx \tag{A.3}$$

And with the aid of the substitution:

$$\begin{aligned} x &= a\sin(t) \\ dx &= a\cos(t)\,dt \end{aligned}$$

the integral changes to:
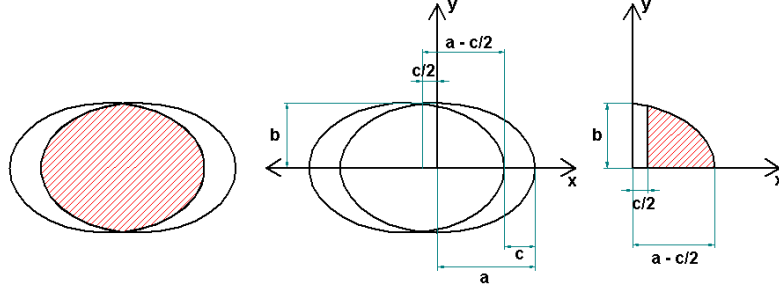
Figure A.1.: The draft shows the intersection of two elliptical capacitor plates. The effective capacitance area A_{eff} with its homogeneous electrical field is red deposited.

$$
\begin{aligned}
\frac{A_{eff}}{4} &= \frac{b}{a} \int_{\frac{c}{2}}^{a-\frac{c}{2}} \sqrt{a^2 - a^2 \sin^2(t)} \cdot a \cos(t)\, dt = \\
&= \frac{b}{a} \int_{\frac{c}{2}}^{a-\frac{c}{2}} a\sqrt{1 - \sin^2(t)} \cdot a \cos(t)\, dt = \\
&= \frac{b}{a} \int_{\frac{c}{2}}^{a-\frac{c}{2}} a\sqrt{\cos^2(t)} \cdot a \cos(t)\, dt = \\
&= ab \int_{\frac{c}{2}}^{a-\frac{c}{2}} \cos^2(t)\, dt = \\
&= \frac{ab}{2} \int_{\frac{c}{2}}^{a-\frac{c}{2}} (1 + \cos(2t))\, dt = \\
&= \frac{ab}{2} \left[t + \frac{1}{2} \sin(2t) \right]_{\frac{c}{2}}^{a-\frac{c}{2}}
\end{aligned}
$$

A back substitution:

$$
t = \arcsin\left(\frac{x}{a}\right)
$$

produces the finally mathematical expression for the effective capacitance area A_{eff}:

$$\frac{A_{eff}}{4} = \frac{ab}{2}\left[\arcsin\left(\frac{x}{a}\right) + \frac{1}{2}\sin\left(2\arcsin\left(\frac{x}{a}\right)\right)\right]_{\frac{c}{2}}^{a-\frac{c}{2}} =$$

$$= \frac{ab}{4}\left[2\arcsin\left(\frac{x}{a}\right) + \sin\left(2\arcsin\left(\frac{x}{a}\right)\right)\right]_{\frac{c}{2}}^{a-\frac{c}{2}} =$$

$$= \frac{ab}{4}\left[2\arcsin\left(\frac{a-\frac{c}{2}}{a}\right) + \sin\left(2\arcsin\left(\frac{a-\frac{c}{2}}{a}\right)\right)\right]$$

$$-\frac{ab}{4}\left[2\arcsin\left(\frac{c}{2a}\right) + \sin\left(2\arcsin\left(\frac{c}{2a}\right)\right)\right] =$$

$$= \frac{ab}{4}\left[2\arcsin\left(\frac{2a-c}{2a}\right) + \sin\left(2\arcsin\left(\frac{2a-c}{2a}\right)\right)\right]$$

$$-\frac{ab}{4}\left[2\arcsin\left(\frac{c}{2a}\right) + \sin\left(2\arcsin\left(\frac{c}{2a}\right)\right)\right]$$

And because of the reason that up to now just the first quadrant and thus a quarter of A_{eff} was viewed we get for the complete area A_{eff}:

$$A_{eff} = ab\left[2\arcsin\left(\frac{2a-c}{2a}\right) + \sin\left(2\arcsin\left(\frac{2a-c}{2a}\right)\right)\right]$$

$$-ab\left[2\arcsin\left(\frac{c}{2a}\right) + \sin\left(2\arcsin\left(\frac{c}{2a}\right)\right)\right] \qquad (A.4)$$

A.2. The first design of the capacitance cell

The detailed construction plans of the first PEEK capacitance cell are registered in the following. They are drafted via the computer software "Solid Edge". The first figure shows the complete PEEK capacitance cell and the next ones present the single parts of the cell from top to bottom:
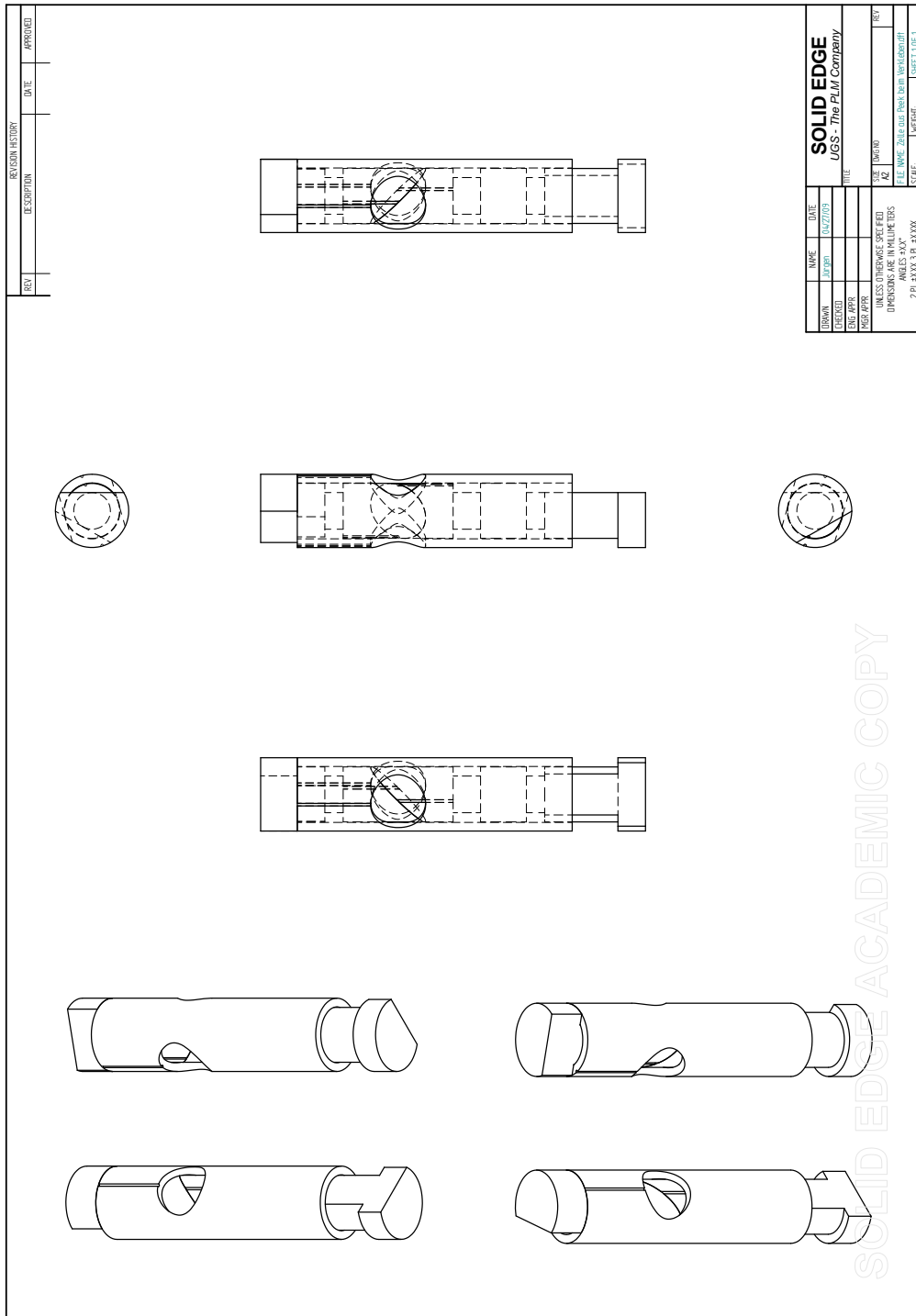
Figure A.2.: complete first PEEK cell design
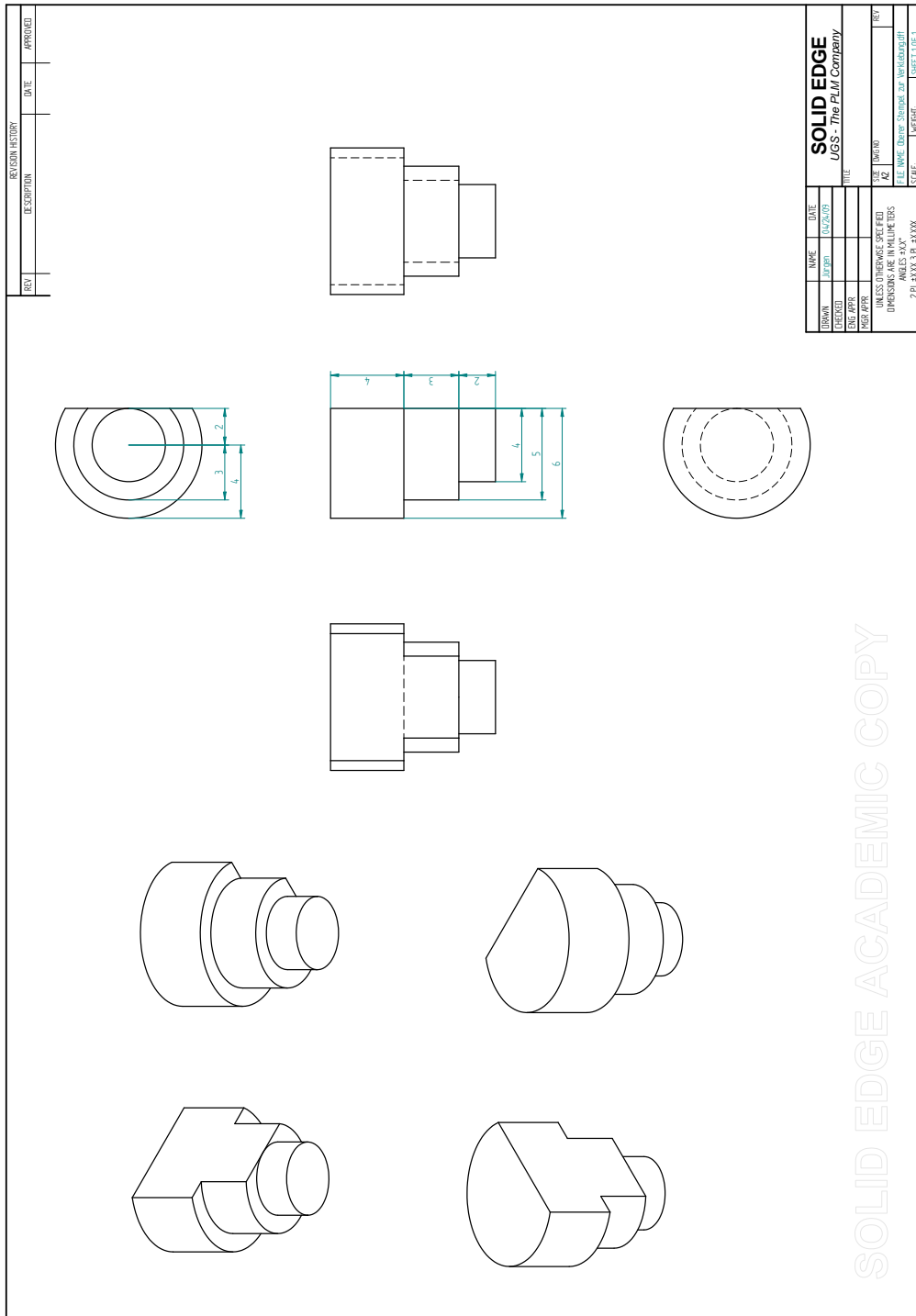
Figure A.3.: upper PEEK cell plunger

Figure A.4.: upper capacitance plunger
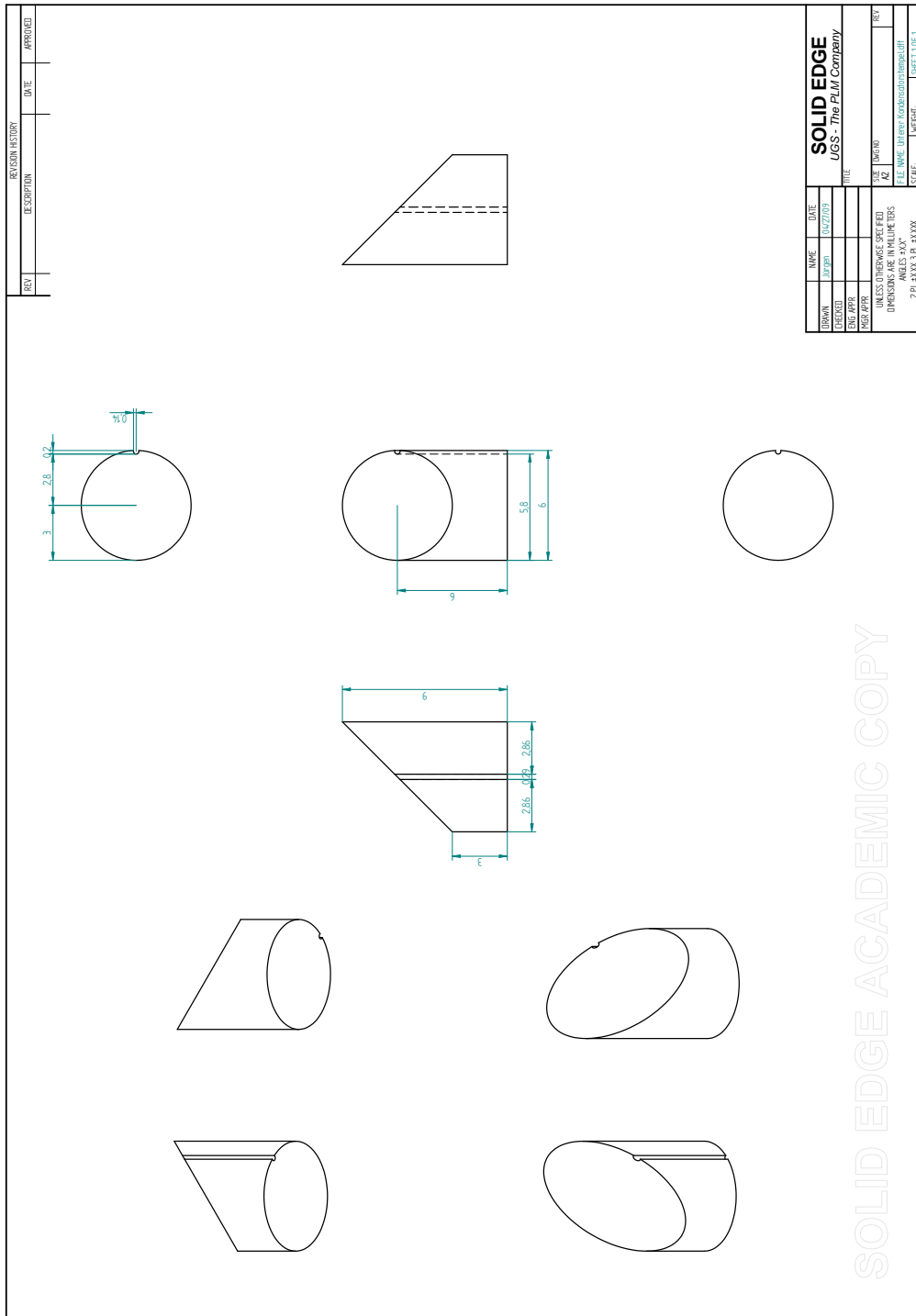
Figure A.5.: lower capacitance plunger

Figure A.6.: sample with its maximum altitude of 3mm
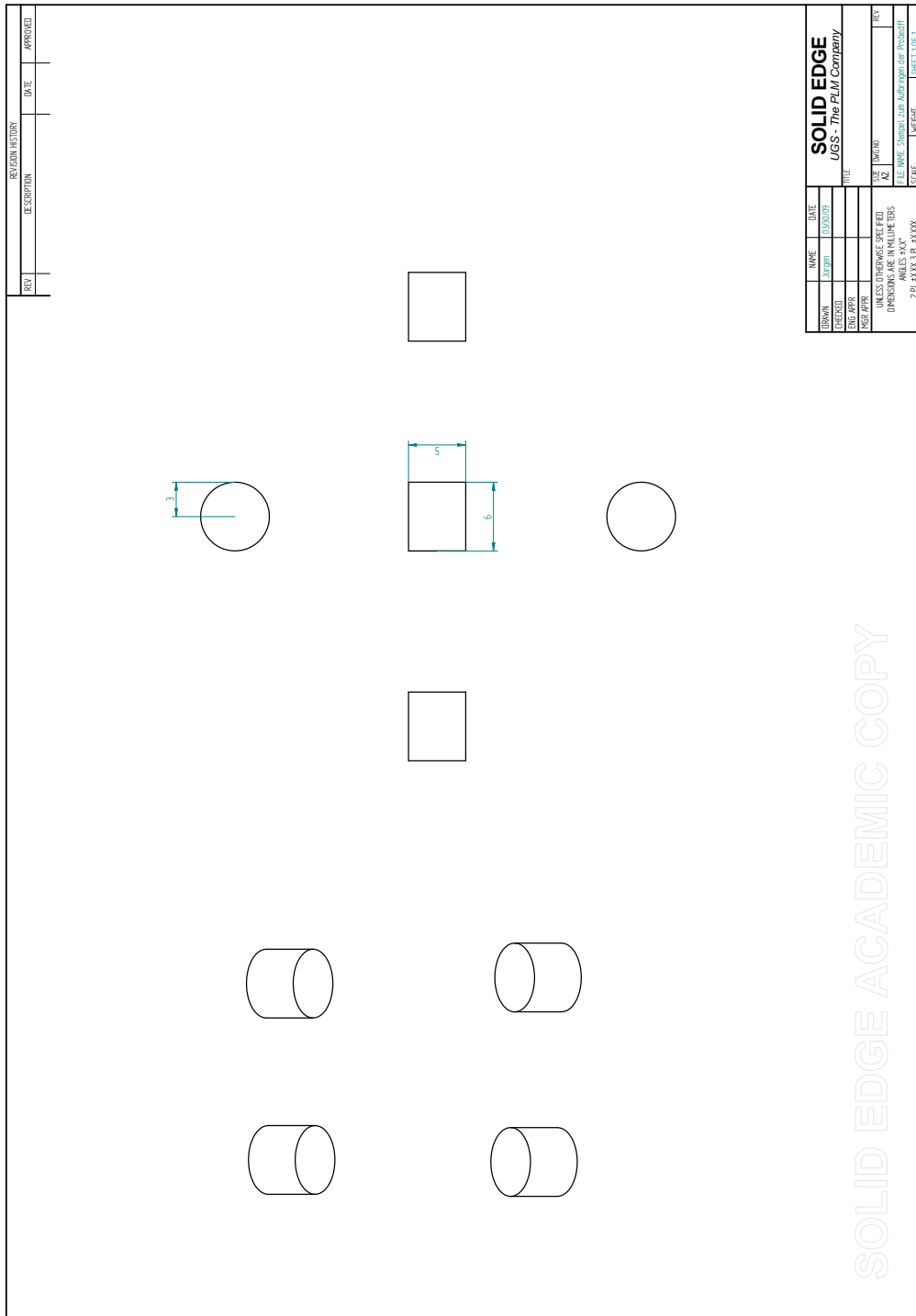
Figure A.7.: sample plunger
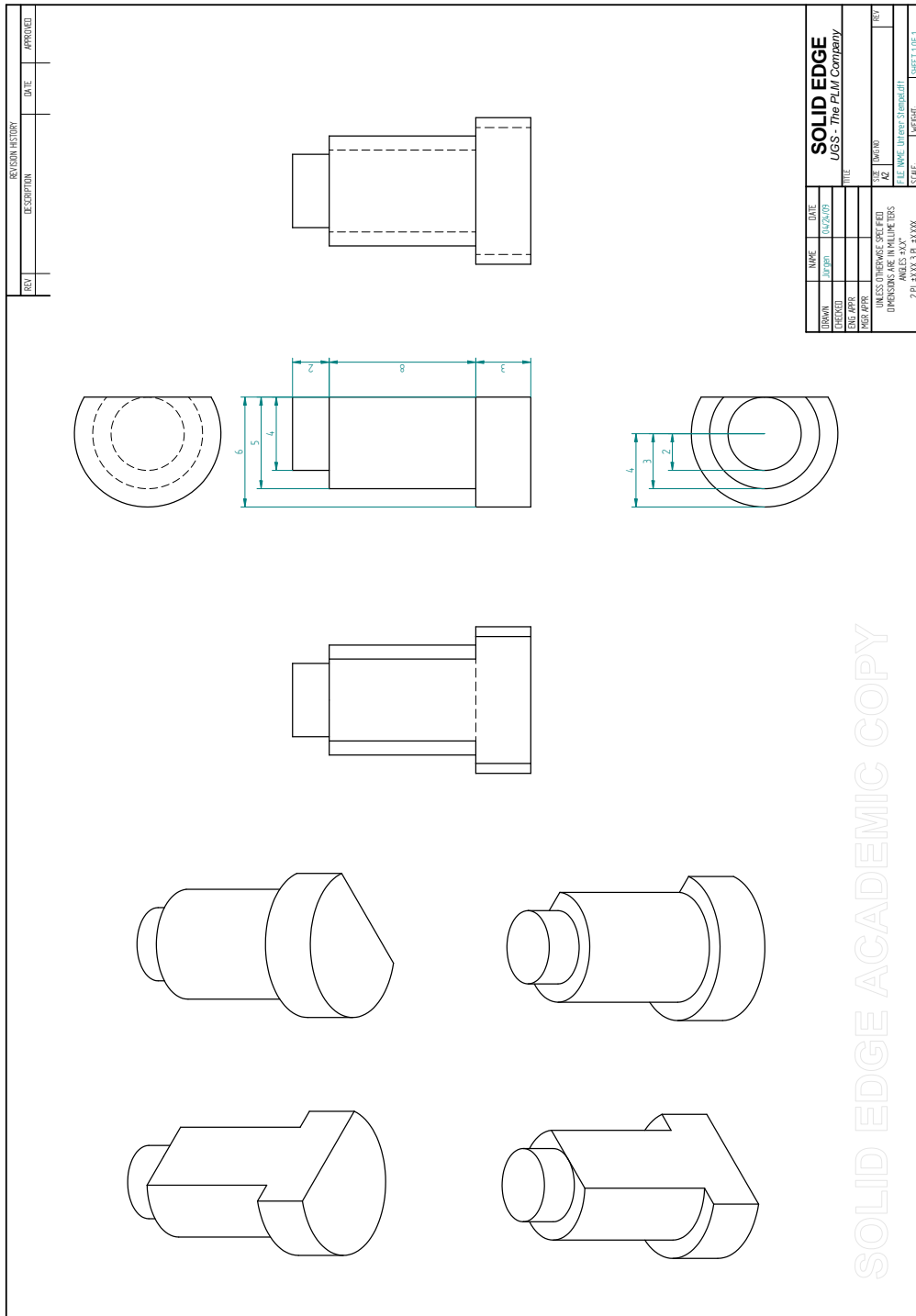
Figure A.8.: lower PEEK cell plunger
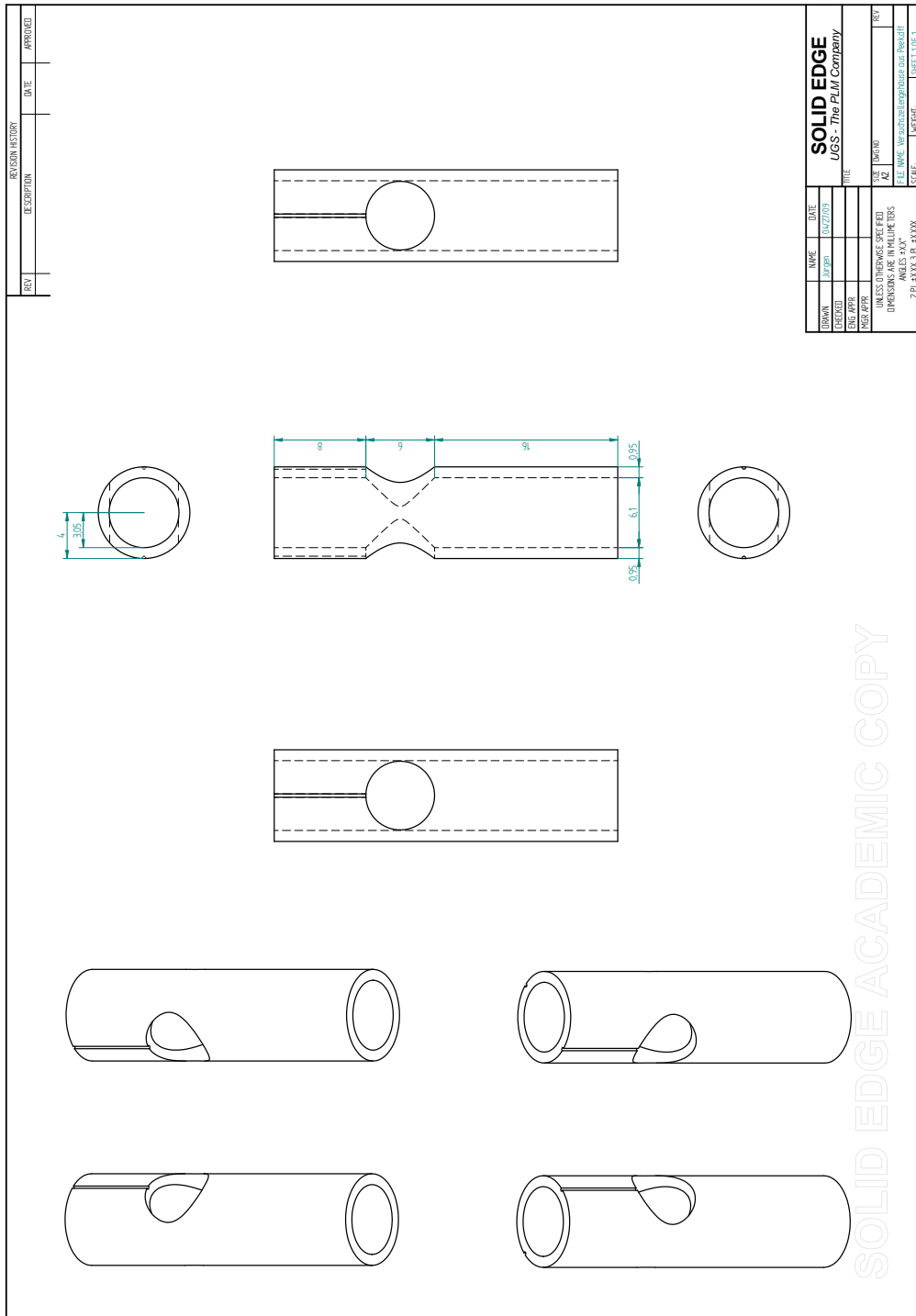
Figure A.9.: PEEK body around

A.3. Horizontal improved PEEK cell

After improving the PEEK cell (section 6.3.1) construction plans of the first PEEK capacitance cell (section A.2) have to be modified via the computer software "Solid Edge". The complete design of the horizontal improved PEEK cell is shown in the first figure A.10. Afterwards the single parts of the cell from top to bottom are presented. Pictures of all components can also be viewed in figure 6.7.
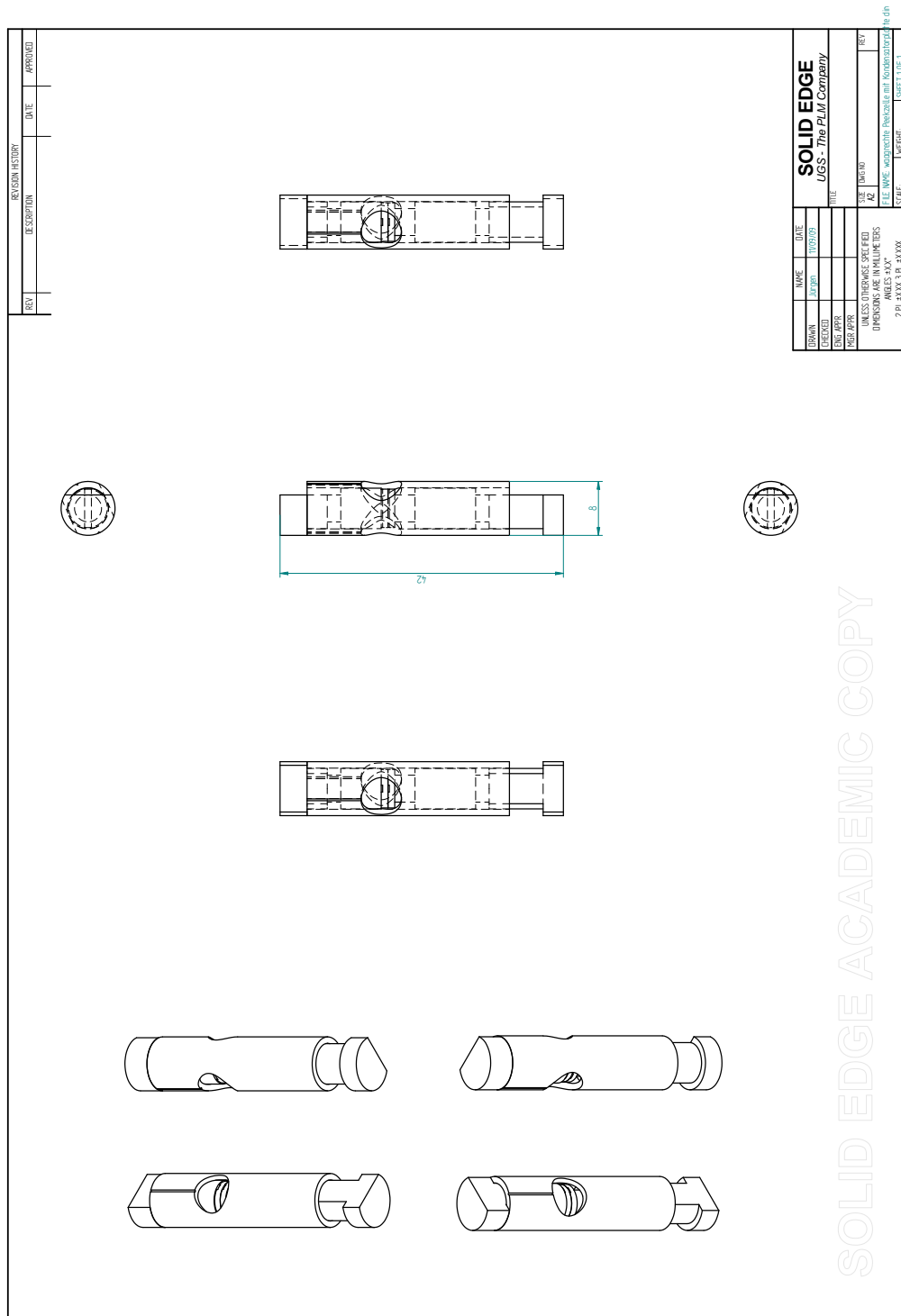
Figure A.10.: complete design of the final improved PEEK cell with horizontal capacitor plates
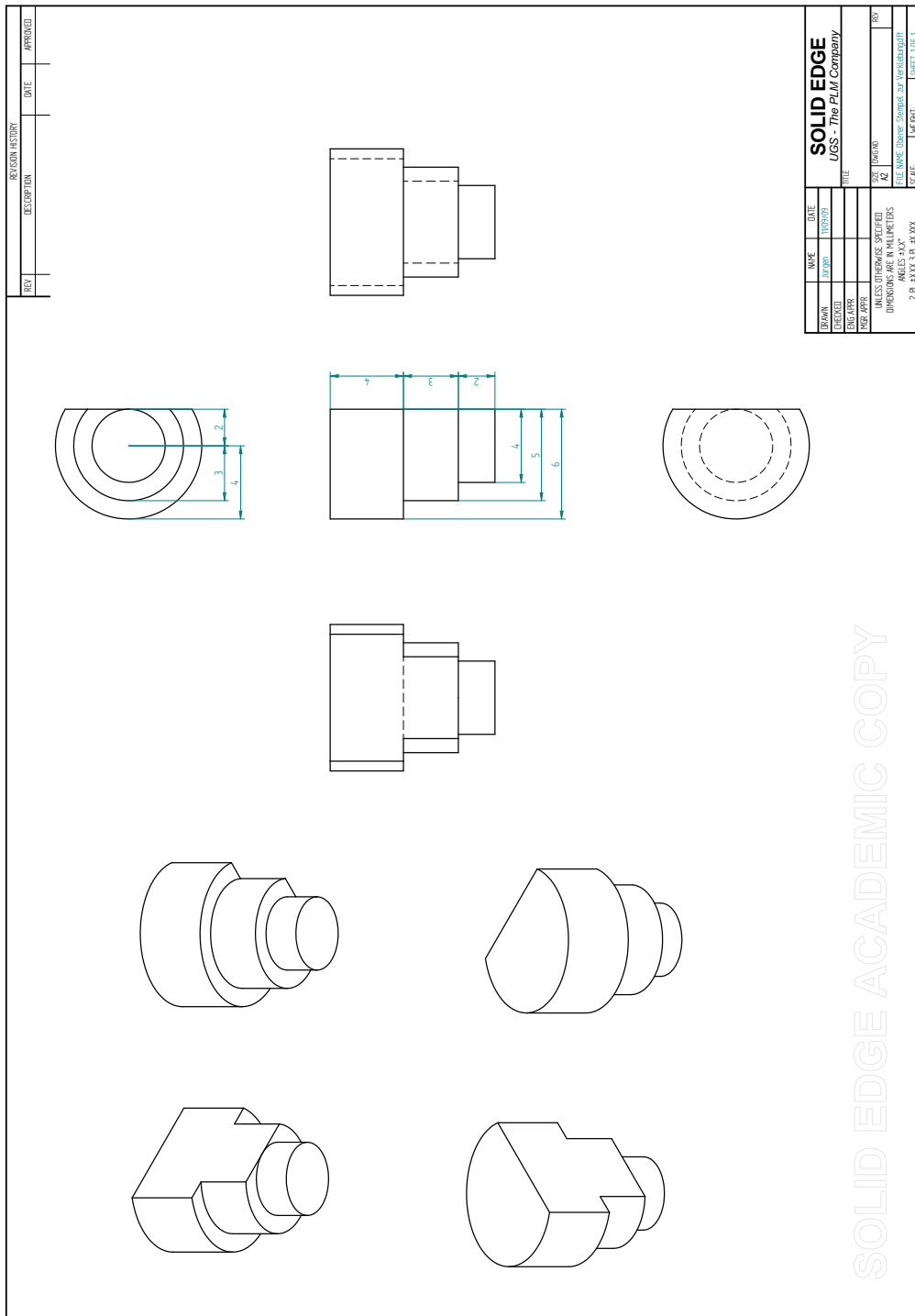
Figure A.11.: upper PEEK cell plunger
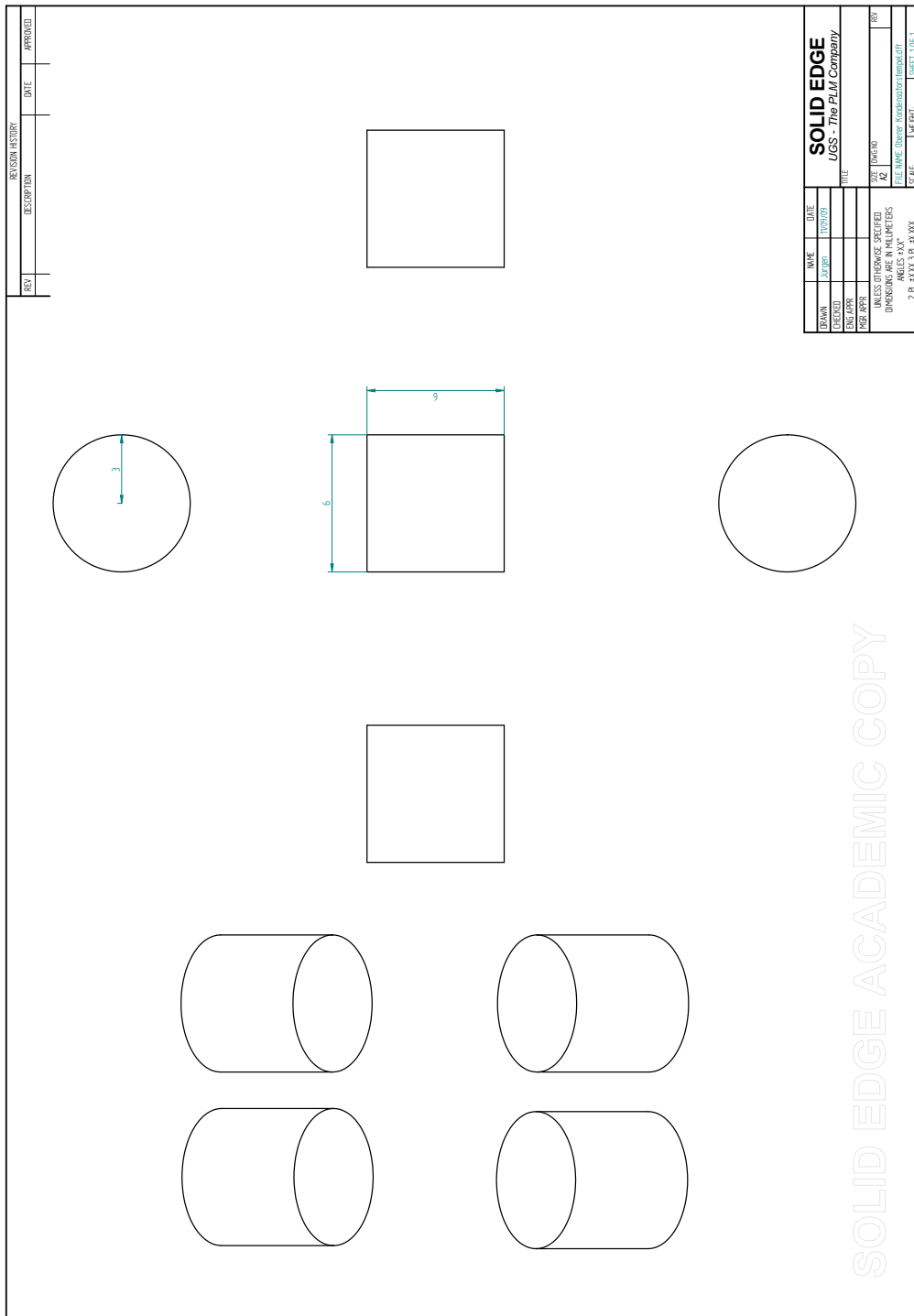
Figure A.12.: upper capacitance plunger
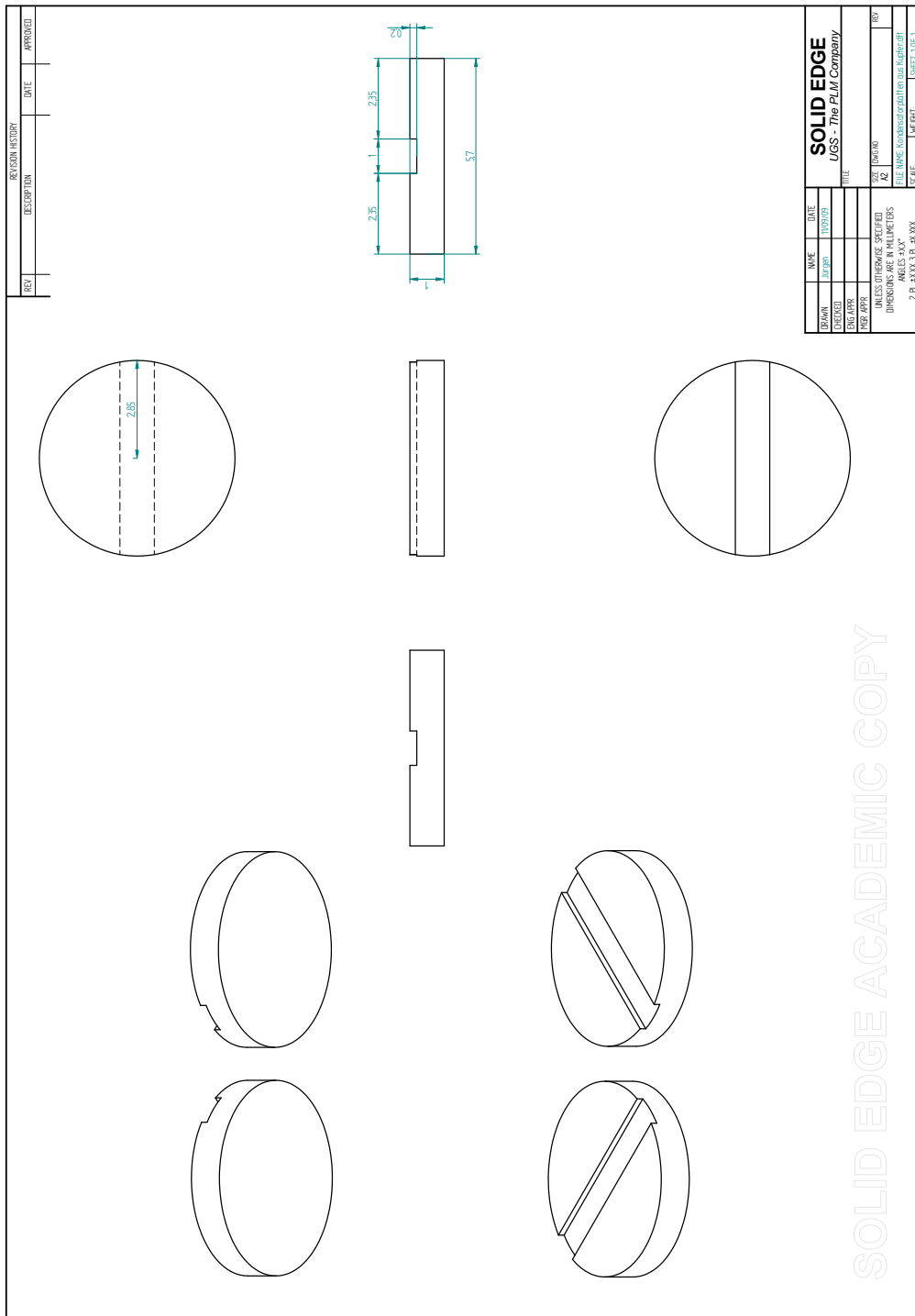
Figure A.13.: the capacitor plates made of copper
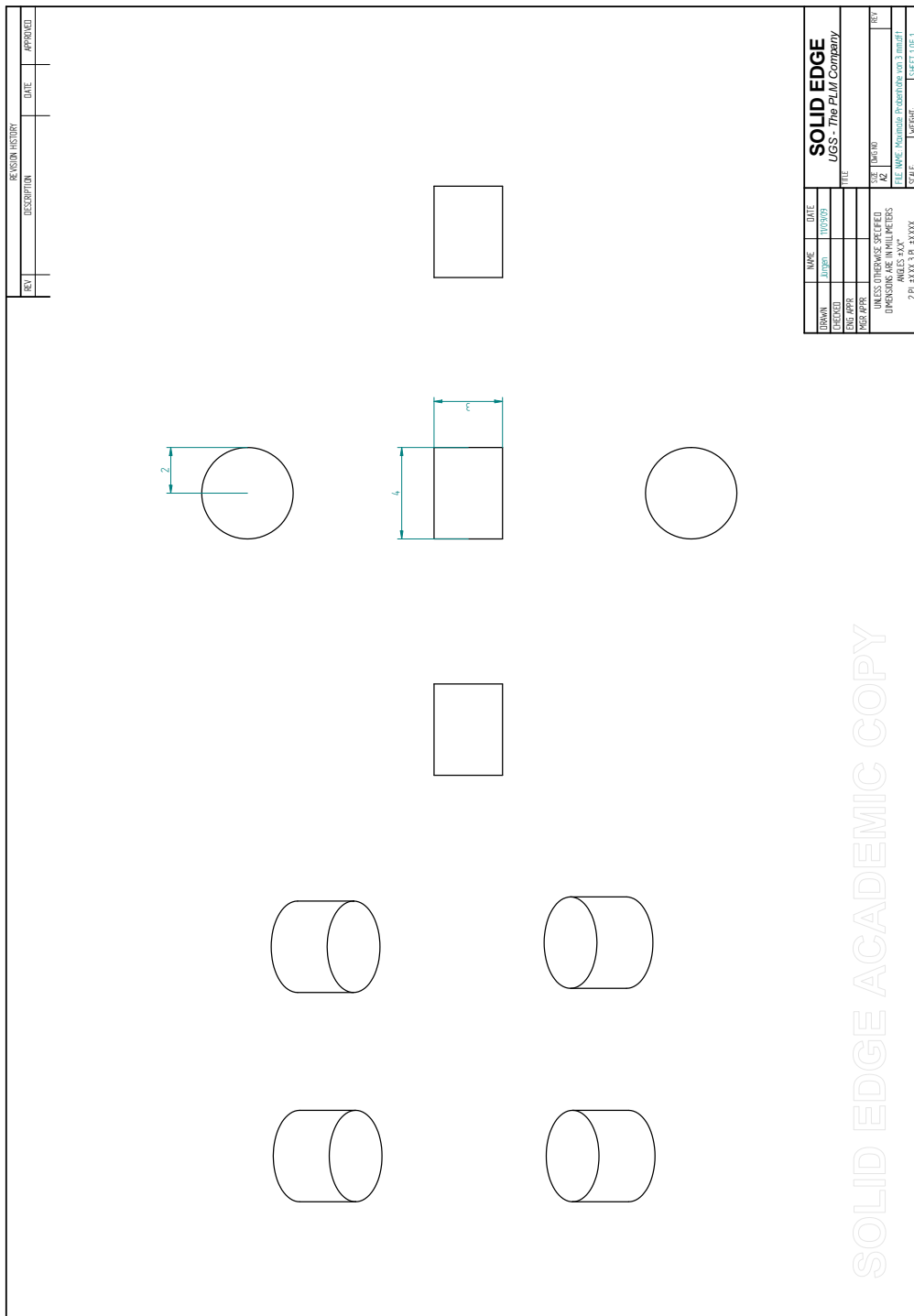
Figure A.14.: for best results the altitude of the sample should vary between 3mm and 4mm (section 6.5.2)
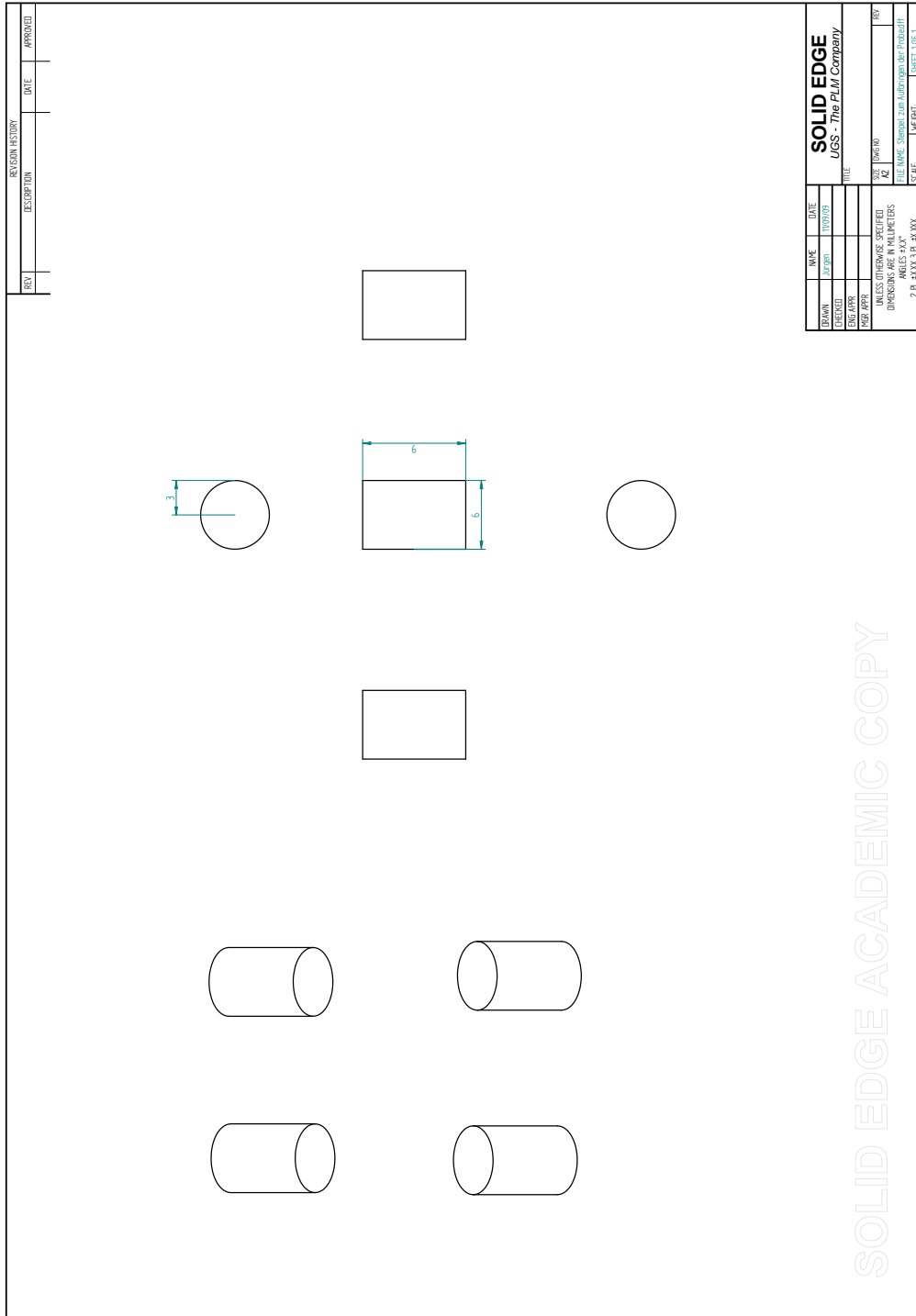
Figure A.15.: sample plunger
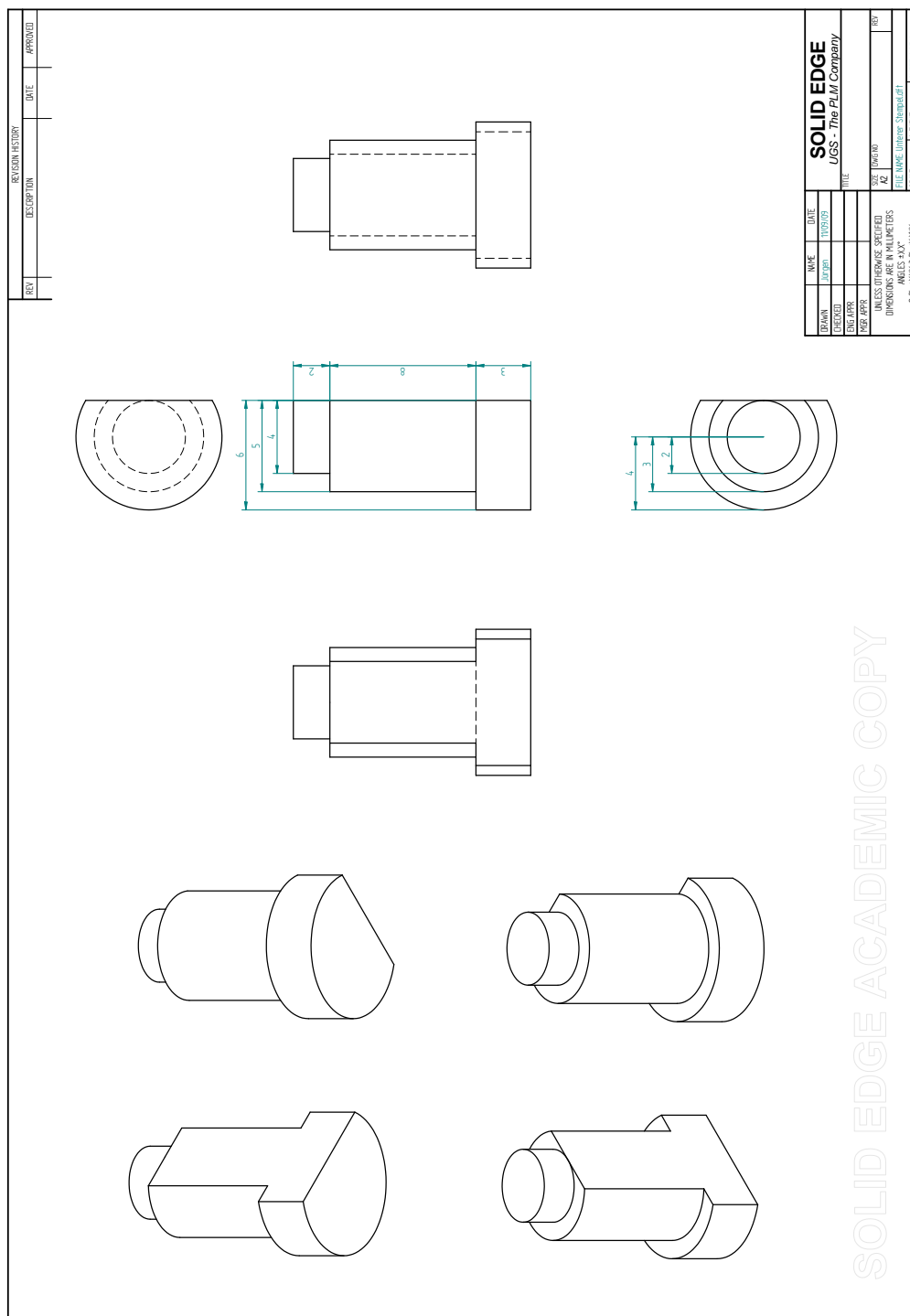
Figure A.16.: lower PEEK cell plunger
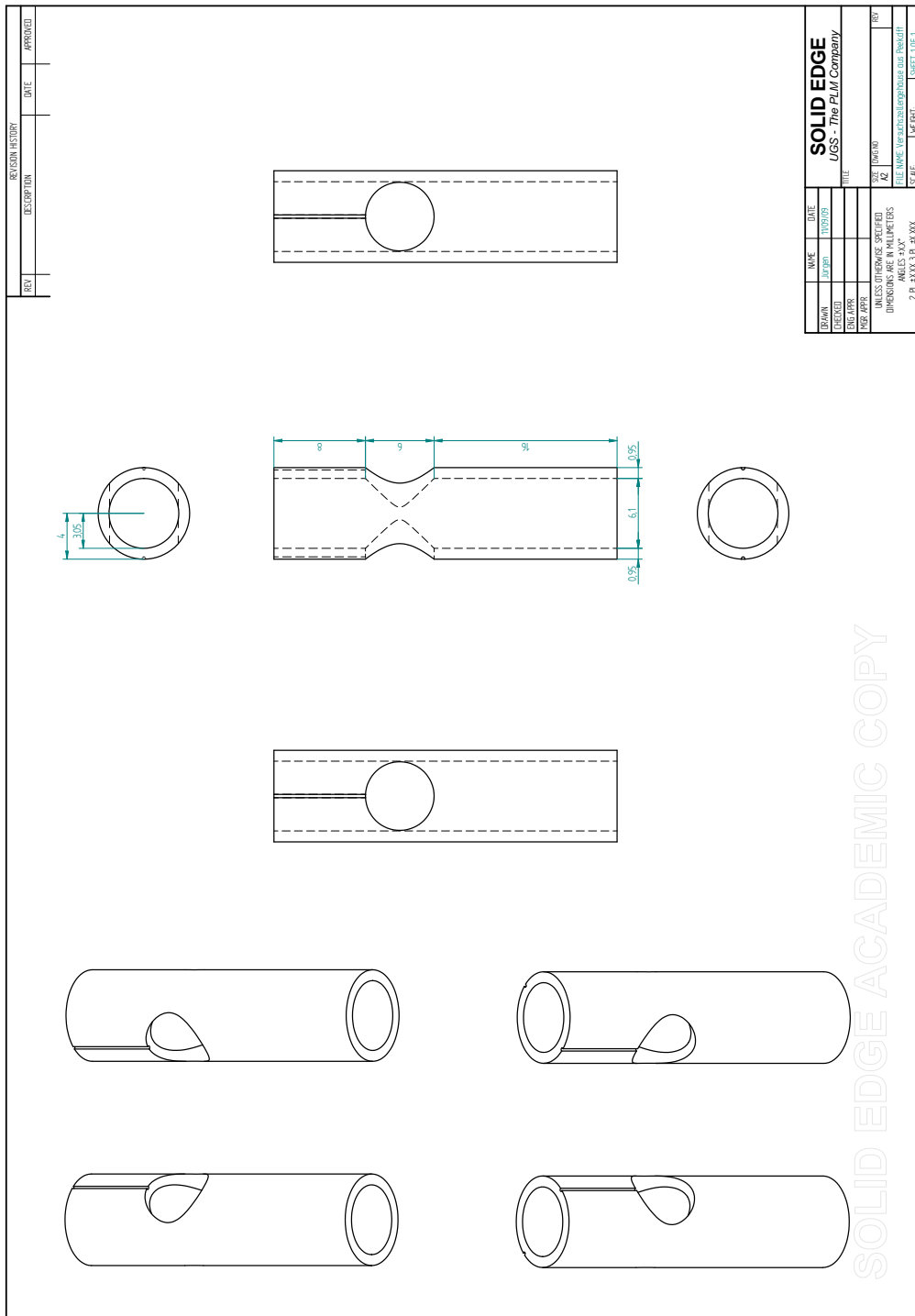
Figure A.17.: PEEK body around

B. Additional information about the MACOR cell

The detailed construction plans of the MACOR capacitance cell, the cell rod and the body of the heating furnace are specified in the following. They are drafted via the computer software "Solid Edge". The first figure shows the complete constructions whereas the next ones present the single parts from top to bottom:

B.1. Horizontal MACOR cell
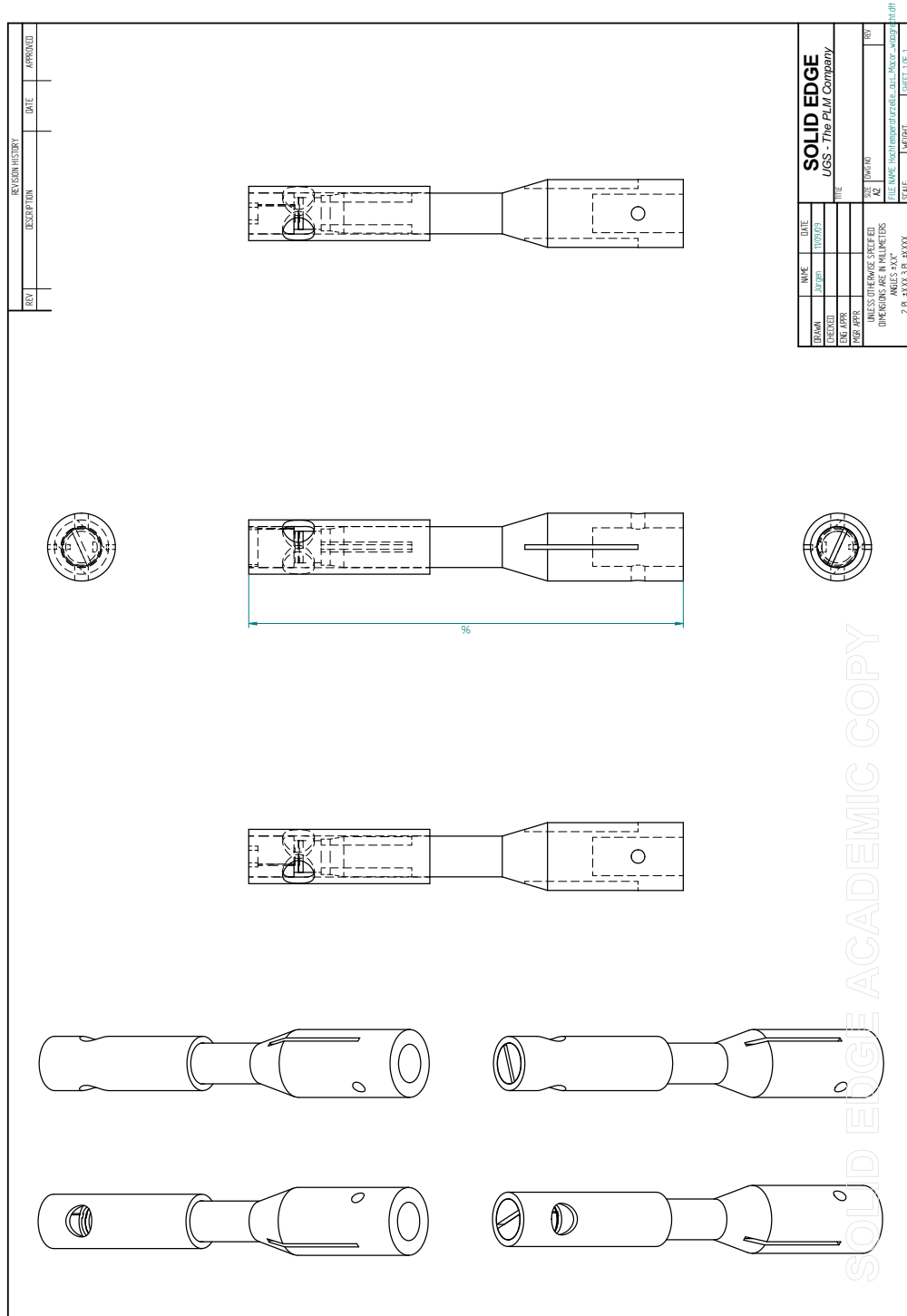
Figure B.1.: complete design of the MACOR cell with horizontal capacitor plates direct on the sample

Figure B.2.: upper MACOR cell plunger

Figure B.3.: tantal capacitor plates

Figure B.4.: for best results the altitude of the sample should vary between 3mm and 4mm (section 6.5.2)

Figure B.5.: the MACOR body around them

Figure B.6.: lower MACOR cell plunger

B.2. The cell rod
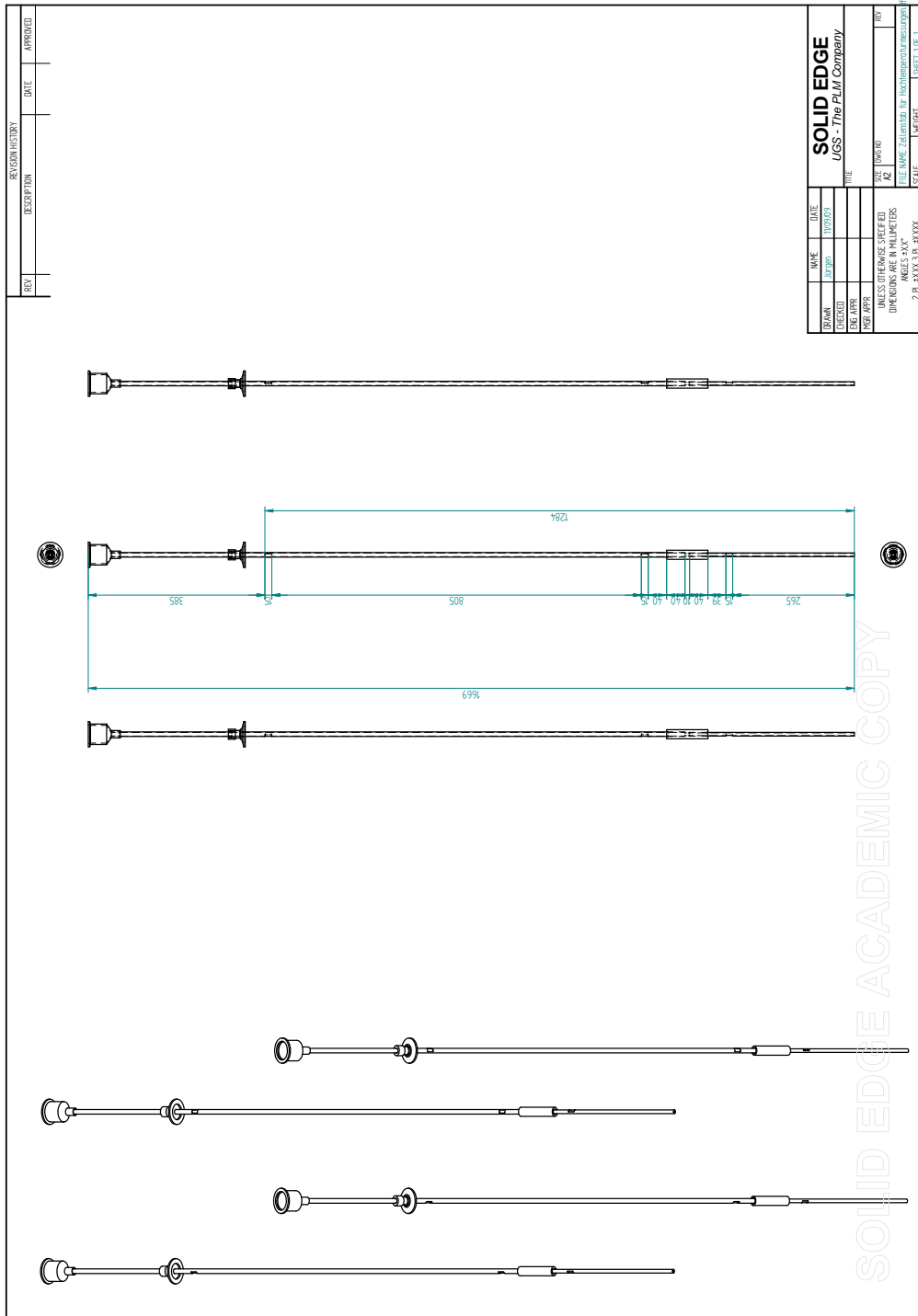
Figure B.7.: non magnetic cell rod with leybold standards for cryostats

B.3. The heating furnace
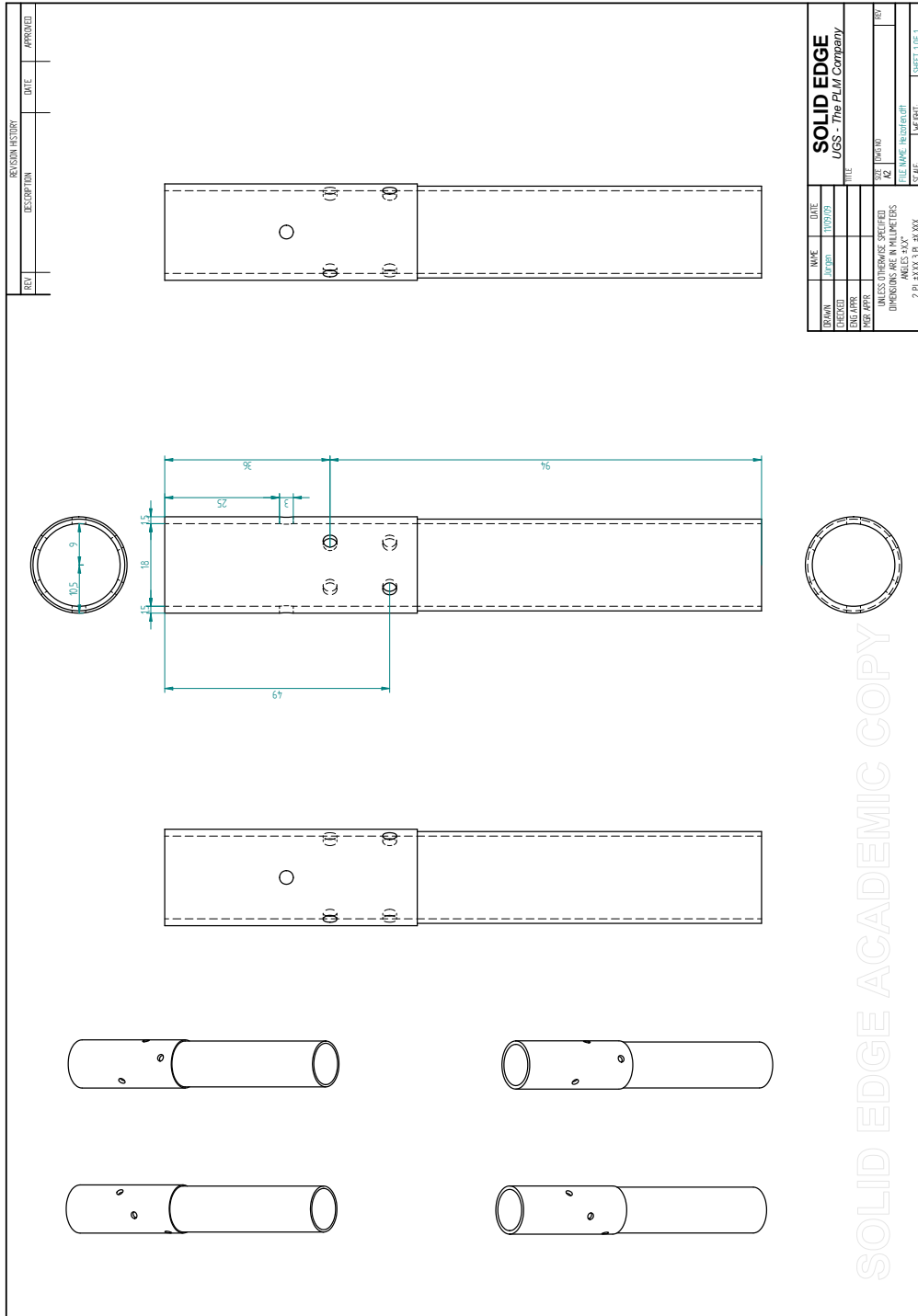
Figure B.8.: the copper body of the heating furnace